

UNCLASSIFIED

AD NUMBER
ADB007733
NEW LIMITATION CHANGE
TO Approved for public release, distribution unlimited
FROM Distribution authorized to U.S. Gov't. agencies only; Test and Evaluation of military hardware; Nov 1975. Other requests shall be referred to Air Force Armament Laboratory [DLJC], Eglin AFB, Florida 32542.
AUTHORITY
USADTC ltr, 5 apr 1979

THIS PAGE IS UNCLASSIFIED

**AEDC-TR-75-149**  
**AFATL-TR-75-141**

*Cy. 1*



**STATIC AND DYNAMIC STABILITY CHARACTERISTICS  
OF THE FIXED-FIN AND INFLATABLE  
STABILIZER RETARDER CONFIGURATIONS OF THE  
MK-82 STORE AT TRANSONIC SPEEDS**

**PROPULSION WIND TUNNEL FACILITY  
ARNOLD ENGINEERING DEVELOPMENT CENTER  
AIR FORCE SYSTEMS COMMAND  
ARNOLD AIR FORCE STATION, TENNESSEE 37389**

**November 1975**

**Final Report for Period May 5 – 27, 1975**

Distribution limited to U. S. Government agencies only; this report contains information on test and evaluation of military hardware; November 1975; other requests for this document must be referred to Air Force Armament Laboratory (DLJC), Eglin AFB, Florida 32542.

A large, stylized handwritten signature in black ink, appearing to be "M. J. ...".

**Prepared for**

**AIR FORCE ARMAMENT LABORATORY (DLJC)  
EGLIN AFB, FLORIDA 32542**

## NOTICES

When U. S. Government drawings specifications, or other data are used for any purpose other than a definitely related Government procurement operation, the Government thereby incurs no responsibility nor any obligation whatsoever, and the fact that the Government may have formulated, furnished, or in any way supplied the said drawings, specifications, or other data, is not to be regarded by implication or otherwise, or in any manner licensing the holder or any other person or corporation, or conveying any rights or permission to manufacture, use, or sell any patented invention that may in any way be related thereto.

Qualified users may obtain copies of this report from the Defense Documentation Center.

References to named commercial products in this report are not to be considered in any sense as an endorsement of the product by the United States Air Force or the Government.

## APPROVAL STATEMENT

This technical report has been reviewed and is approved for publication.

FOR THE COMMANDER



JOHN C. CARDOSI  
Lt Colonel, USAF  
Chief Air Force Test Director, PWT  
Directorate of Test



CRAIG E. MAHAFFY  
Colonel, USAF  
Director of Test

# UNCLASSIFIED

REPORT DOCUMENTATION PAGE		READ INSTRUCTIONS BEFORE COMPLETING FORM
1. REPORT NUMBER AEDC-TR-75-149 AFATL-TR-75-141	2. GOVT ACCESSION NO.	3. RECIPIENT'S CATALOG NUMBER
4. TITLE (and Subtitle) STATIC AND DYNAMIC STABILITY CHARACTERISTICS OF THE FIXED-FIN AND INFLATABLE STABILIZER RETARDER CONFIGURATIONS OF THE MK-82 STORE AT TRANSONIC SPEEDS	5. TYPE OF REPORT & PERIOD COVERED Final Report - May 5 - 27, 1975	
	6. PERFORMING ORG. REPORT NUMBER	
7. AUTHOR(s)  C. F. Anderson and W. E. Carleton, ARO, Inc.	8. CONTRACT OR GRANT NUMBER(s)	
9. PERFORMING ORGANIZATION NAME AND ADDRESS Arnold Engineering Development Center (XO) Arnold Air Force Station, Tennessee 37389	10. PROGRAM ELEMENT, PROJECT, TASK AREA & WORK UNIT NUMBERS Program Element 64602F Project 5613-02	
11. CONTROLLING OFFICE NAME AND ADDRESS Air Force Armament Laboratory (DLJC) Eglin AFB, Florida 32542	12. REPORT DATE November 1975	
	13. NUMBER OF PAGES 90	
14. MONITORING AGENCY NAME & ADDRESS (if different from Controlling Office)	15. SECURITY CLASS. (of this report)  UNCLASSIFIED	
	15a. DECLASSIFICATION DOWNGRADING SCHEDULE N/A	
16. DISTRIBUTION STATEMENT (of this Report) Distribution limited to U.S. Government agencies only; this report contains information on test and evaluation of military hardware; November 1975; other requests for this document must be referred to Air Force Armament Laboratory (DLJC), Eglin AFB, Florida 32542.		
17. DISTRIBUTION STATEMENT (of the abstract entered in Block 20, if different from Report)  1. Stores -- MK 82 2. " -- Stability		
18. SUPPLEMENTARY NOTES  3. " -- E  Available in DDC		
19. KEY WORDS (Continue on reverse side if necessary and identify by block number)  static shapes Mach numbers dynamic MK-82 Reynolds numbers stability external stores characteristics transonic flow		
20. ABSTRACT (Continue on reverse side if necessary and identify by block number)  An investigation was conducted in the Aerodynamic Wind Tunnel (4T) to obtain the static stability and pitch-damping characteristics of the Fixed-Fin (FF) and Inflatable Stabilizer Retarder (ISRe) configurations of the MK-82 store with solid and slotted fins and with various fin tabs. The static phase was conducted using 0.20-scale models, and the dynamic phase was conducted using 0.442-scale models. The tests were conducted at Mach numbers from		

## UNCLASSIFIED

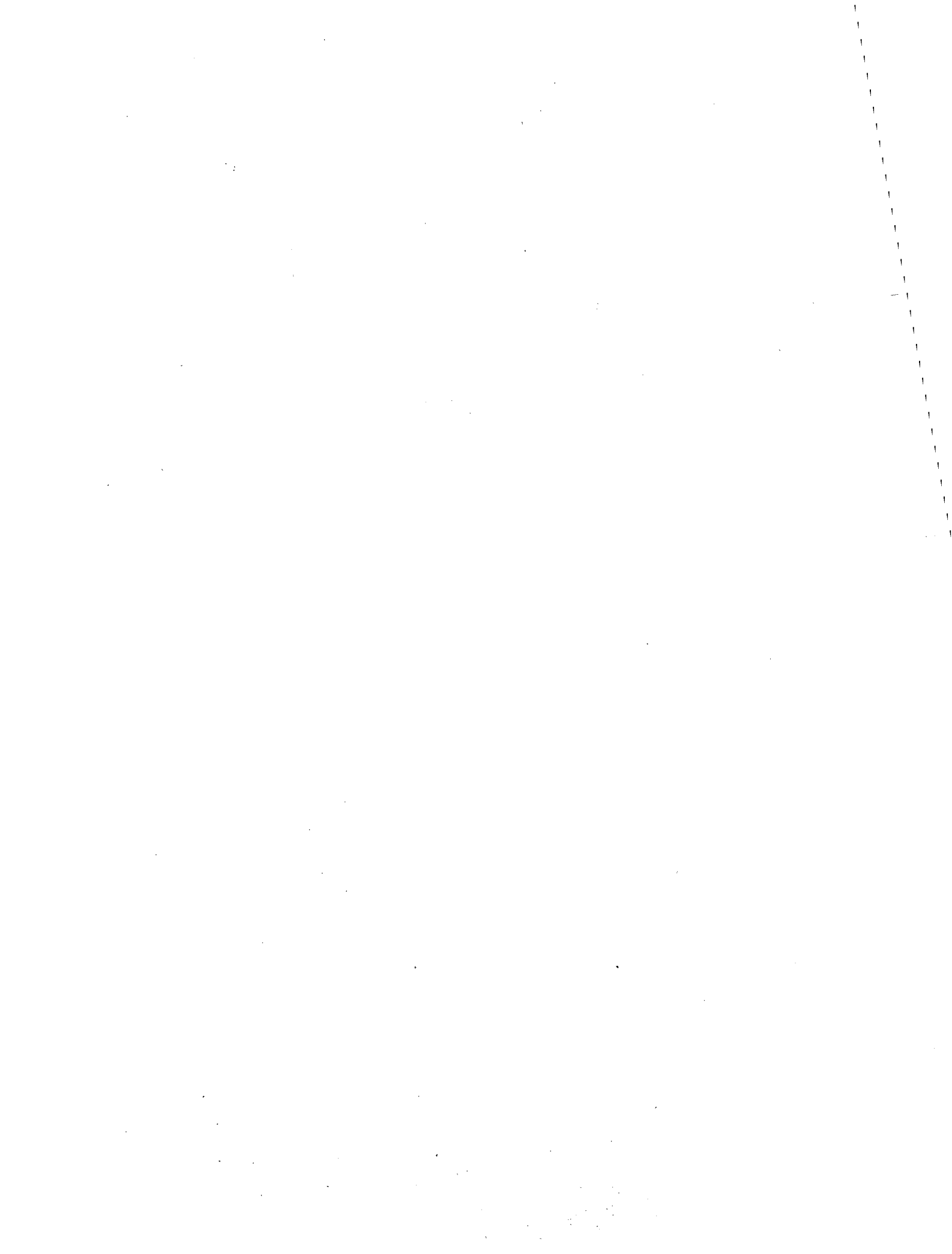
# UNCLASSIFIED

## 20. ABSTRACT (Continued)

0.4 to 1.3 for angles of attack up to 42 deg and Reynolds numbers from 0.2 to  $1.0 \times 10^6$  based on the centerbody maximum diameter. All configurations tested were statically and dynamically stable. The ISRe configurations had a greater static stability margin than the FF configurations. Use of the slotted fin reduced the static stability margin of the FF configurations but had no significant effect on the ISRe configurations. The slotted fin had little or no effect on the dynamic stability characteristics. Increasing fin tab angle generally caused an increase in dynamic stability for subsonic Mach numbers and a decrease for supersonic Mach numbers. The dynamic stability generally increased with increasing angle of attack.

## PREFACE

The work reported herein was conducted by the Arnold Engineering Development Center (AEDC), Air Force Systems Command (AFSC), for the Air Force Armament Laboratory (AFATL/DLJC) under Program Element 64602F, Project No. 5613-02. The AFATL project monitor was Mr. Paul D. Shirey. The results of the test were obtained by ARO, Inc. (a subsidiary of Sverdrup & Parcel and Associates, Inc.), contract operator of AEDC, AFSC, Arnold Air Force Station, Tennessee. The work was done under ARO Project No. P41C-86A. The authors of this report were C. F. Anderson and W. E. Carleton, ARO, Inc. The data analysis was completed on July 24, 1975, and the manuscript (ARO Control No. ARO-PWT-TR-75-140) was submitted for publication on September 11, 1975.



## CONTENTS

	<u>Page</u>
1.0 INTRODUCTION . . . . .	5
2.0 APPARATUS	
2.1 Test Facility and Model Support System . . . . .	5
2.2 Models . . . . .	5
2.3 Instrumentation . . . . .	7
3.0 TEST PROCEDURES	
3.1 Test Description . . . . .	8
3.2 Precision of Measurements . . . . .	9
4.0 RESULTS	
4.1 Static Stability Tests . . . . .	10
4.2 Pitch-Damping Tests . . . . .	11
5.0 SUMMARY OF RESULTS . . . . .	12
REFERENCES . . . . .	13

## ILLUSTRATIONS

### Figure

1. Schematic of Model Installation . . . . .	15
2. Photographs of Model Installation . . . . .	17
3. Static Stability Model Details . . . . .	20
4. Pitch-Damping Model Details . . . . .	22
5. Schematic of the 1,200-lb Pitch-Damping Balance . . . . .	25
6. Schematic of the Forced-Oscillation Balance Control and Electromechanical Data Acquisition Instrumentation . . . . .	26
7. Schematic of the Electronic Resolver Data Acquisition Instrumentation . . . . .	27
8. Nominal Variation of Reynolds Number and Dynamic Pressure with Mach Number for Static Stability Test . . . . .	28
9. Variation of Reynolds Number and Reduced Frequency with Mach Number for Pitch-Damping Test . . . . .	29
10. Static Stability Characteristics of Configurations FFW1 and FFSW1 with $\phi_m = -22.5$ . . . . .	30
11. Static Stability Characteristics of Configurations ISReW1 and ISReSW1 with $\phi_m = -22.5$ . . . . .	37
12. Effects of Roll Angle on the Static Stability Characteristics of Configuration FFSW1 . . . . .	44
13. Effects of Roll Angle on the Static Stability Characteristics of Configuration ISReW1 . . . . .	51

<u>Figure</u>	<u>Page</u>
14. Effects of Fin Spin Wedge Angle on the Static Stability Characteristics of the FF Configuration . . . . .	58
15. Effects of Fin Spin Wedge Angle on the Static Stability Characteristics of the ISRe Configuration, $\phi_m = -22.5$ . . . . .	65
16. Effects of High Angles of Attack on the Static Stability Characteristics of Configuration FFSW1 with $\phi_m = 45$ . . . . .	72
17. Variation of $C_{m_q} + C_{m_{\dot{\alpha}}}$ and $C_{m_{\alpha}}$ with Angle of Attack . . . . .	79
18. Variation of $C_{m_q} + C_{m_{\dot{\alpha}}}$ and $C_{m_{\alpha}}$ with Mach Number at Zero Angle of Attack . . . . .	86
 NOMENCLATURE . . . . .	 88

## 1.0 INTRODUCTION

An investigation to evaluate the static stability, pitch-damping, and magnus characteristics of two candidate concepts for an MK-82 store replacement at transonic speeds was conducted in the Aerodynamic Wind Tunnel (4T) of the Propulsion Wind Tunnel Facility (PWT). Static stability, pitch-damping, and magnus data were obtained at Mach numbers from 0.4 to 1.3 at a constant total pressure of 1,200 psfa. The Reynolds number range, based on centerbody maximum diameter, was from  $2.1 \times 10^5$  to  $3.8 \times 10^5$  for the static stability tests and from  $5.5 \times 10^5$  to  $1.0 \times 10^6$  for the pitch-damping and magnus tests. Both configurations were designed for air inflatable retardation devices that can be deployed for low altitude delivery; however, the purpose of this series of tests was to evaluate the high-speed aerodynamic characteristics of the stores, and the retarders were not installed. This report presents the results of the static stability and pitch-damping tests. The results of the magnus tests are presented in Ref. 1.

## 2.0 APPARATUS

### 2.1 TEST FACILITY AND MODEL SUPPORT SYSTEM

Tunnel 4T is a continuous flow, closed-loop, variable density wind tunnel equipped with a sonic nozzle. The normal Mach number range is from 0.1 to 1.3; however, removable nozzle blocks can be installed to provide Mach numbers of 1.6 and 2.0. The stagnation pressure can be varied from 300 to 3,700 psfa. The test section is 4 ft square and 12.5 ft long with variable porosity perforated walls (0.5- to 10-percent open). A detailed description of the tunnel and its capabilities may be found in Ref. 2.

The model support system consists of a pitch sector, boom, and sting which provide a pitch capability from -11 to 28 deg with respect to the tunnel centerline. The pitch center is located at tunnel station 108. The model support system also has a remote-controlled roll system that allows the model to be rolled  $\pm 180$  deg. An adjustable offset adaptor was used in the static stability test in order to permit testing at angles of attack up to 42 deg.

Schematics of the test section showing the model locations are presented in Fig. 1, and model installation photographs are presented in Fig. 2.

### 2.2 MODELS

Two proposed configurations of an MK-82 store replacement were tested. The Fixed-Fin (FF) models had four fins attached to a cylindrical afterbody, while the Inflatable Stabilizer Retarder (ISRe) model had eight fins attached to a conic afterbody. The conic

afterbody of the full-scale ISRe configuration initially is folded down to give a cylindrical afterbody and inflates when released from an aircraft. The ISRe model was a simulation of the conic afterbody in the inflated position. The air inflatable, high drag, retardation device used for low altitude delivery was not installed for the current series of tests. Both the FF and ISRe configurations use spin wedges on the fins to induce rotation during free flight.

### 2.2.1 Static Stability Models

Details of the 0.20-scale static stability models are shown in Fig. 3. The nose and centerbody of the FF and ISRe configurations were identical, and interchangeable afterbody sections with solid and slotted fins were used. Also, spin wedges with 15- and 25-deg included angle could be attached to each fin.

### 2.2.2 Pitch-Damping Models

Details of the 0.442-scale models of the FF and ISRe configurations are shown in Fig. 4. The ogive nose and centerbody portion aft to the cylindrical section were common to both configurations. Solid and slotted fins along with 15- and 25-deg fin spin wedges were the configuration variables for the two different tail sections as shown in Fig. 4. The models contained provisions for mounting the tail fins at different roll orientations as shown in the figure and for adjusting the model center of gravity to the balance pivot. A photograph showing the tail section of the ISRe model is presented in Fig. 4.

Special effort was afforded the design and fabrication of these models to obtain a model pitch resonant frequency and a model support sting resonant frequency such that the ratio of the model frequency to the sting frequency would be less than 0.50. This was done to avoid any complications that could occur, in controlling the balance drive system and in correcting the data, because of excessive coupling between frequencies. The model resonant frequency is a function of (balance spring plus aerodynamic restoring spring)/(model mass moment of inertia) and the sting resonant frequency is a function of the (sting stiffness)/(mass of sting plus mass of model). A relatively limber support sting had to be used because of the small internal diameter of the model at the model base and the long length from the balance pivot to the model base for the FF configuration. The models were constructed of aluminum for minimum model mass, and the minimum balance restoring spring was used which resulted in the following:

	FF	FFS	ISRe	ISReS
I	0.427 to 0.436	0.420 to 0.428	0.460 to 0.474	0.453 to 0.468
$\omega_s$	115.5		112.5	
$\omega_m/\omega_s$	0.371 to 0.417		0.356 to 0.475	

The ranges indicated for  $I$  and  $\omega_m/\omega_s$  correspond to the values obtained for different fin spin wedge configurations.

## 2.3 INSTRUMENTATION

### 2.3.1 Static Stability Instrumentation

Static forces and moments were measured with a six-component, internal, strain-gage balance. Model base static pressures were measured with two differential pressure transducers. The base pressure was defined as the average of two pressures measured above and below the sting in the plane of the model base. The model angle of attack and roll angle were measured with the pitch sector angle-of-attack and roll indicators and corrected for sting and balance deflections resulting from aerodynamic forces and moments on the model. Electrical signals from the balance, pressure transducers, and tunnel instrumentation were processed by the PWT data acquisition system and digital computer for online data reduction. Balance outputs were recorded on an oscillograph for monitoring of model dynamics.

### 2.3.2 Dynamic Balance and Instrumentation

A schematic of the 1,200-lb pitch-derivative, forced-oscillation balance is shown in Fig. 5. The balance consists of a cross-flexure pivot connected to a hydraulic cylinder through a force-measuring flexure. The hydraulic cylinder is operated with a servo-valve to obtain sinusoidal oscillatory motion at constant oscillation amplitude, up to  $\pm 3$  deg, and constant frequency, from 2 to 30 Hz. The cross flexure is instrumented to measure rotational displacement and supports the model loads (up to 1,200-lb normal force and 600-lb axial force) and provides the restoring moment (758 ft-lb/radian) to cancel the inertia moment when the system is operating at the natural frequency. The balance has provisions for changing the restoring moment by installing leaf springs on the sides of the balance as shown in the figure.

A schematic of the forced-oscillation balance control and electromechanical data acquisition instrumentation and a schematic of the electronic resolver data acquisition instrumentation are presented in Figs. 6 and 7, respectively.

The balance control instrumentation, Fig. 6, provides a system for varying oscillation frequency and oscillation amplitude, within the cross-flexure limits, and a torque nulling system. The latter centers the balance servovalve-controlled, hydraulic-driven piston so that the force-measuring flexure is not subjected to the model static aerodynamic moment. This allows the use of a force-measuring flexure suitable to the particular range of damping moments expected for a particular model. An electronic position feedback loop is used

to maintain a constant oscillation amplitude under aerodynamic loads and permits testing dynamically stable and unstable configurations.

Data are normally obtained at the natural frequency of the model flexure system; however, the data acquisition instrumentation provides the measurement of the in-phase and quadrature components for off-resonant conditions. The electromechanical data acquisition process, Fig. 6, corresponds to an integration of the strain-gage signal over an integral number of cycles. The integration interval may be varied from about 0.5 to 8 sec. The electronic resolver data acquisition system, Fig. 7, is used as a backup system for balance data and is used to measure sting dynamic moment components. This system uses a 5-Hz bandpass, tracking filter to separate out any extraneous excitations superimposed on the fundamental output waveform of the strain-gage signal.

The digital readouts of the data acquisition instrumentation are input to the tunnel scanner and sent to the computer for reduction data to the final aerodynamic coefficients.

### 3.0 TEST PROCEDURES

#### 3.1 TEST DESCRIPTION

##### 3.1.1 Static Stability Tests

Steady-state force and moment data were obtained at Mach numbers from 0.4 to 1.3. The angle-of-attack range was from 0 to 27 deg for most configurations; however, an offset adaptor was used to extend the maximum angle of attack to 42 deg for one configuration. The maximum angle of attack was limited to 18 deg at the beginning of the test by high dynamics in the yaw plane. The balance and support sting were replaced with a stiffer balance and support sting, and no further dynamic problems were encountered at any angle of attack. Data were obtained at roll angles of -22.5, 0, and 45 deg. The remote-controlled roll mechanism in the sting support was used to set roll angles when the offset adaptor was set at zero deflection angle. When the offset adaptor was set at 15 deg, the fins and afterbody were rotated on the model to vary roll angle; however, in this case, incremental roll angles were limited to 45 deg because of the location of the afterbody attachment screws.

The total pressure was held constant at 1,200 psf, and the nominal variation of Reynolds number and dynamic pressure with Mach number is shown in Fig. 8. The models were tested with free transition throughout the test program.

The data were reduced to coefficient form in the aeroballistic axis system with the moment reference 3.866 calibers from the nose of the FF model and 3.644 calibers from the nose of the ISRe model.

### 3.1.2 Pitch-Damping Test

The model was oscillated at an amplitude of  $\pm 1$  deg and at the natural frequency for each angle-of-attack setting, while a set tunnel Mach number and total pressure were maintained. The maximum angle of attack was determined by the static aerodynamic pitching moment that deflected the balance cross flexure to a static trim angle of approximately 1 and 2 deg, respectively, for the FF and ISRe models. Balance force and position measurements were obtained for a 50-cycle interval at each test point, and a minimum of three test points were obtained at each angle of attack. The data presented are averages of the test point values obtained at each angle of attack.

Data were obtained for Mach numbers 0.40 to 1.3 at a constant tunnel free-stream total pressure of 1,200 psfa. The variation of Reynolds number and reduced frequency,  $\omega d/2V_\infty$ , are presented in Fig. 9.

## 3.2 PRECISION OF MEASUREMENTS

### 3.2.1 Test Conditions

The estimated uncertainty for Mach number due to instrumentation errors and data acquisition techniques is  $\pm 0.003$ . The deviations from the mean value of Mach number based on the tunnel empty centerline calibration are  $\pm 0.005$  for Mach numbers up to 1.05,  $\pm 0.010$  for Mach number 1.2, and  $\pm 0.015$  for Mach number 1.3. The uncertainty in  $q_\infty$  is  $\pm 1.1$  psf for  $M_\infty \leq 0.8$  and  $\pm 0.8$  psf for  $M_\infty > 0.8$ . The uncertainties in angle of attack and roll angle are  $\pm 0.1$  deg and  $\pm 0.85$  deg, respectively.

### 3.2.2 Static Stability Tests

The estimated uncertainties associated with the measured coefficients are as follows:

	<u><math>M_\infty = 0.4</math></u>	<u><math>M_\infty = 0.8</math></u>	<u><math>M_\infty = 1.0</math></u>	<u><math>M_\infty = 1.3</math></u>
$\Delta C_N$	$\pm 0.081$	$\pm 0.028$	$\pm 0.022$	$\pm 0.019$
$\Delta C_A$	$\pm 0.050$	$\pm 0.017$	$\pm 0.014$	$\pm 0.012$
$\Delta C_Y$	$\pm 0.049$	$\pm 0.017$	$\pm 0.013$	$\pm 0.012$
$\Delta C_\ell$	$\pm 0.044$	$\pm 0.015$	$\pm 0.012$	$\pm 0.010$
$\Delta C_m$	$\pm 0.124$	$\pm 0.043$	$\pm 0.033$	$\pm 0.029$
$\Delta C_n$	$\pm 0.081$	$\pm 0.028$	$\pm 0.022$	$\pm 0.019$

### 3.2.3 Pitch-Damping Tests

The estimated uncertainties are as follows:

$$\begin{aligned}
 C_{m_\alpha} & \quad \pm 0.50/\text{radian for } M_\infty = 0.4 \\
 & \quad \pm 0.17/\text{radian for } M_\infty = 0.8 \text{ to } 1.0 \\
 & \quad \pm 0.11/\text{radian for } M_\infty = 1.1 \text{ to } 1.3 \\
 \\
 C_{m_q} + C_{m_{\dot{\alpha}}} & \quad \pm 15/\text{radian for } M_\infty = 0.4 \\
 & \quad \pm 10/\text{radian for } M_\infty = 0.8 \text{ to } 1.3
 \end{aligned}$$

Uncertainties quoted for  $C_{m_\alpha}$  and  $C_{m_q} + C_{m_{\dot{\alpha}}}$  are based on a 95-percent confidence level and include probable inaccuracies in the balance calibration constants, instrumentation measurements, and setting and measuring tunnel flow parameters. Data scatter resulting from support sting and sector vibration and/or unsteady flow conditions in the tunnel test section acting on the model and balance cannot be accounted for in the estimated uncertainties. However, a minimum of three data points were taken at each test condition, and the uncertainties of the average of these points probably fall within the uncertainties quoted for the coefficients.

## 4.0 RESULTS

### 4.1 STATIC STABILITY TESTS

The effects of fin slots on the static stability characteristics of the FF and ISRe configurations with 15-deg fin spin wedges installed are presented in Figs. 10 and 11. These data were obtained at a model roll angle of -22.5 deg. Adding slots to the FF configuration generally decreased  $C_N$ , and shifted  $X_{cp}$  forward, but had little effect on  $C_{A,F}$ . Increasing the angle of attack of the FF model produced significant variations of  $C_Y$ ,  $C_n$ , and  $C_\ell$  as might be expected for a roll angle of -22.5 deg. Adding slots generally decreased the variations in  $C_Y$  and  $C_n$  but increased the variations in  $C_\ell$  with angle of attack. However, at Mach numbers 0.8 and 0.9, and  $\alpha > 24$  deg,  $C_\ell$  was reduced by adding slots to the FF configuration. Adding slots to the ISRe configuration (Fig. 11) produced only small changes in the static stability coefficients.

The effects of roll angle on the static stability characteristics of the FF and ISRe configurations with 15-deg fin spin wedges and no fin slots are presented in Figs. 12 and 13. Variation of roll angle with the FF configuration produced large variations in  $C_Y$ ,  $C_n$ ,  $C_\ell$ , and  $X_{cp}$  for angles of attack above 4 deg. The static stability characteristics of the ISRe configuration were relatively insensitive to roll angle except for angles of attack above 20 deg where some variation of  $C_Y$ ,  $C_n$ , and  $C_\ell$  was observed.

The effect of fin spin wedge angle on the static stability characteristics of the FF and ISRe configurations without fin slots are presented in Figs. 14 and 15. The data presented for the FF configuration with fin spin wedge angles of 15 and 25 deg and

all ISRe data were obtained at a roll angle of -22.5 deg. No data were obtained for the FF configuration without fin spin wedges at this roll angle. Therefore, data obtained at  $\phi_m = 0$  with no fin spin wedges and with 15-deg fin spin wedges are presented with solid symbols.

Adding fin spin wedges had little effect on the aerodynamic coefficients for the FF configuration except to increase  $C_{\ell}$  and, at zero roll angle, shift the center of pressure forward. Adding fin spin wedges to the ISRe configuration produced small changes in  $C_Y$  and  $C_n$  and gave a significant increase in  $C_{A,F}$  as well as increasing  $C_{\ell}$ .

The FFSW1 configuration was tested at angles of attack up to 42 deg to determine if the forward shift of the center of pressure with angle of attack would cause the model to become longitudinally unstable. The sting roll angle was set at zero and the tail installed at 45-deg roll angle for the high angle-of-attack data. The results of this investigation are presented in Fig. 16. The maximum forward shift of  $X_{cp}$  occurs at  $M = 0.8$ ; however, the center of pressure never moves forward of the moment reference point, and the most forward  $X_{cp}$  is approximately the same at all Mach numbers.

Comparison of data obtained with the sting offset angle at 0 and 15 deg shows excellent agreement for  $C_N$  and  $C_A$ , some mismatch for  $C_{\ell}$  and  $X_{np}$  at  $M_{\infty} = 0.8$ , and a large difference in  $C_Y$  and  $C_n$  for angles of attack between 20 and 30 deg at all Mach numbers. Asymmetric vortex shedding can be triggered by small surface imperfections on the forebody and can generate large side forces and yawing moments in either direction. Rolling the complete model from 0 to 45 deg generated small side forces in opposite directions for angles of attack above 20 deg (Fig. 12). Therefore, it is conjectured that differences in the asymmetric vortex shedding induced by the different forebody roll angles was the most probable cause of the difference in aerodynamic coefficients observed in Fig. 16 for angles of attack above 20 deg.

## 4.2 PITCH-DAMPING TESTS

The variations of the pitch-damping derivative,  $C_{m_q} + C_{m_{\dot{\alpha}}}$ , and the pitch static stability parameter,  $C_{m_{\alpha}}$ , with angle of attack are presented in Fig. 17 for each configuration. The variations of  $C_{m_q} + C_{m_{\dot{\alpha}}}$  and  $C_{m_{\alpha}}$  with Mach number at zero angle of attack are presented in Fig. 18. In general, all configurations were dynamically and statically stable throughout the Mach number and angle-of-attack ranges at which the pitch-damping test was conducted.

The slotted fin, FFS and ISReS configurations, and fin orientation change of 22.5 deg, FFSW1 ( $\phi_m = 45$ ) and ISReW1 ( $\phi_m = -22.5$ ) configurations had little or no effect on the pitch-damping and static stability parameter characteristics compared to the basic

FF and ISRe configurations. Increasing fin spin wedge angle generally caused an increase in pitch damping for Mach numbers less than 0.9 and a decrease in pitch damping for Mach numbers above 0.9 at zero angle of attack. Pitch damping increased with increasing angle of attack except for the unexplainable instance where the FFSW1 ( $\phi_m = 22.5$ ) configuration exhibited the opposite trend at Mach numbers 1.2 and 1.3.

Increasing fin spin wedge angle had only small effects on  $C_{m_\alpha}$ . The values of  $C_{m_\alpha}$  from the static stability tests of the FFW1, FFSW1, and ISReW1 with  $\phi_m = -22.5$  and the ISReW1 with  $\phi_m = 0$  were calculated and are included in Fig. 18 for comparison purposes. The static and dynamic values of  $C_{m_\alpha}$  are in fairly good agreement for the FF and FFS configurations but exhibited significant differences for the ISRe configuration, especially at the higher Mach numbers. It should be noted that the tunnel blockage was approximately 0.5 and 1.75 percent, respectively, for the static and dynamic models. The latter value is considered to be in the range of possible wall interference effects for models of this type. Also, the large conical tail of the ISRe model was in the field of possible shock wave reflections from the tunnel walls. Moreover, some of the difference might be attributed to differences in Reynolds number between the static and dynamic tests (compare Figs. 8 and 9).

## 5.0 SUMMARY OF RESULTS

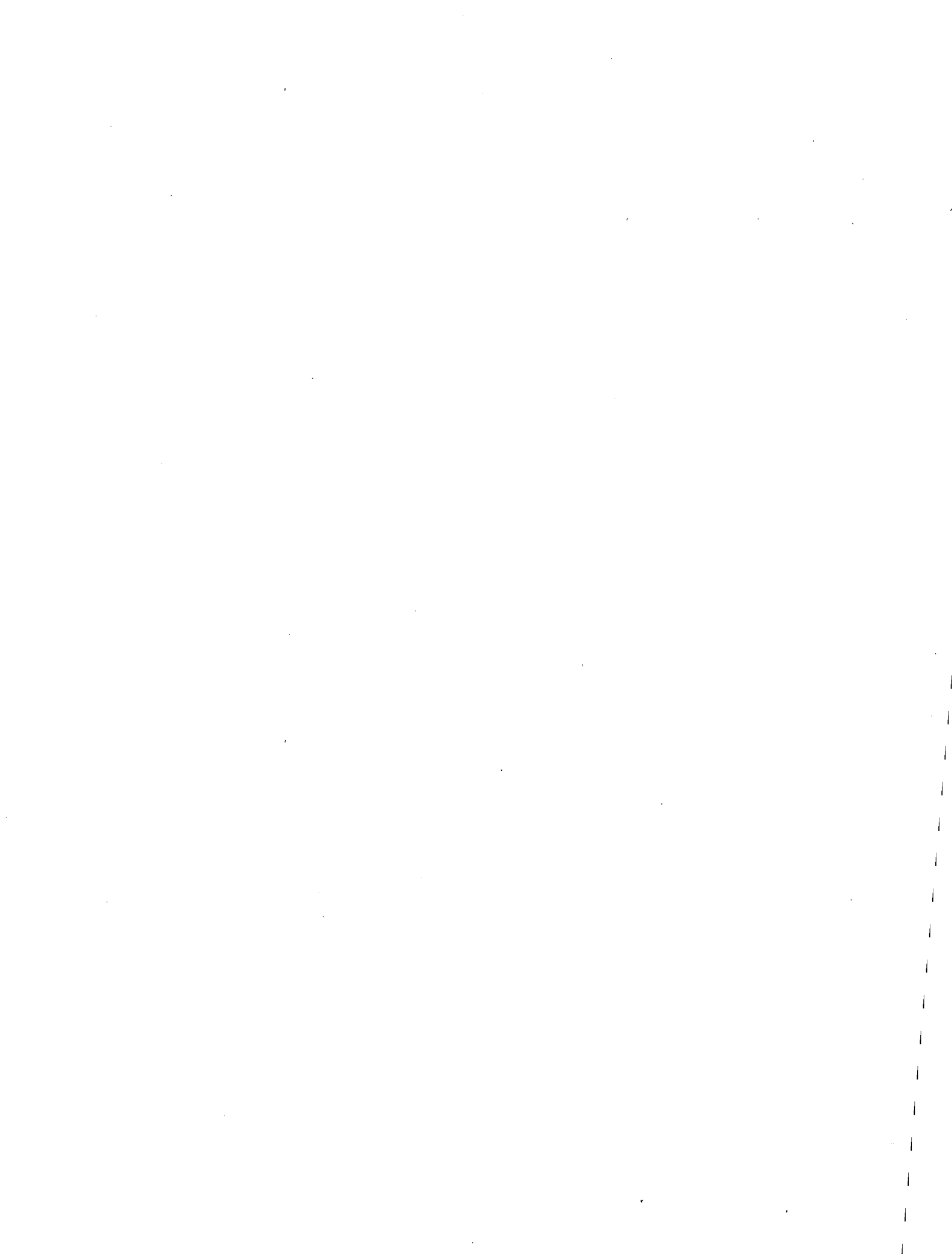
Static stability and pitch-damping tests were conducted for the FF and ISRe MK-82 store configurations. Results of the test are summarized as follows:

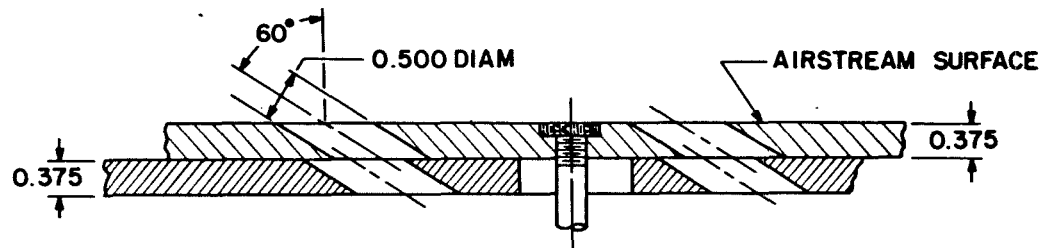
1. All configurations were statically and dynamically stable throughout the angle-of-attack and Mach number range. The inflatable stabilizer retarder configuration had a greater static stability margin than the fixed-fin configurations.
2. The fixed-fin configuration exhibited large variations in side force and yawing moment with model roll angle. The inflatable stabilizer retarder model had no significant variations in aerodynamic coefficients with roll angle.
3. Fin slots reduced the static stability margin of the fixed-fin configuration but had no significant effect on the inflatable stabilizer retarder configuration.
4. Fin slots and fin orientation had little or no effect on the pitch-damping characteristics.

5. Increasing fin spin wedge angle generally caused an increase in pitch damping for subsonic Mach numbers and a decrease for supersonic Mach numbers at zero angle of attack.

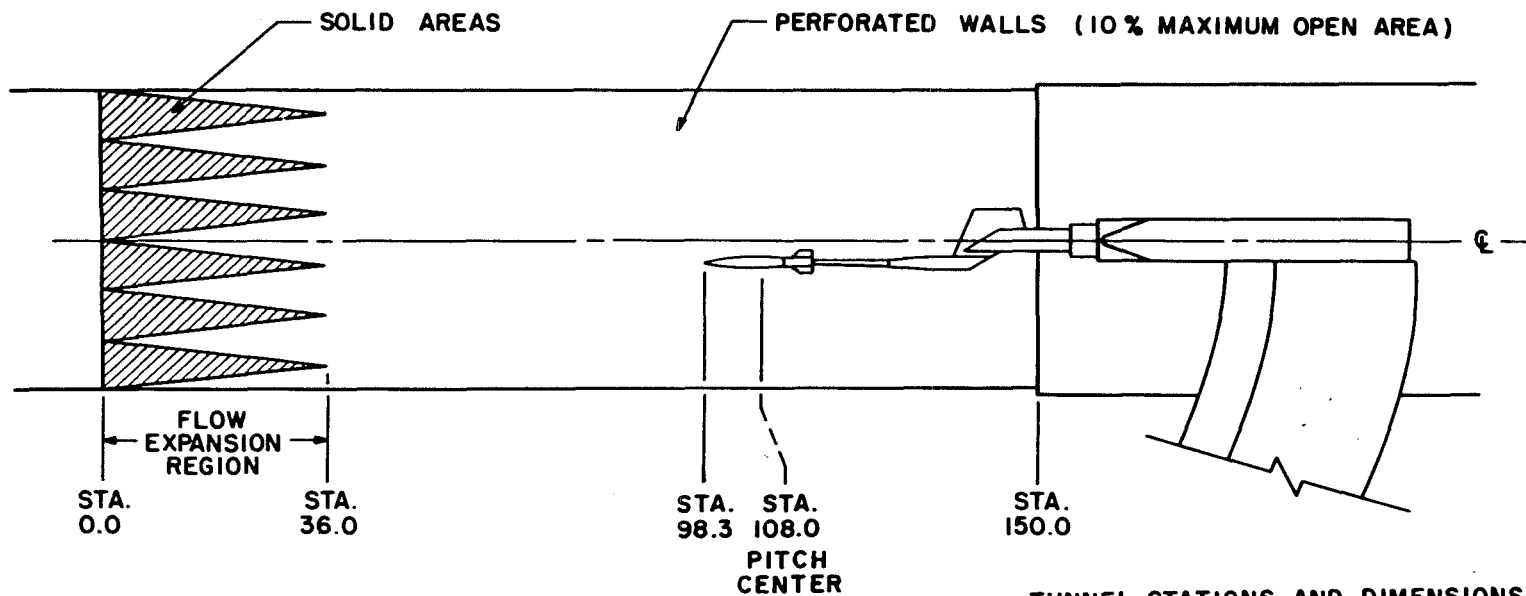
#### REFERENCES

1. Wallace, A. R. and Shadow, T. O. "Magnus and Roll-Damping Characteristics of the Fixed-Fin and Inflatable Stabilizer Retarder Configurations of the MK-82 Store at Transonic Speeds." AEDC-TR-75-163.
2. Test Facilities Handbook (Tenth Edition). "Propulsion Wind Tunnel Facility, Vol. 4." Arnold Engineering Development Center, May 1974.



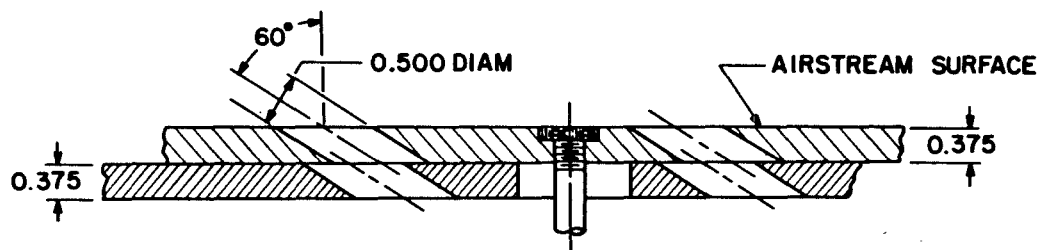


TYPICAL PERFORATED WALL CROSS SECTION

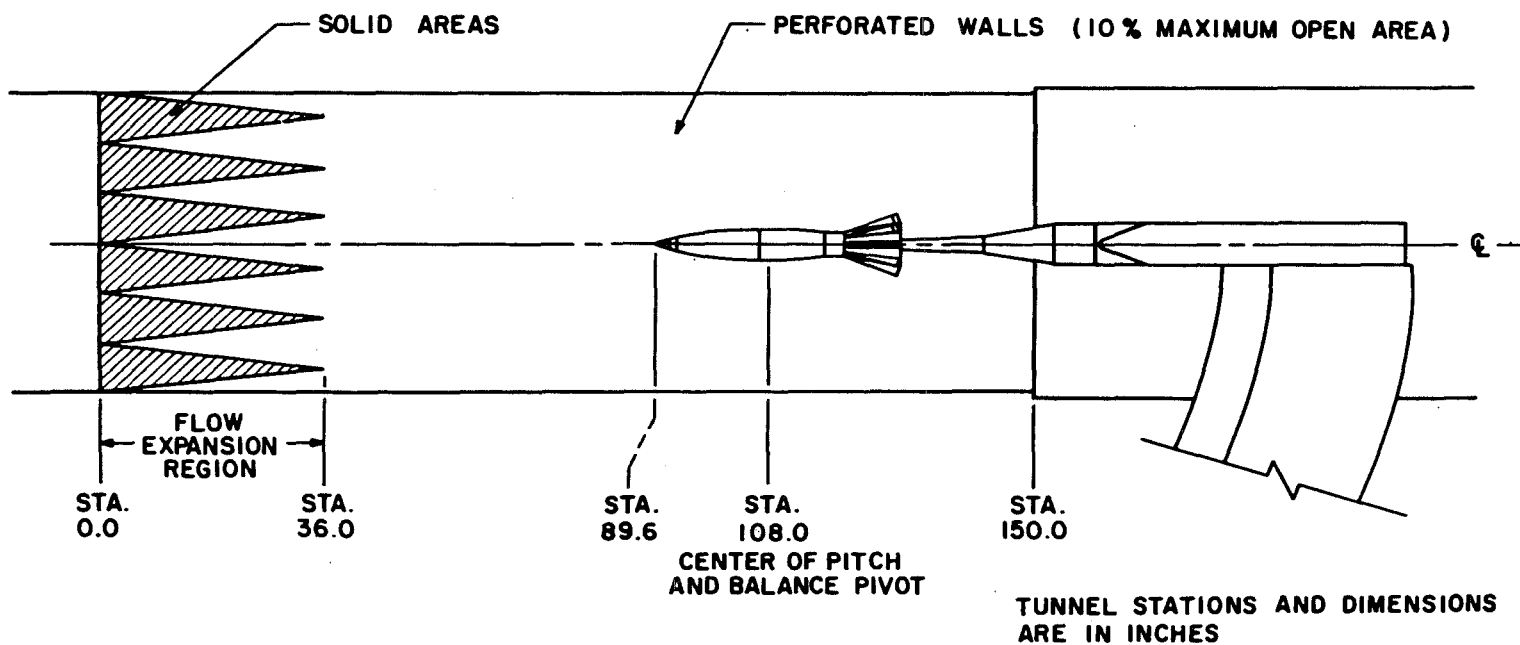


TUNNEL STATIONS AND DIMENSIONS ARE IN INCHES

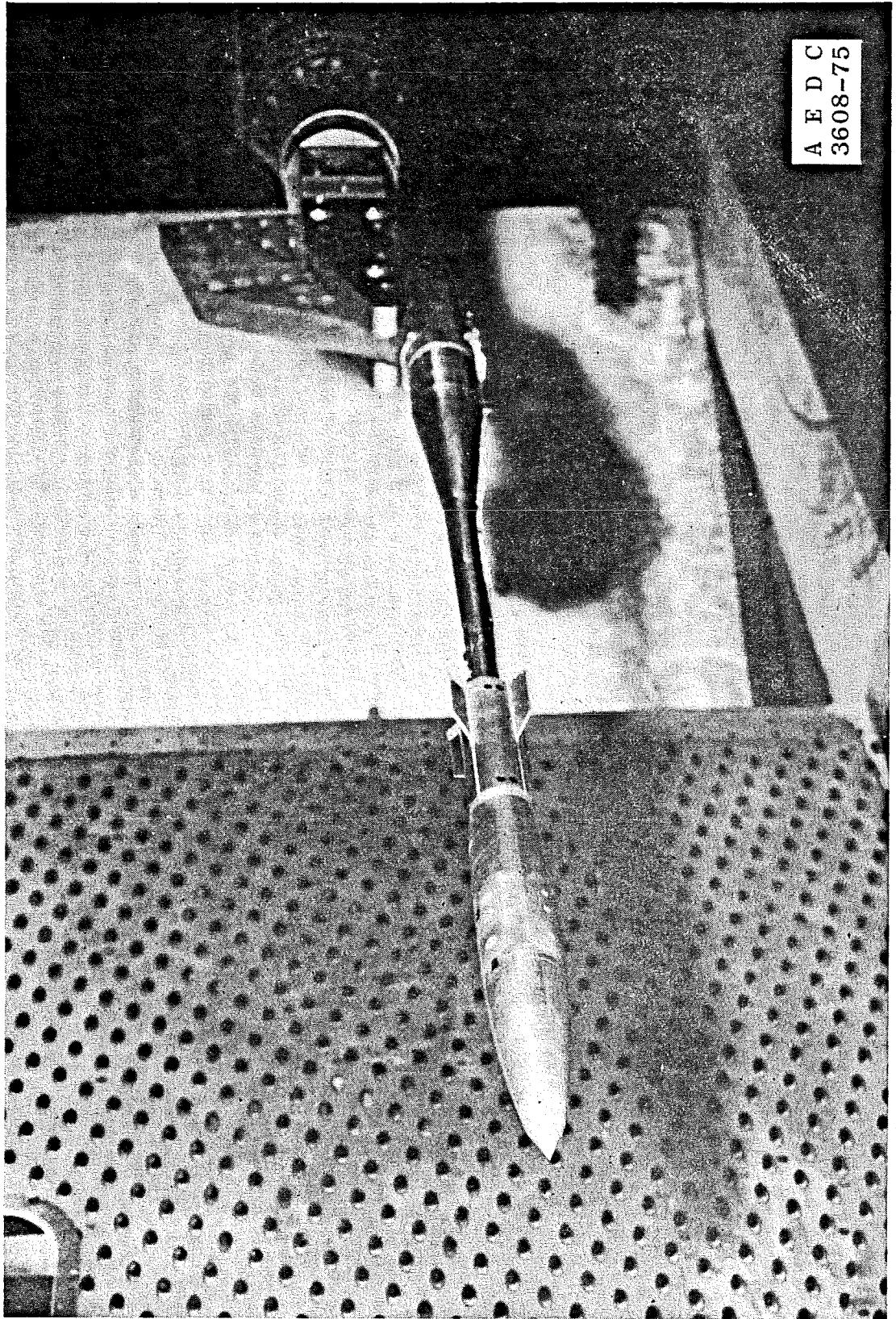
a. Static stability test  
Figure 1. Schematic of model installation.



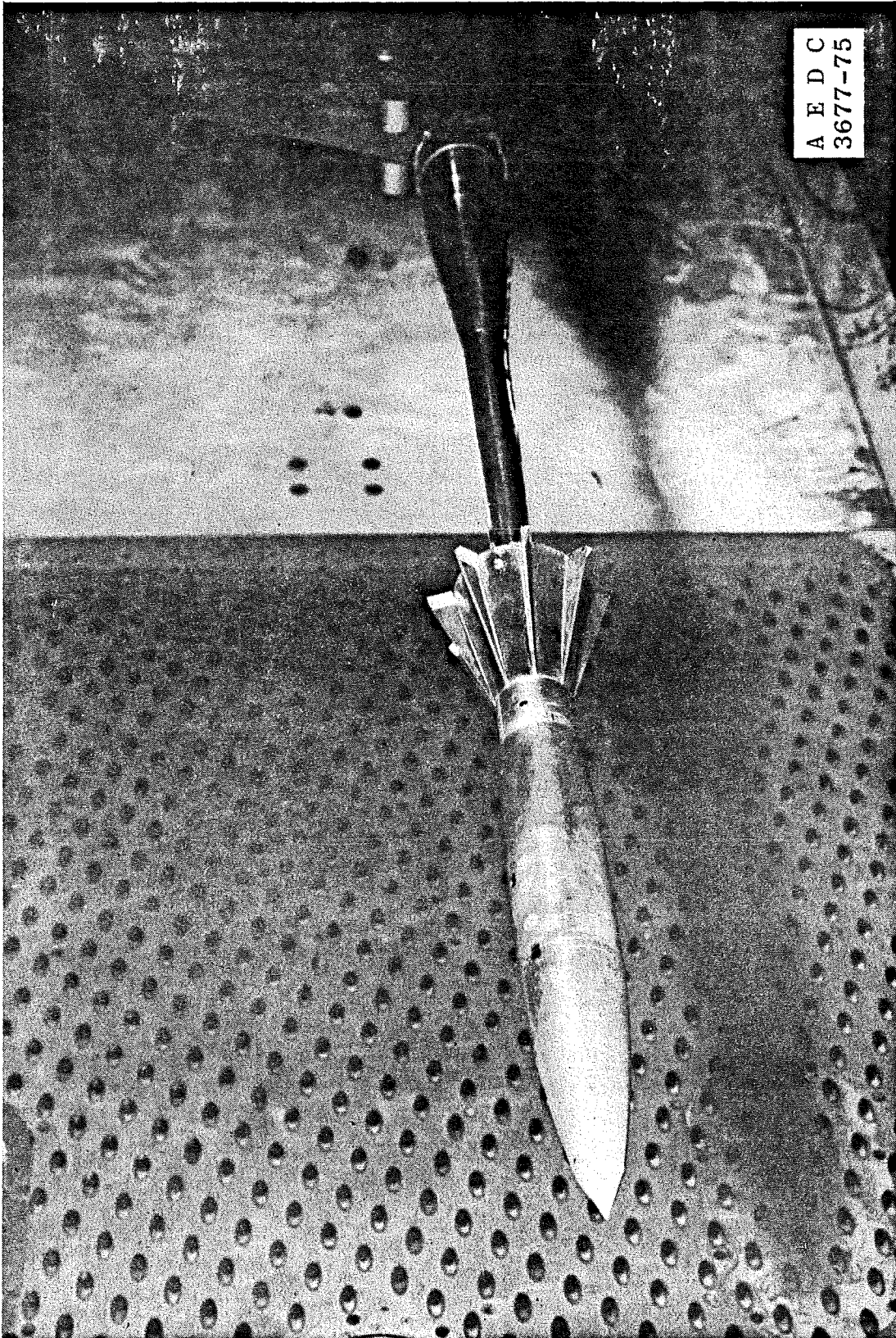
TYPICAL PERFORATED WALL CROSS SECTION



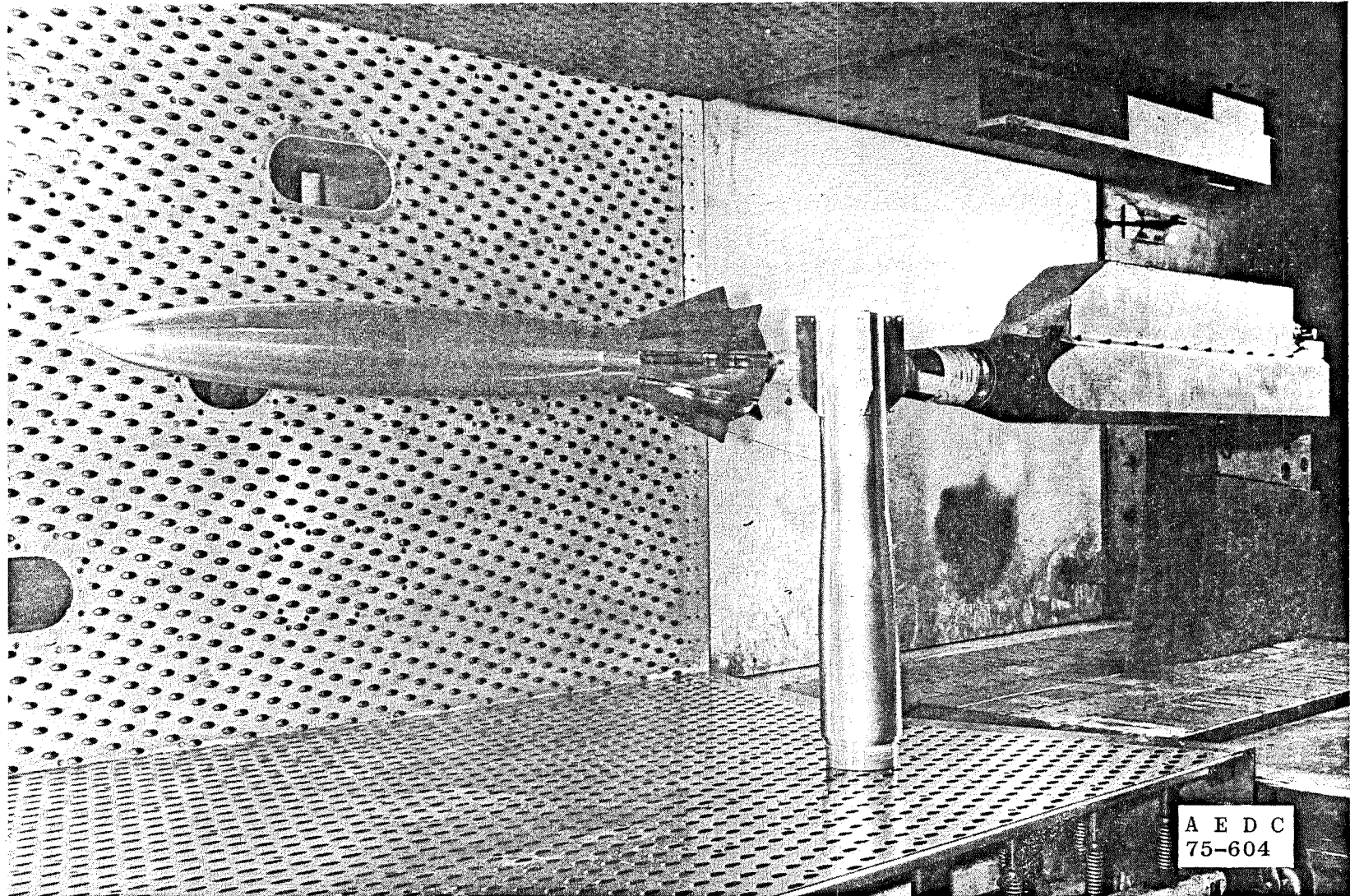
b. Pitch-damping test  
Figure 1. Concluded.



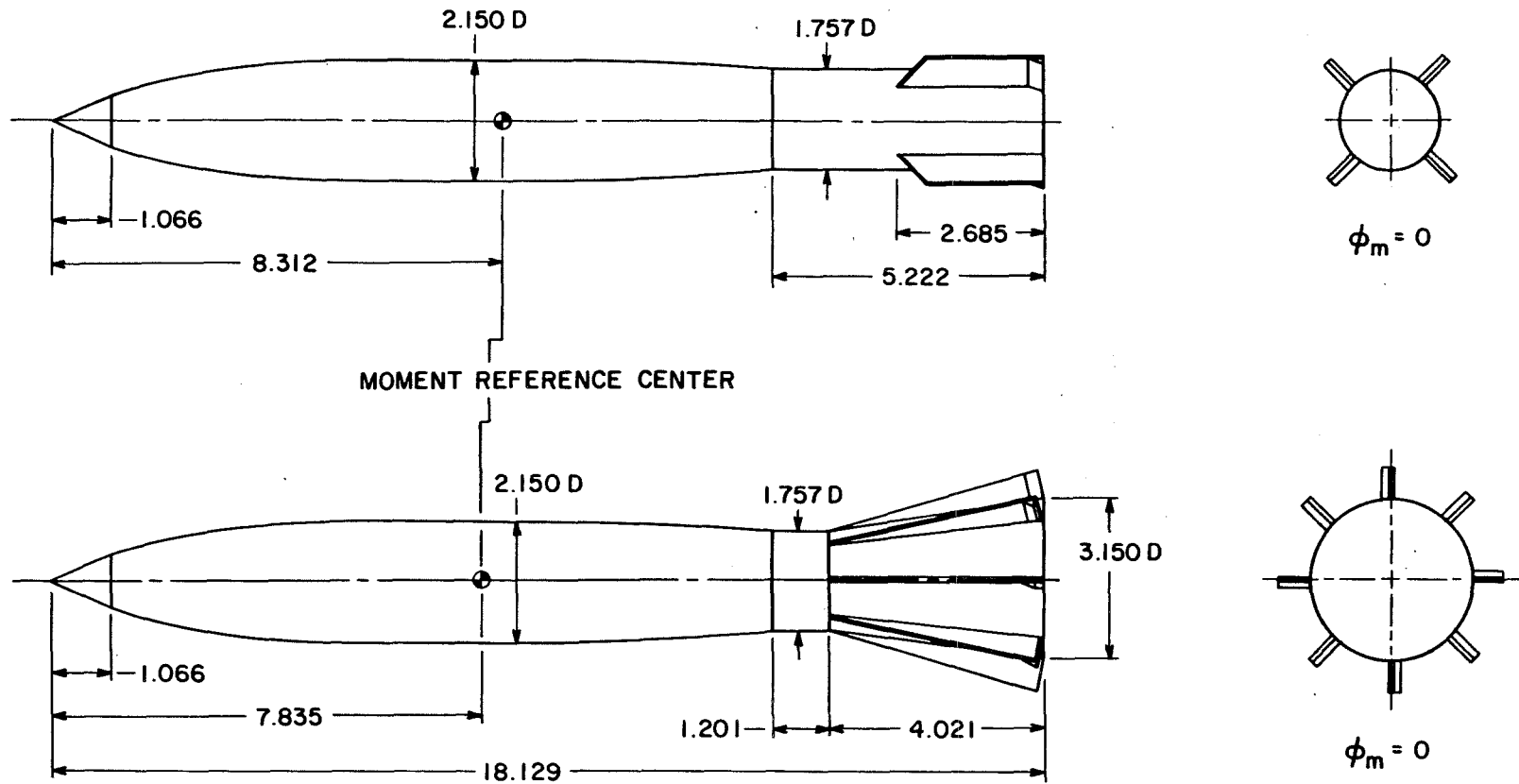
a. Fixed-fin static stability model  
Figure 2. Photographs of model installation.



b. Inflatable stabilizer retarder static stability model  
Figure 2. Continued.

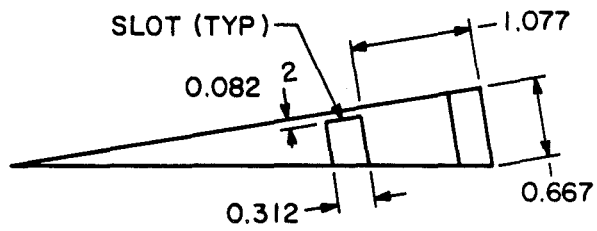
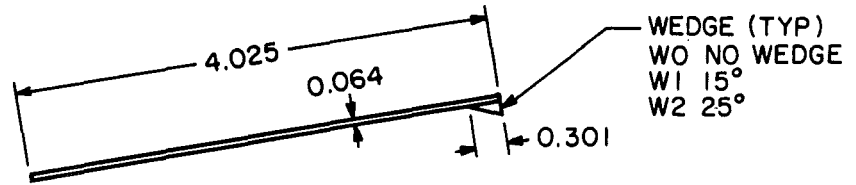


c. Pitch-damping models  
Figure 2. Concluded.

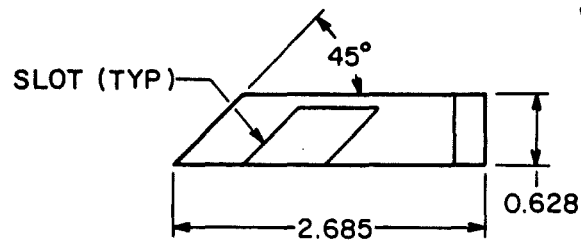
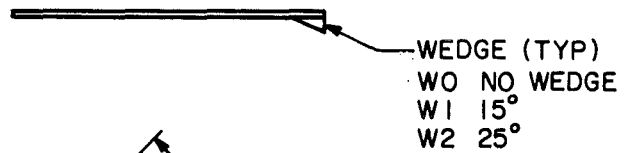


DIMENSIONS IN INCHES

a. Model dimensions  
 Figure 3. Static stability model details.



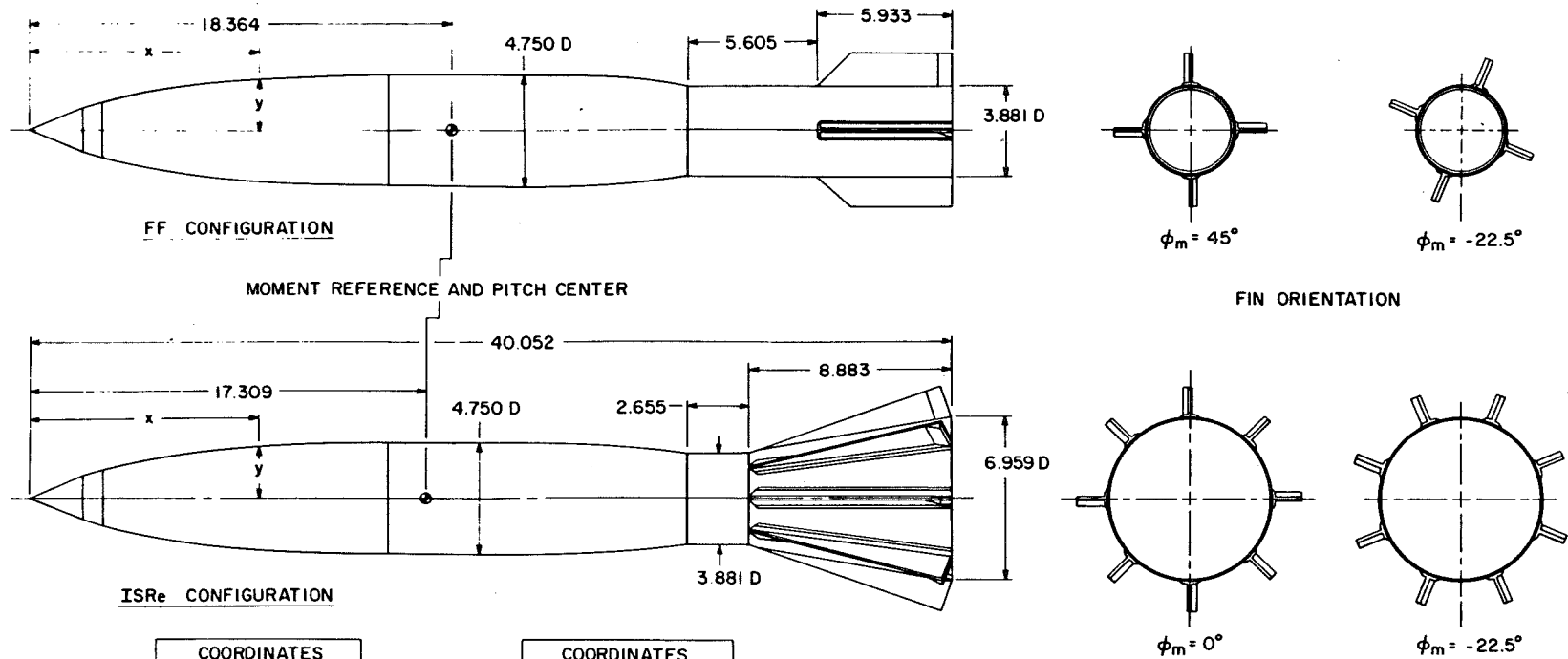
ISReS FIN



FFS FIN

DIMENSIONS IN INCHES

b. Fin dimensions and identification  
 Figure 3. Concluded.

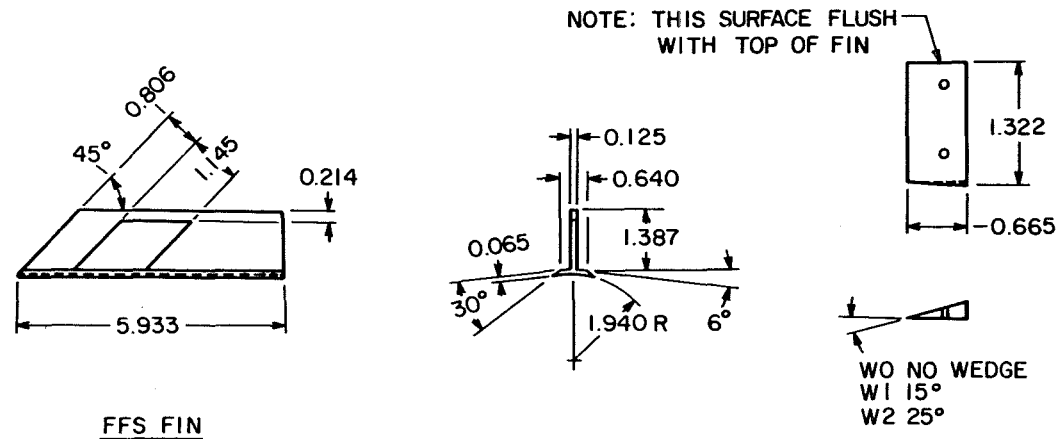
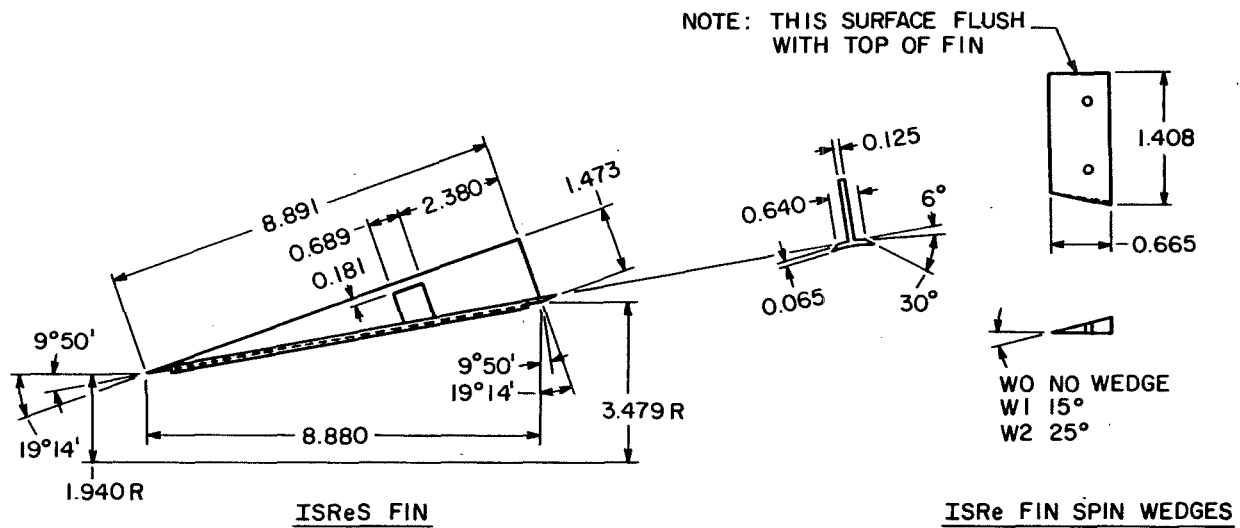


COORDINATES	
x	y
0.0000	0.0000
2.3560	1.0218
2.4273	1.0429
3.1493	1.2372
3.3345	1.2813
3.7858	1.3813
4.2370	1.4754
5.1443	1.6350
6.0468	1.7680
6.9540	1.8813
7.8565	1.9798
8.7638	2.0675
9.6663	2.1463
10.5735	2.2169
11.4760	2.2783

COORDINATES	
x	y
12.3833	2.3282
13.2858	2.3622
14.1930	2.3750
20.0735	2.3750
20.9760	2.3693
21.8833	2.3529
22.7858	2.3258
23.6930	2.2886
24.5955	2.2420
25.4980	2.1862
26.4053	2.1218
27.3078	2.0494
28.2150	1.9694
28.5143	1.9404

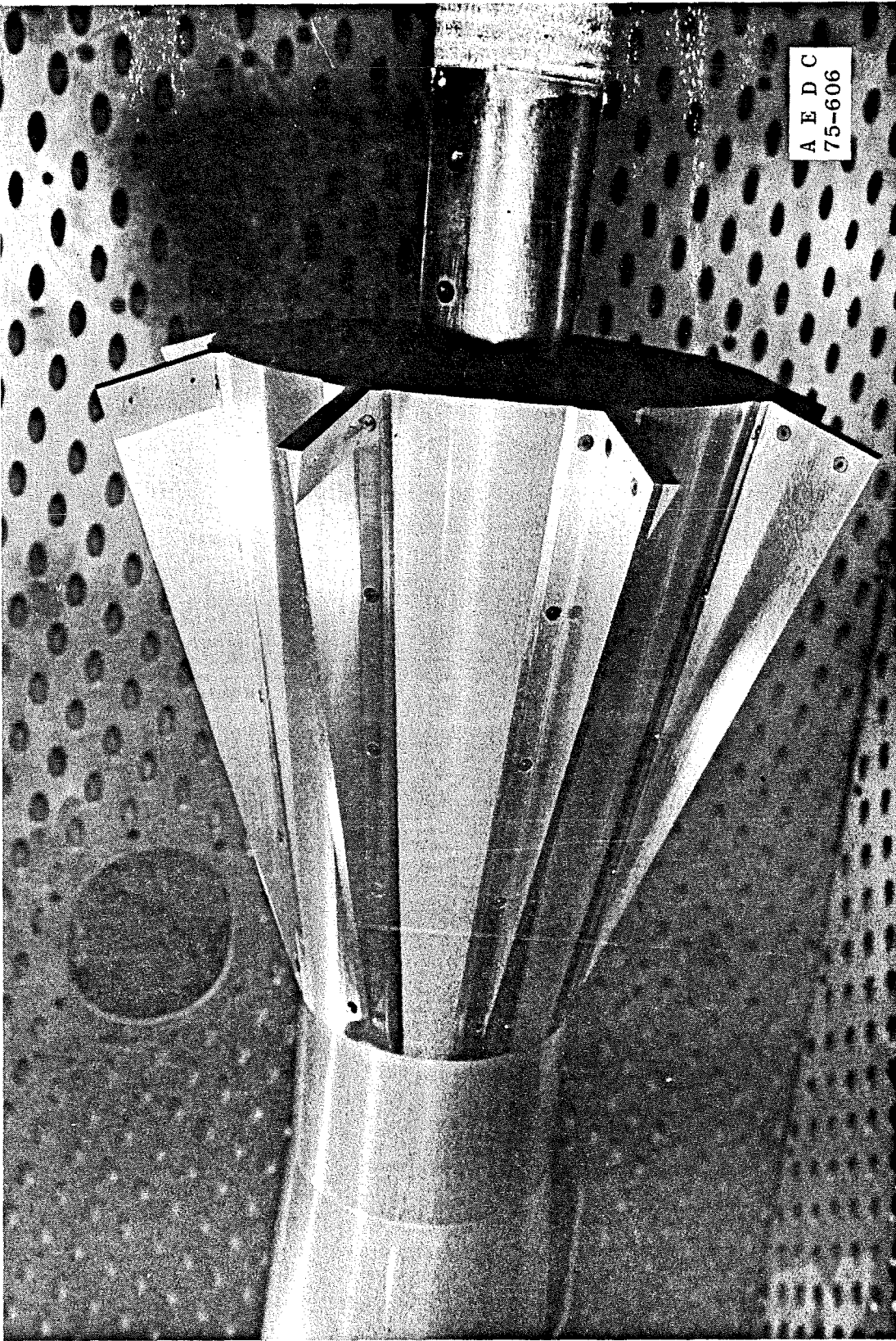
DIMENSIONS IN INCHES

a. Model dimensions and fin orientation  
Figure 4. Pitch-damping model details.



DIMENSIONS IN INCHES

b. Fin dimensions and identification  
Figure 4. Continued.



c. Photograph viewing tail of the ISReW1 configuration  
Figure 4. Concluded.

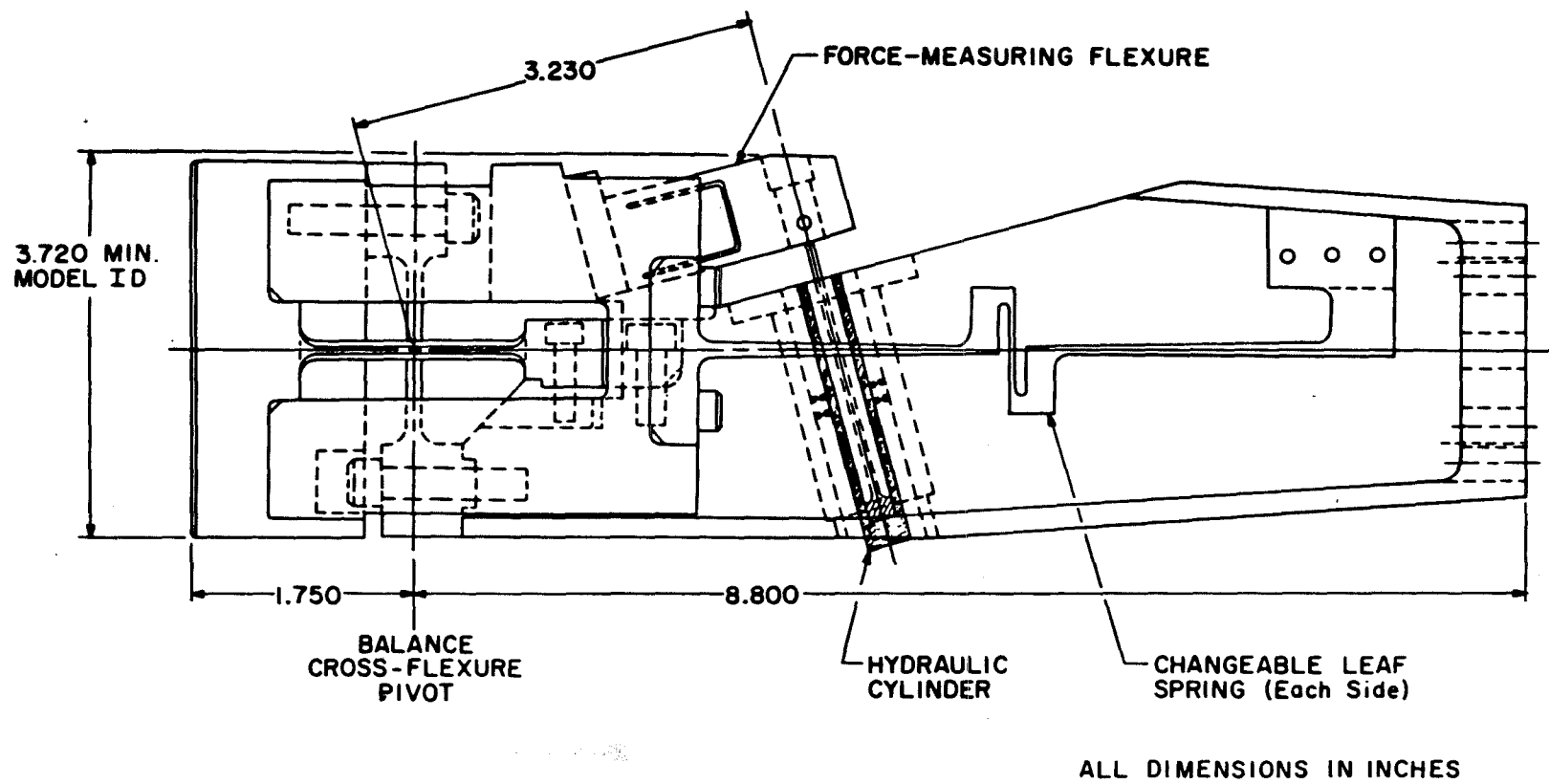
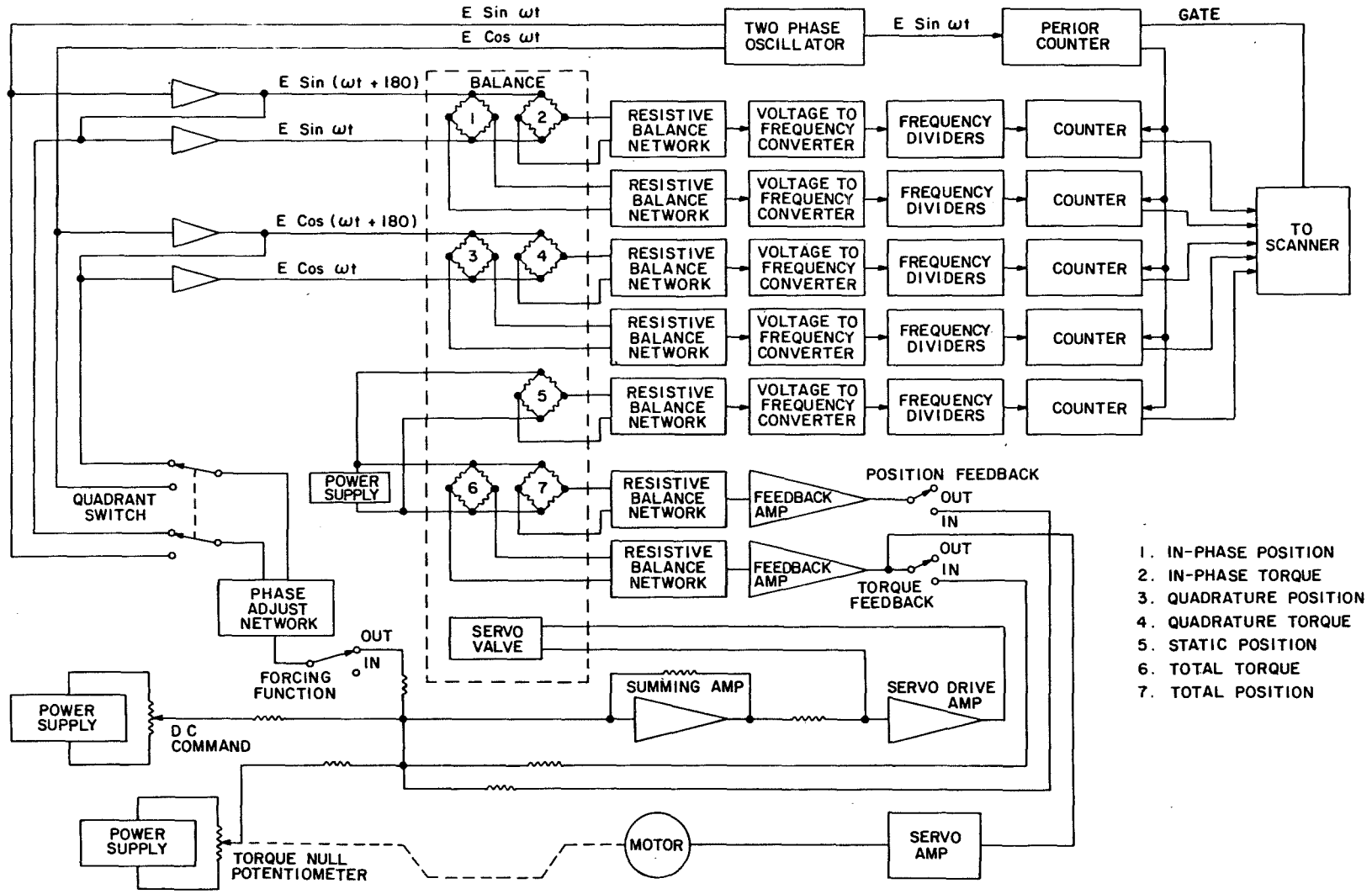
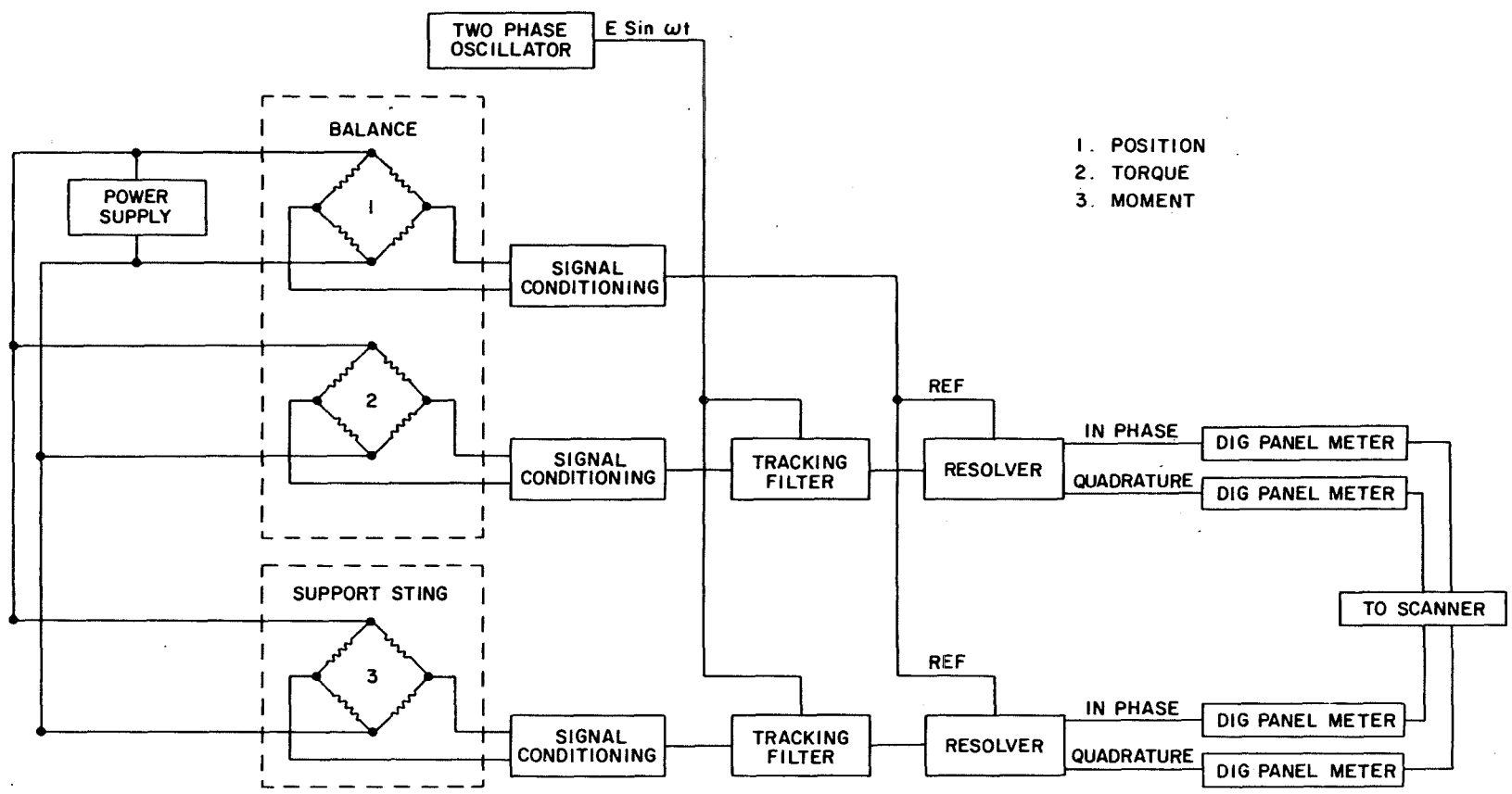


Figure 5. Schematic of the 1,200-lb pitch-damping balance.



1. IN-PHASE POSITION
2. IN-PHASE TORQUE
3. QUADRATURE POSITION
4. QUADRATURE TORQUE
5. STATIC POSITION
6. TOTAL TORQUE
7. TOTAL POSITION

Figure 6. Schematic of the forced-oscillation balance control and electromechanical data acquisition instrumentation.



- 1. POSITION
- 2. TORQUE
- 3. MOMENT

Figure 7. Schematic of the electronic resolver data acquisition instrumentation.

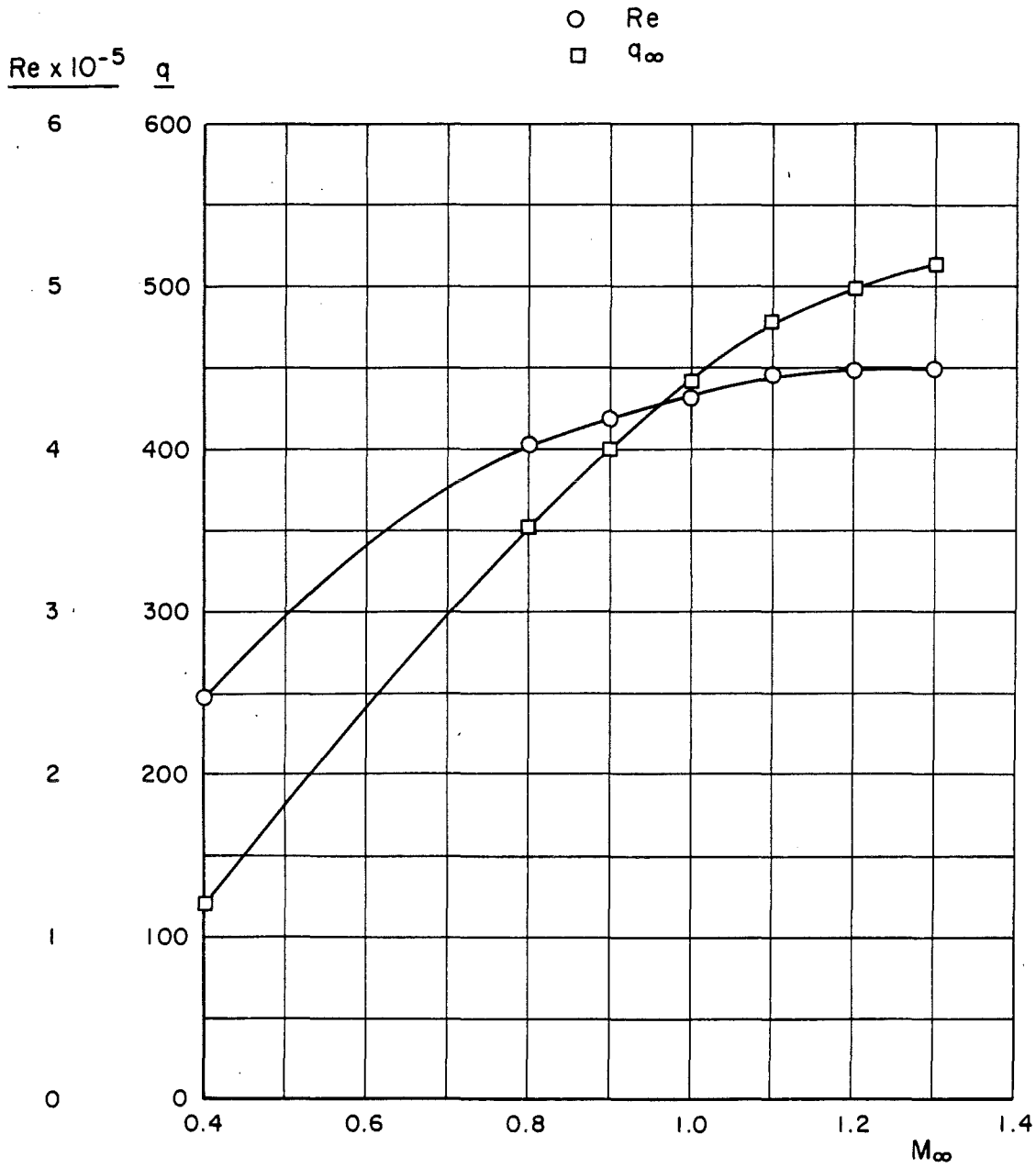


Figure 8. Nominal variation of Reynolds number and dynamic pressure with Mach number for static stability test.

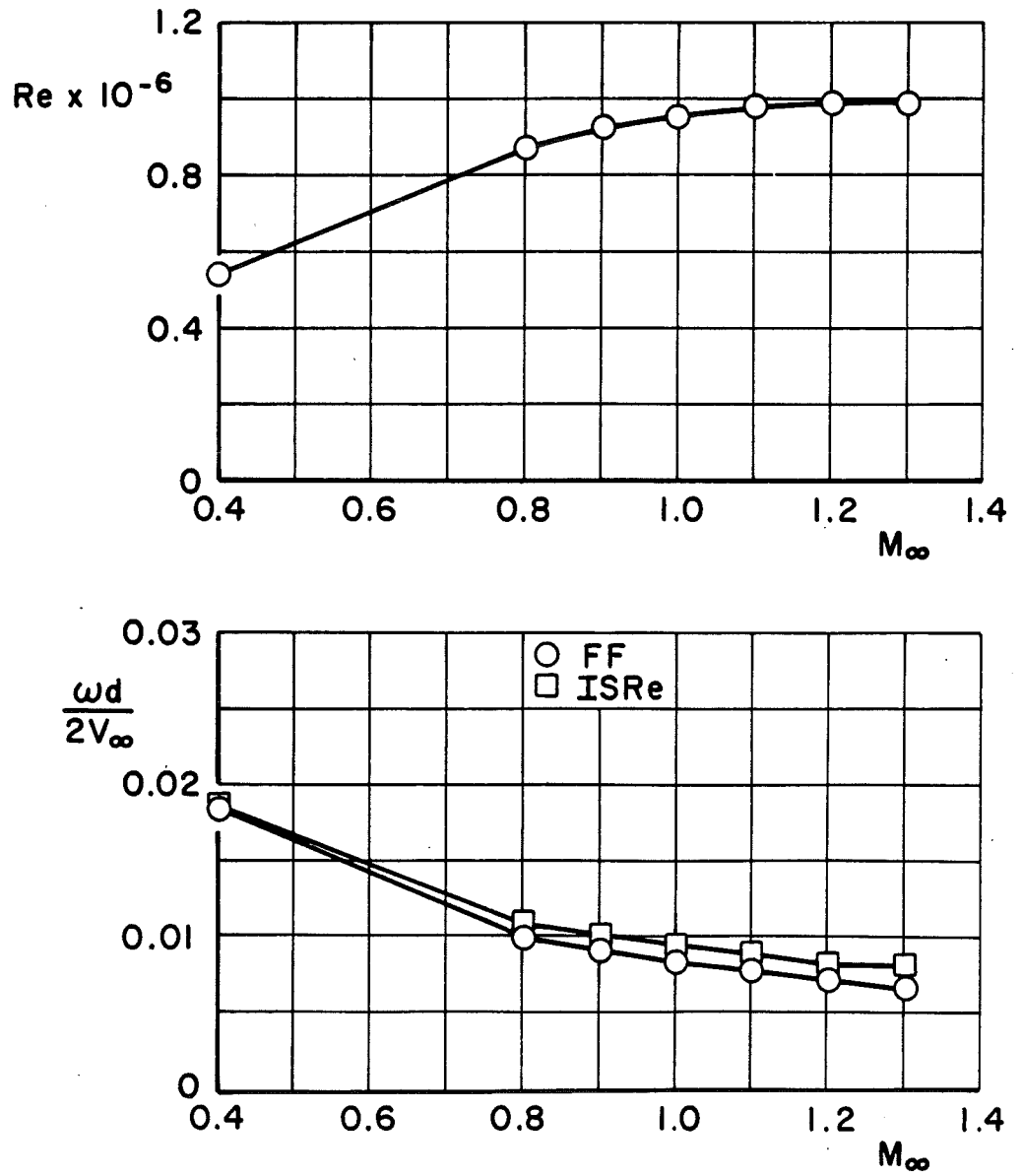
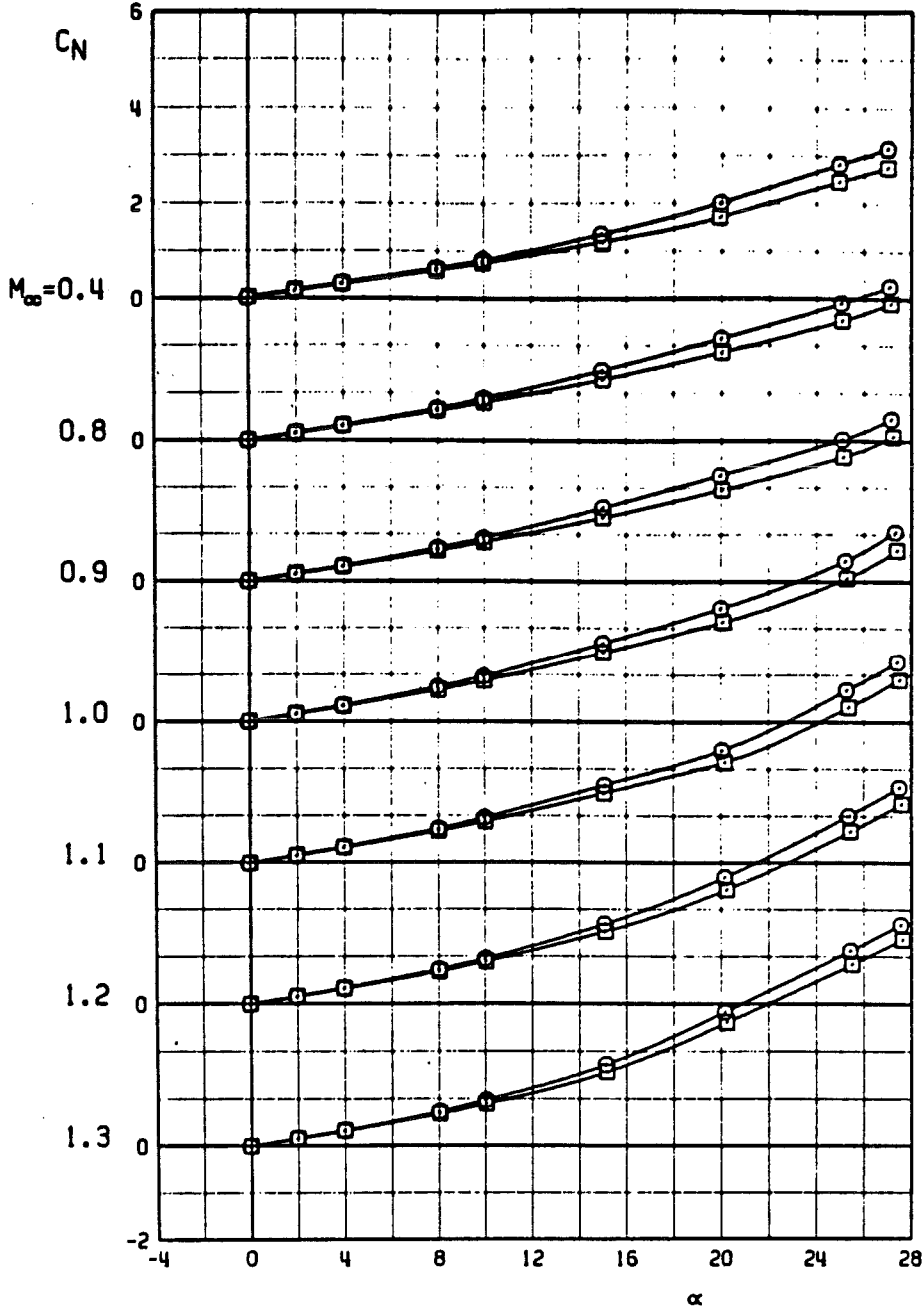


Figure 9. Variation of Reynolds number and reduced frequency with Mach number for pitch-damping test.

○ FFW1  
 □ FFSW1

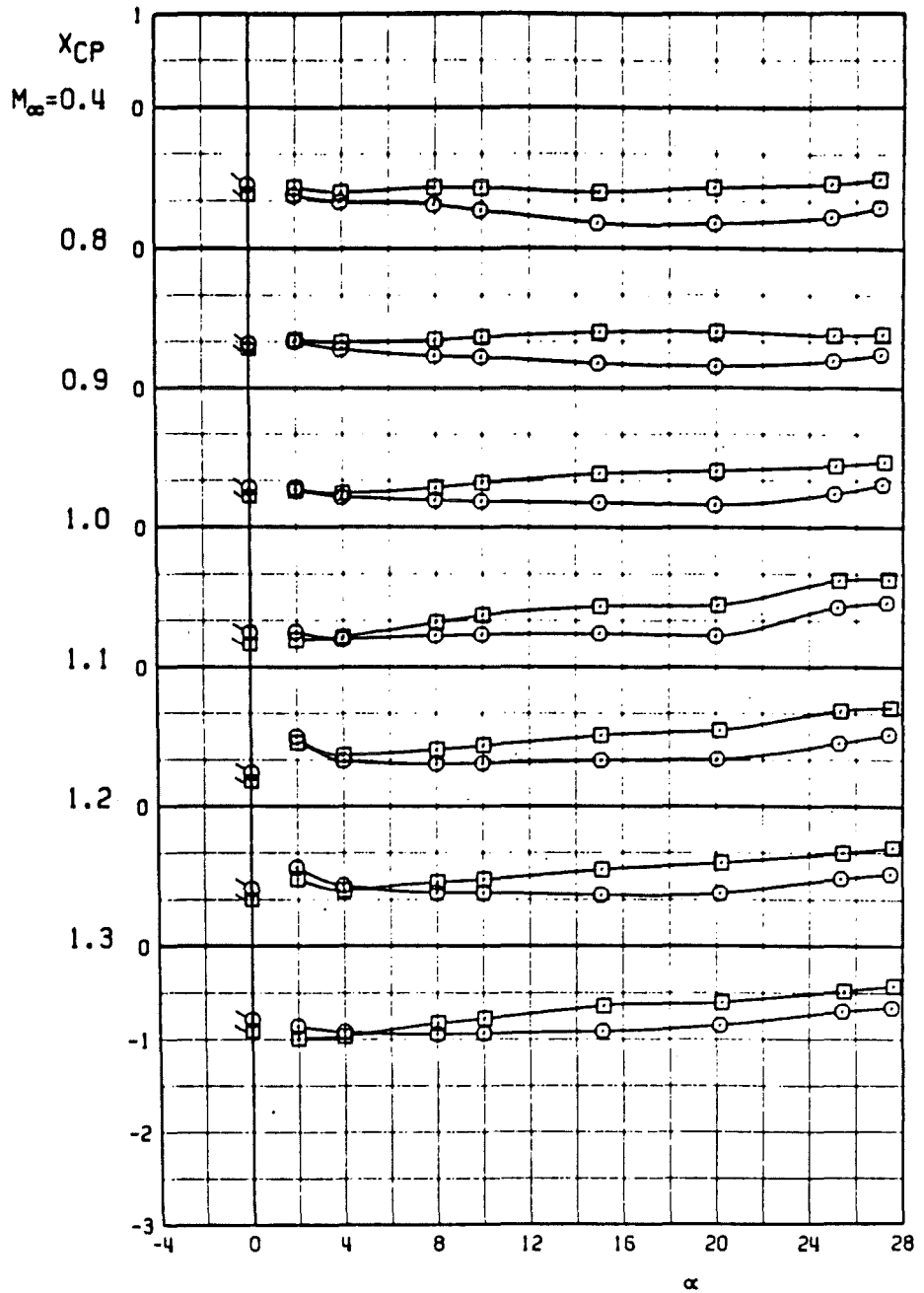


a.  $C_N$  versus  $\alpha$

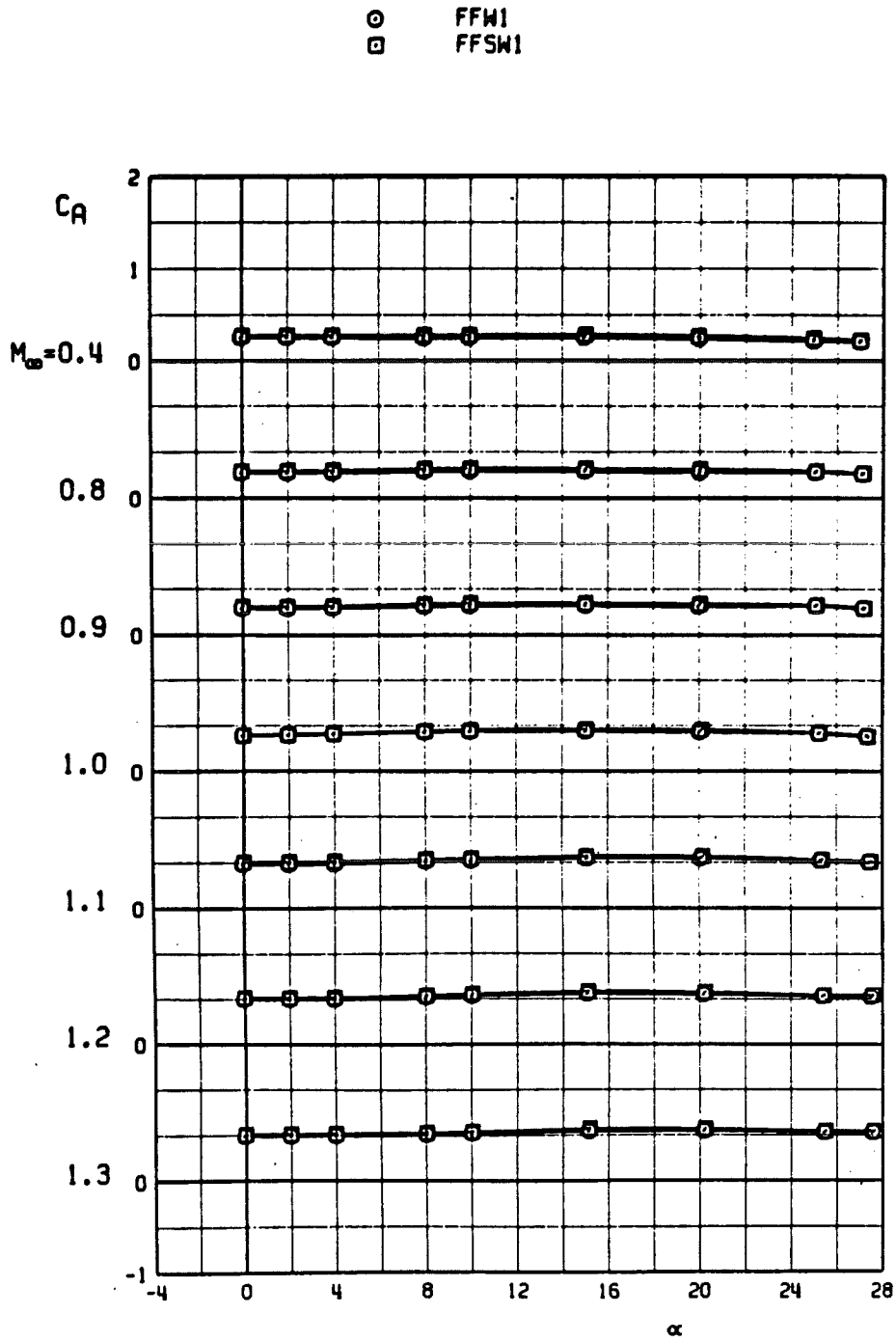
Figure 10. Static stability characteristics of configurations FFW1 and FFSW1 with  $\phi_m = -22.5$ .

○ FFWI  
 □ FFSWI

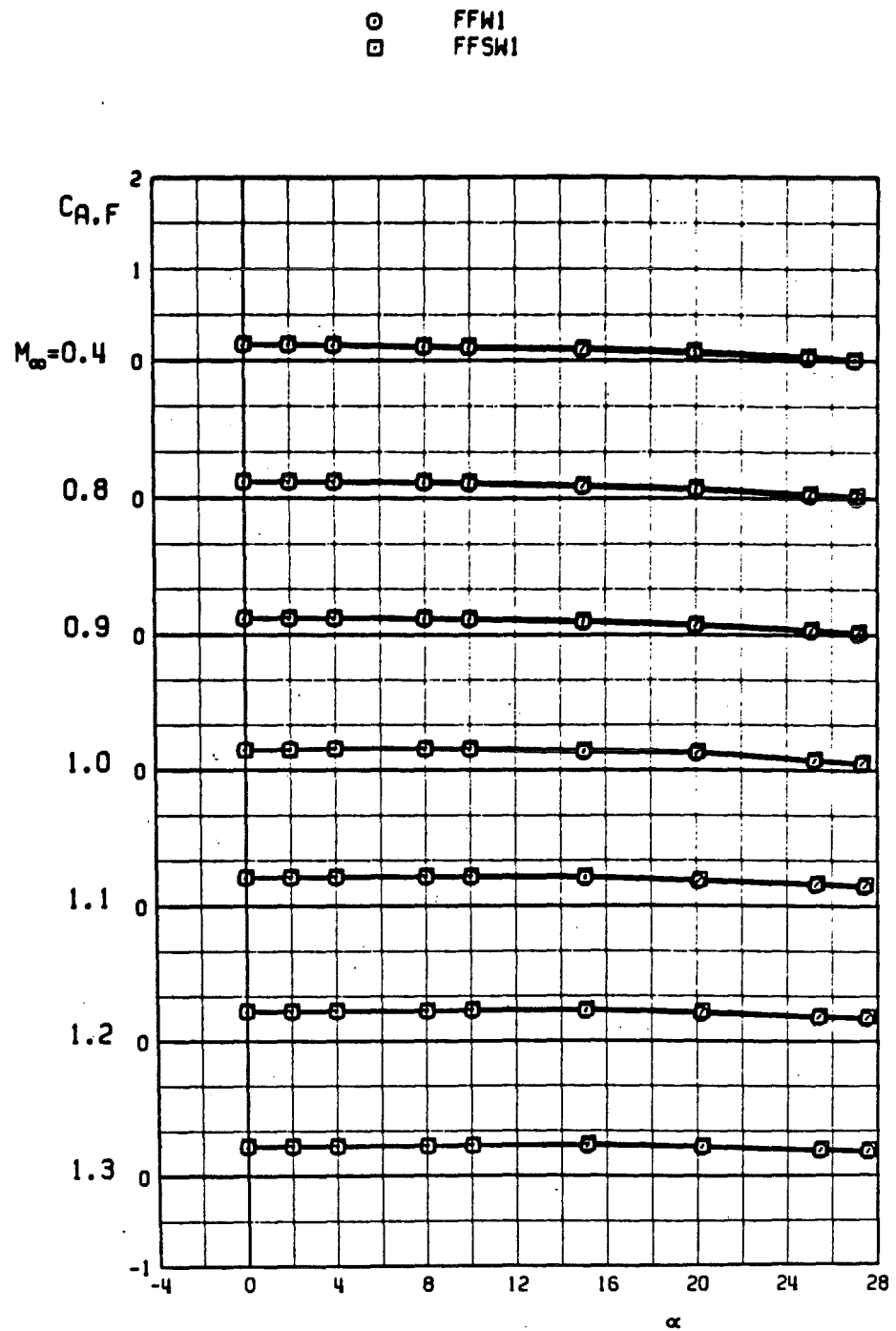
FLAGGED SYMBOLS INDICATE NEUTRAL-POINT LOCATION



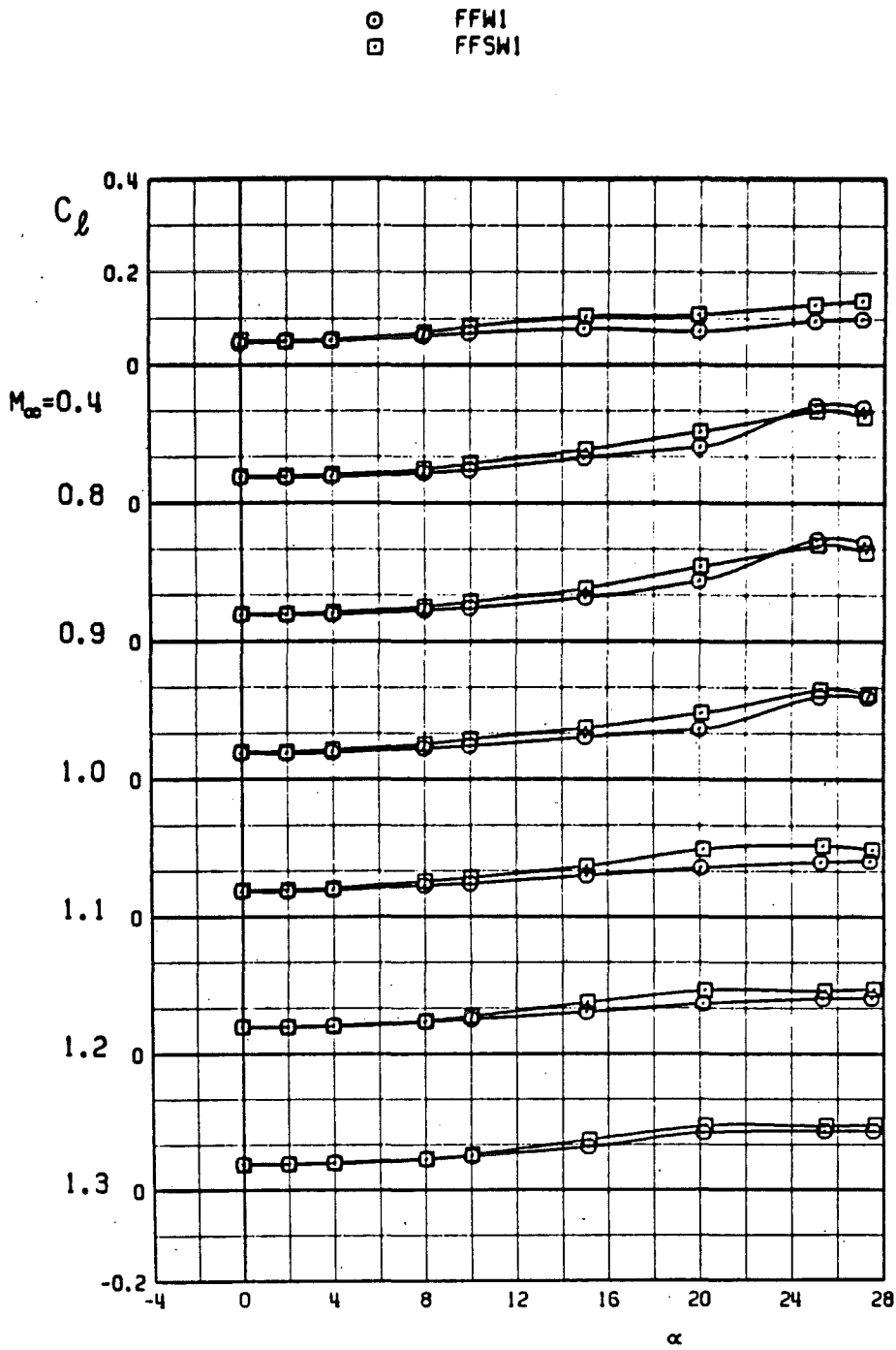
b. Center-of-pressure locations  
 Figure 10. Continued.



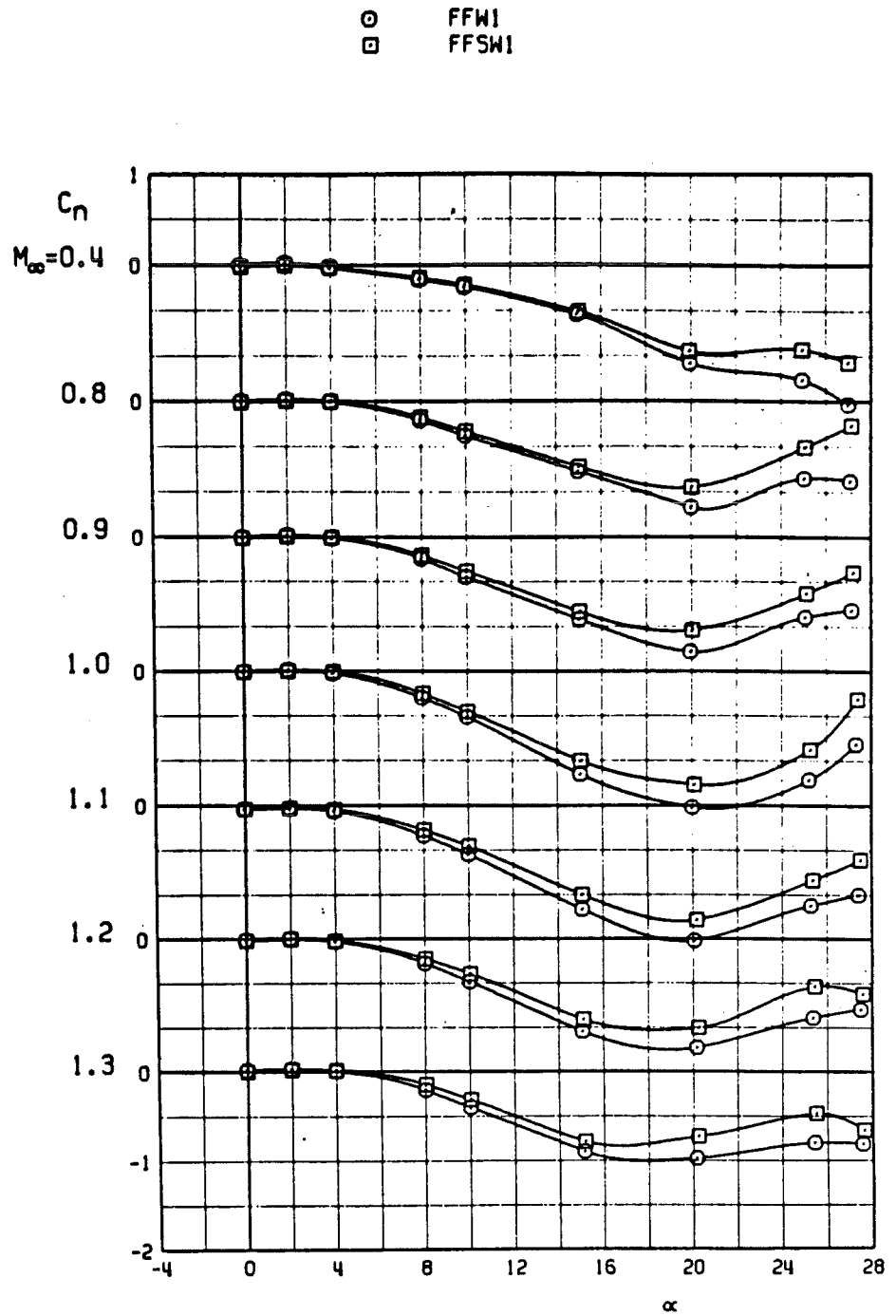
c. Axial-force coefficients  
 Figure 10. Continued.



d. Forebody axial-force coefficients  
 Figure 10. Continued.

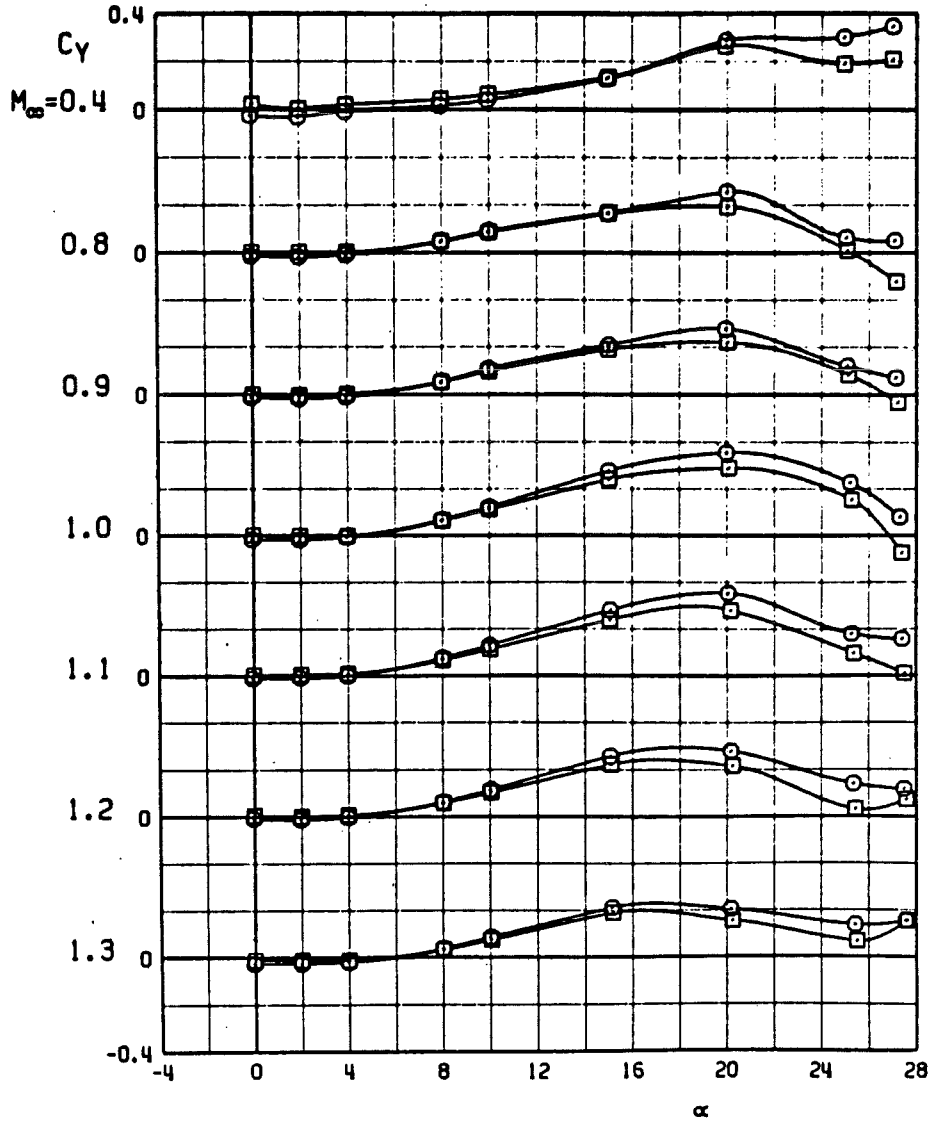


e. Rolling-moment coefficients  
 Figure 10. Continued.



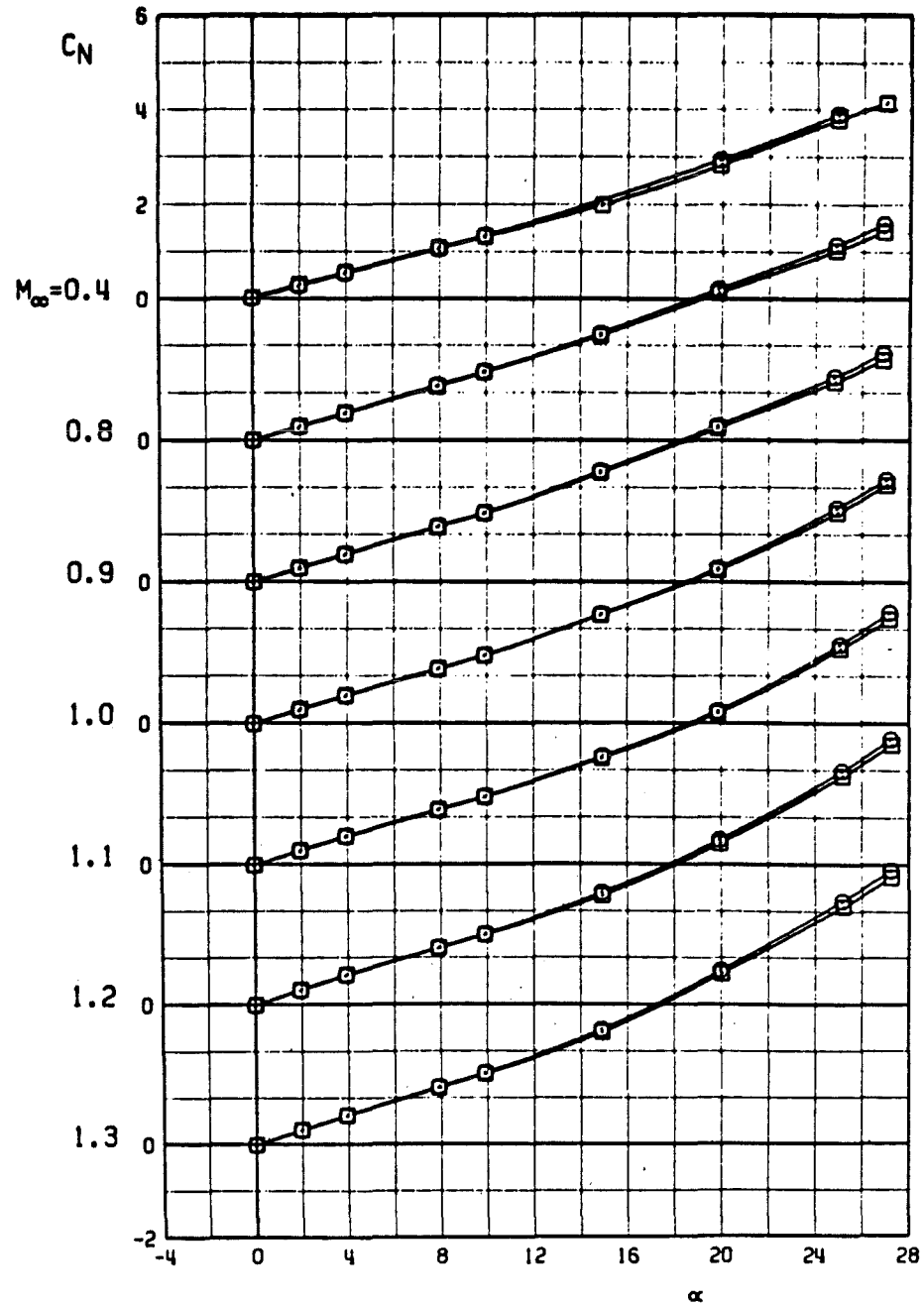
f. Yawing-moment coefficients  
Figure 10. Continued.

○ FFW1  
 □ FFSW1



g. Side-force coefficients  
 Figure 10. Concluded.

○ ISReW1  
 □ ISReSW1

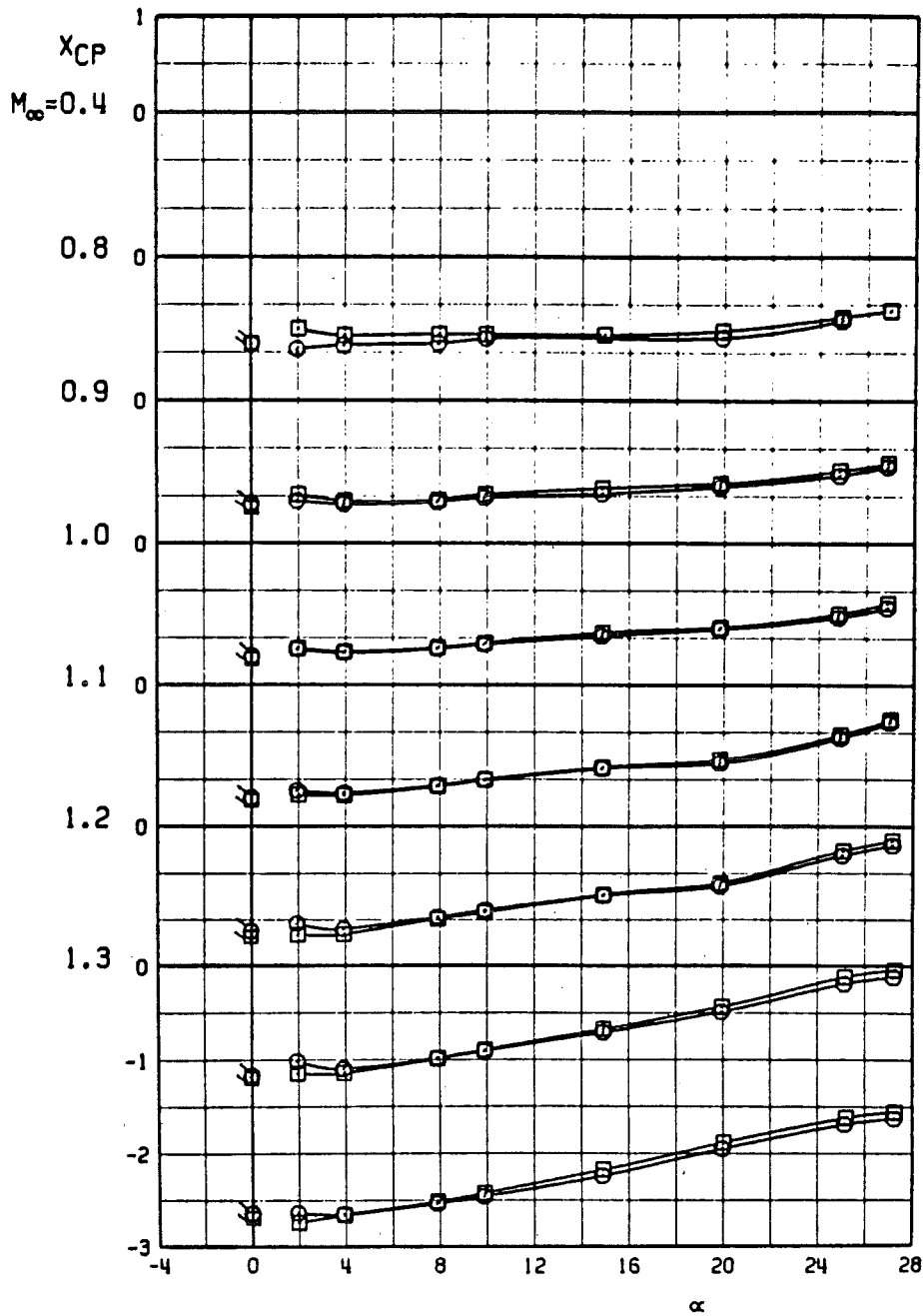


a. Normal-force coefficients

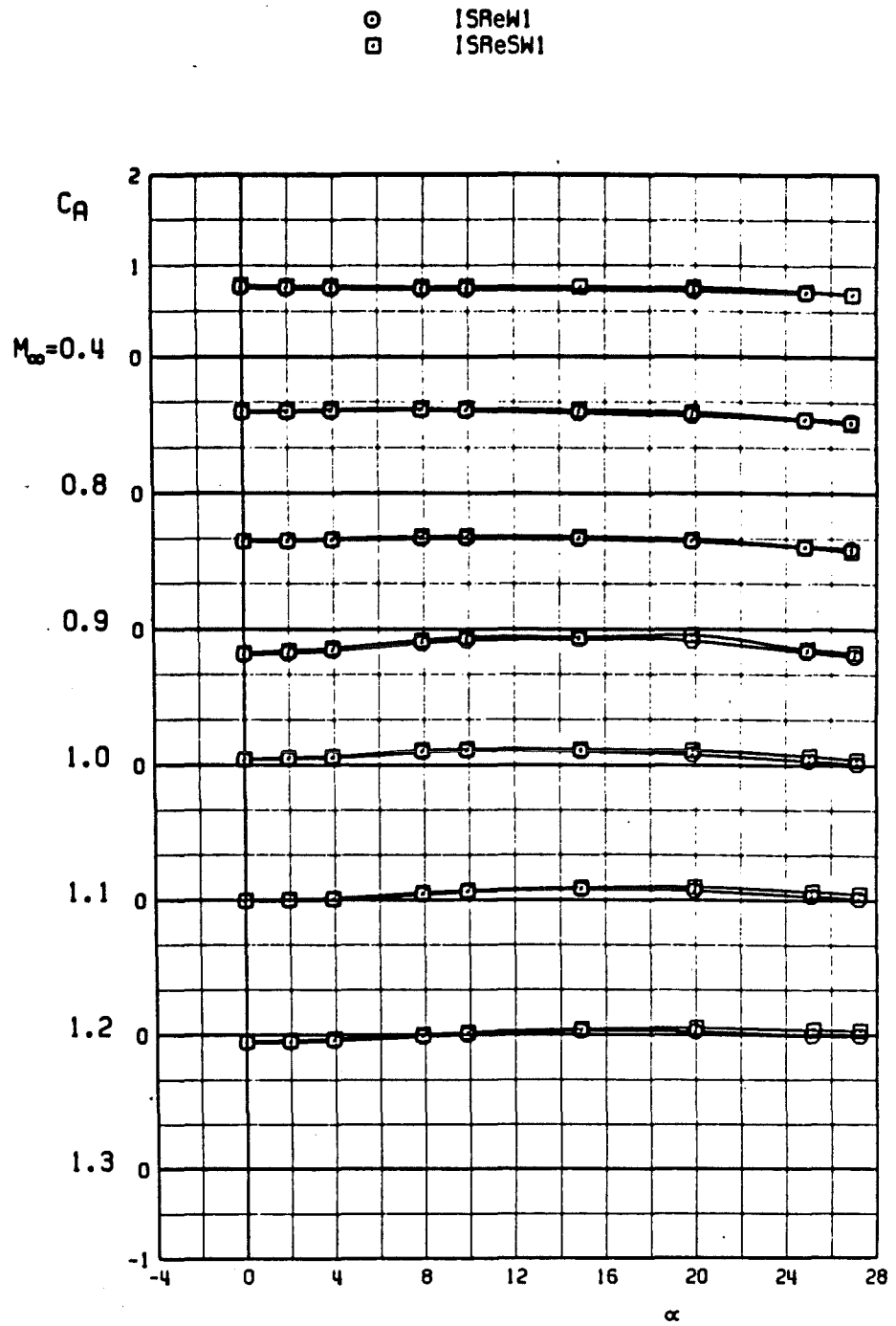
Figure 11. Static stability characteristics of configurations ISReW1 and ISReSW1 with  $\phi_m = -22.5$ .

○ ISReW1  
 □ ISReSW1

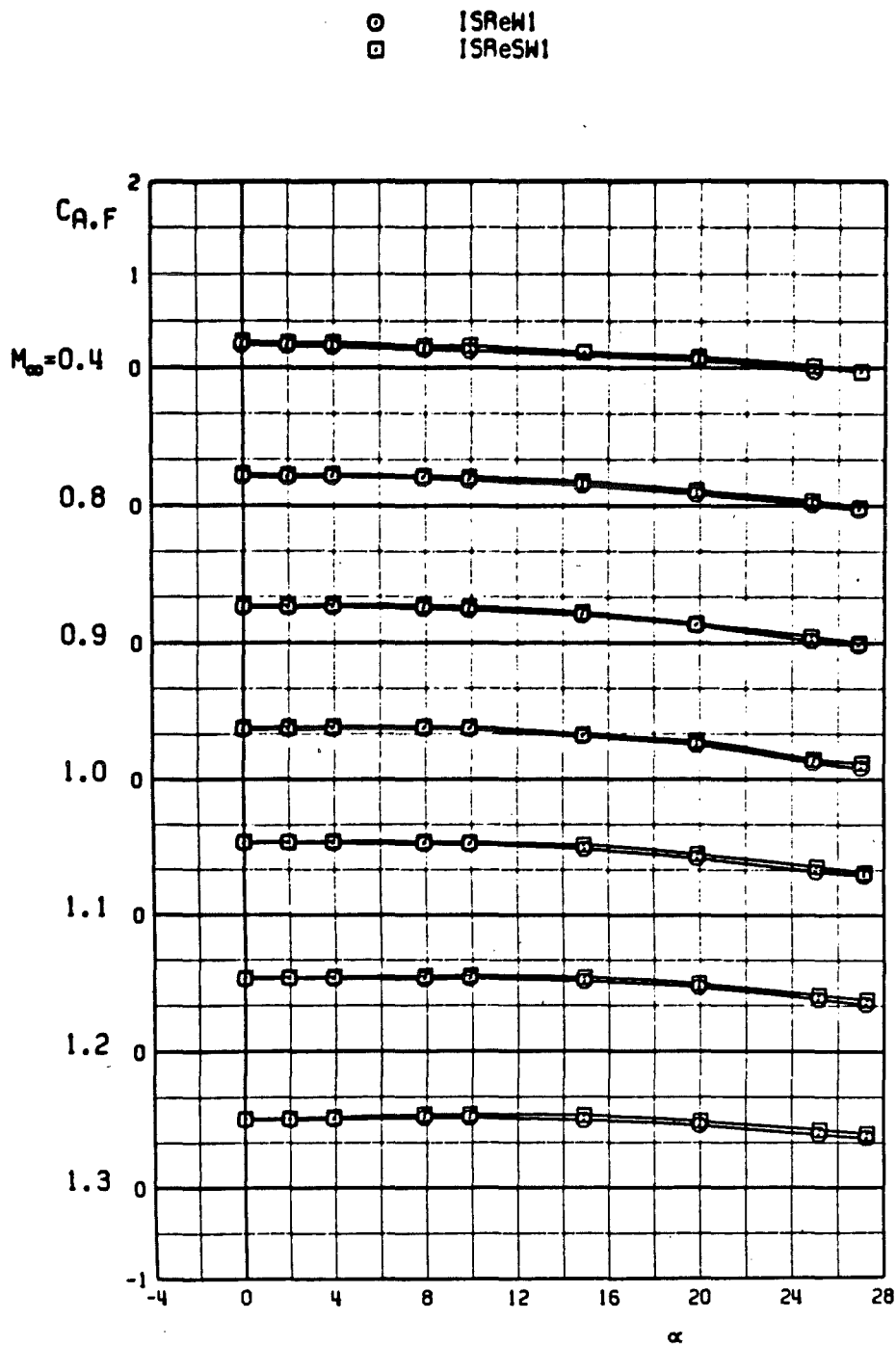
FLAGGED SYMBOLS INDICATE NEUTRAL-POINT LOCATION



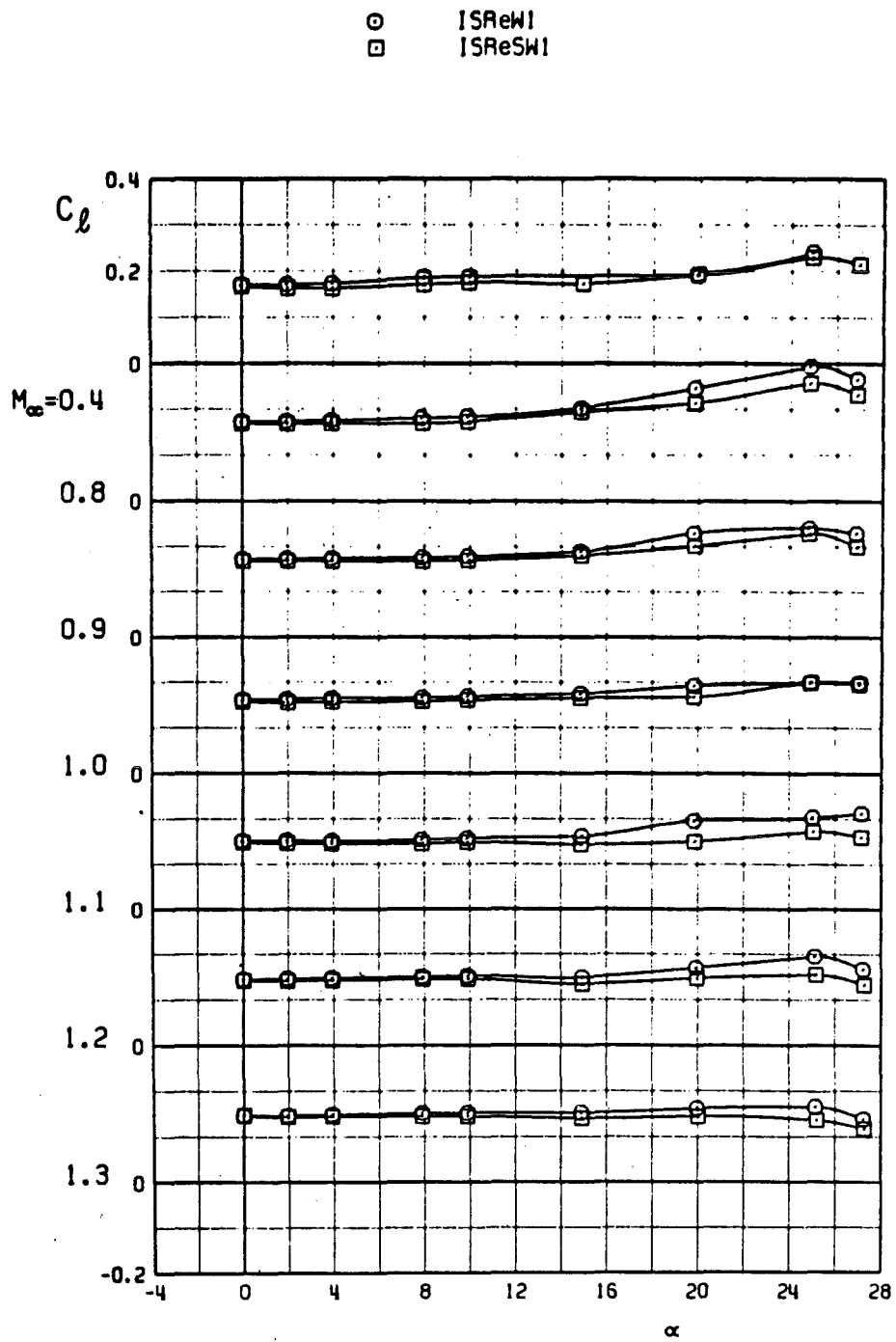
b. Center-of-pressure locations  
 Figure 11. Continued.



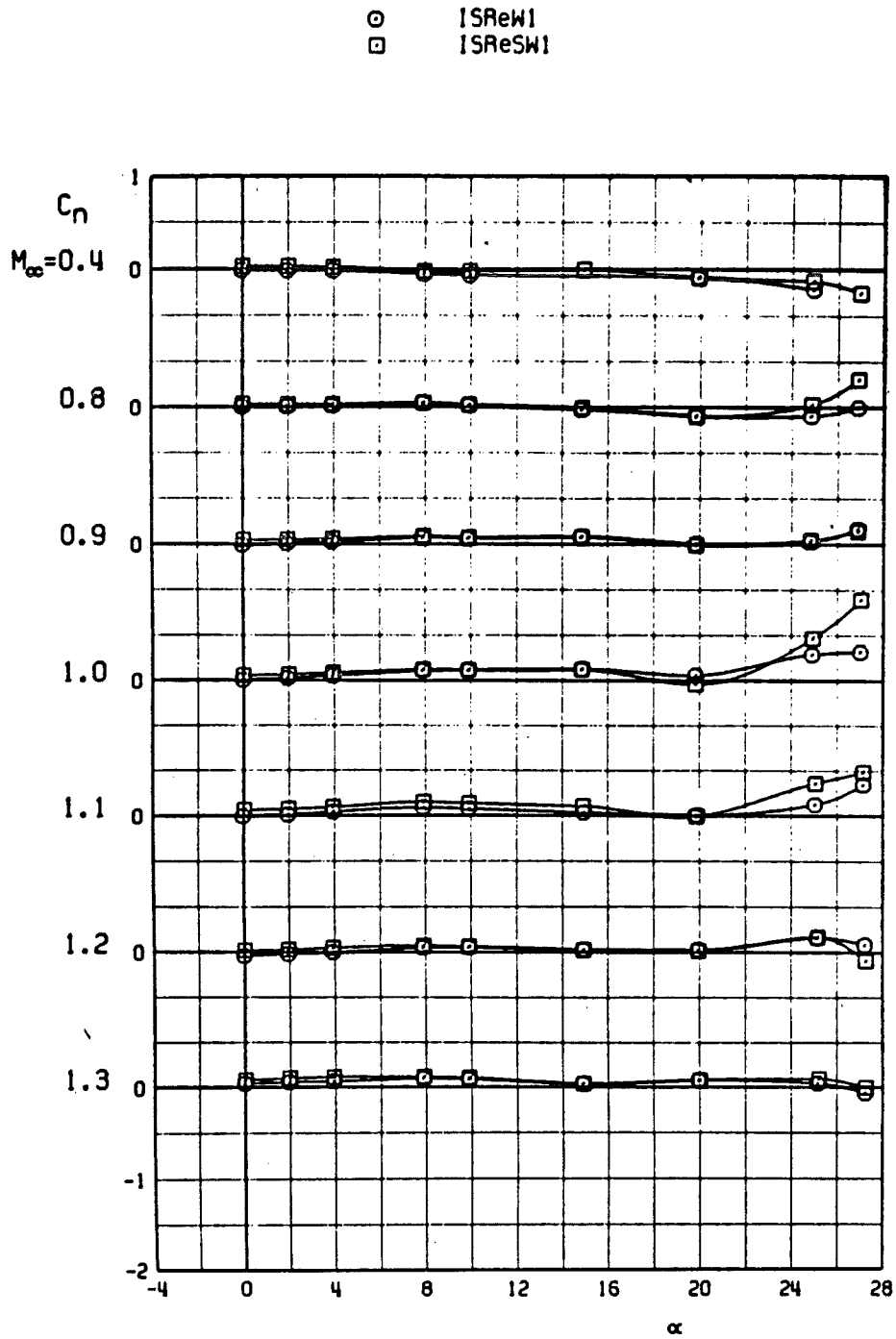
c. Axial-force coefficients  
 Figure 11. Continued.



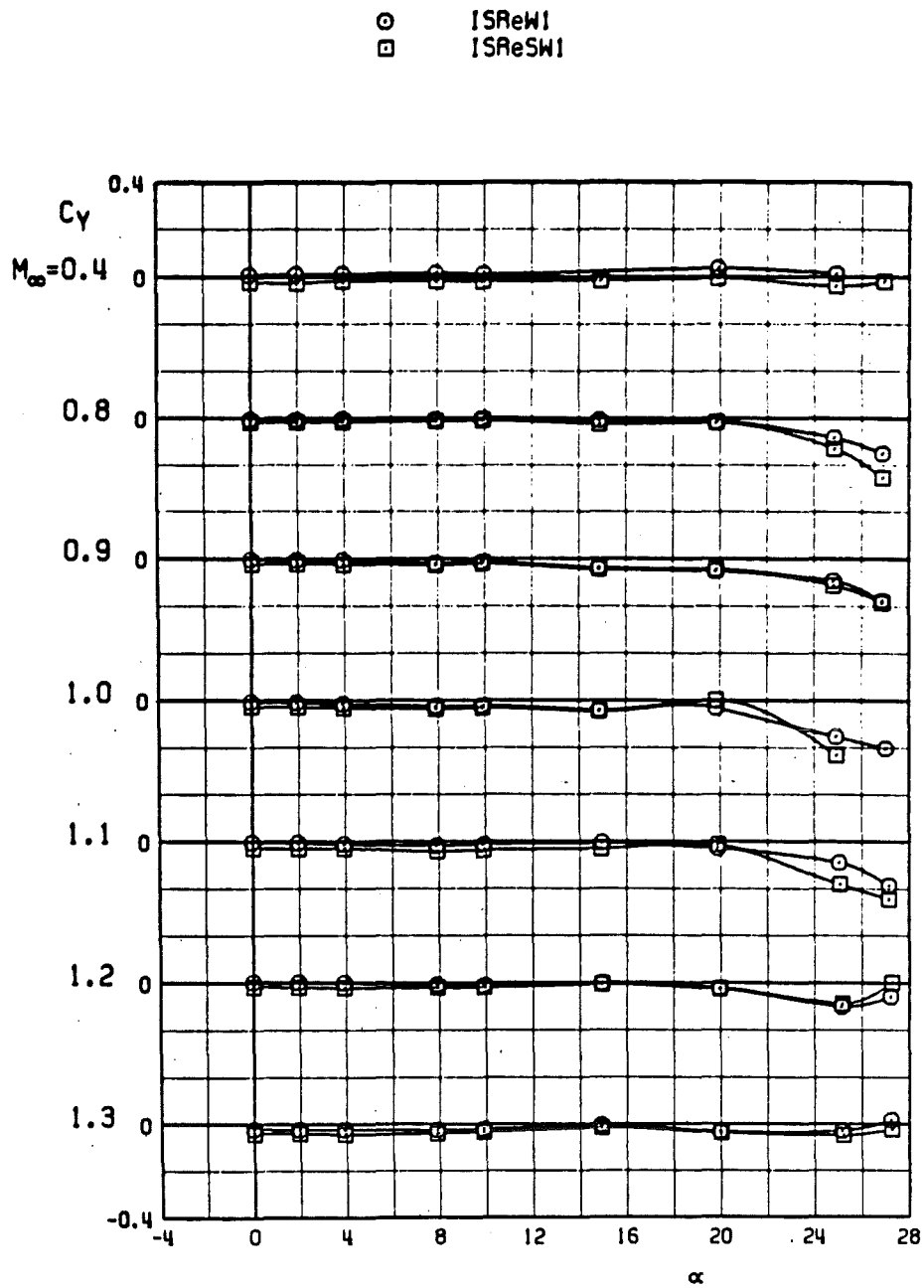
d. Forebody axial-force coefficients  
 Figure 11. Continued.



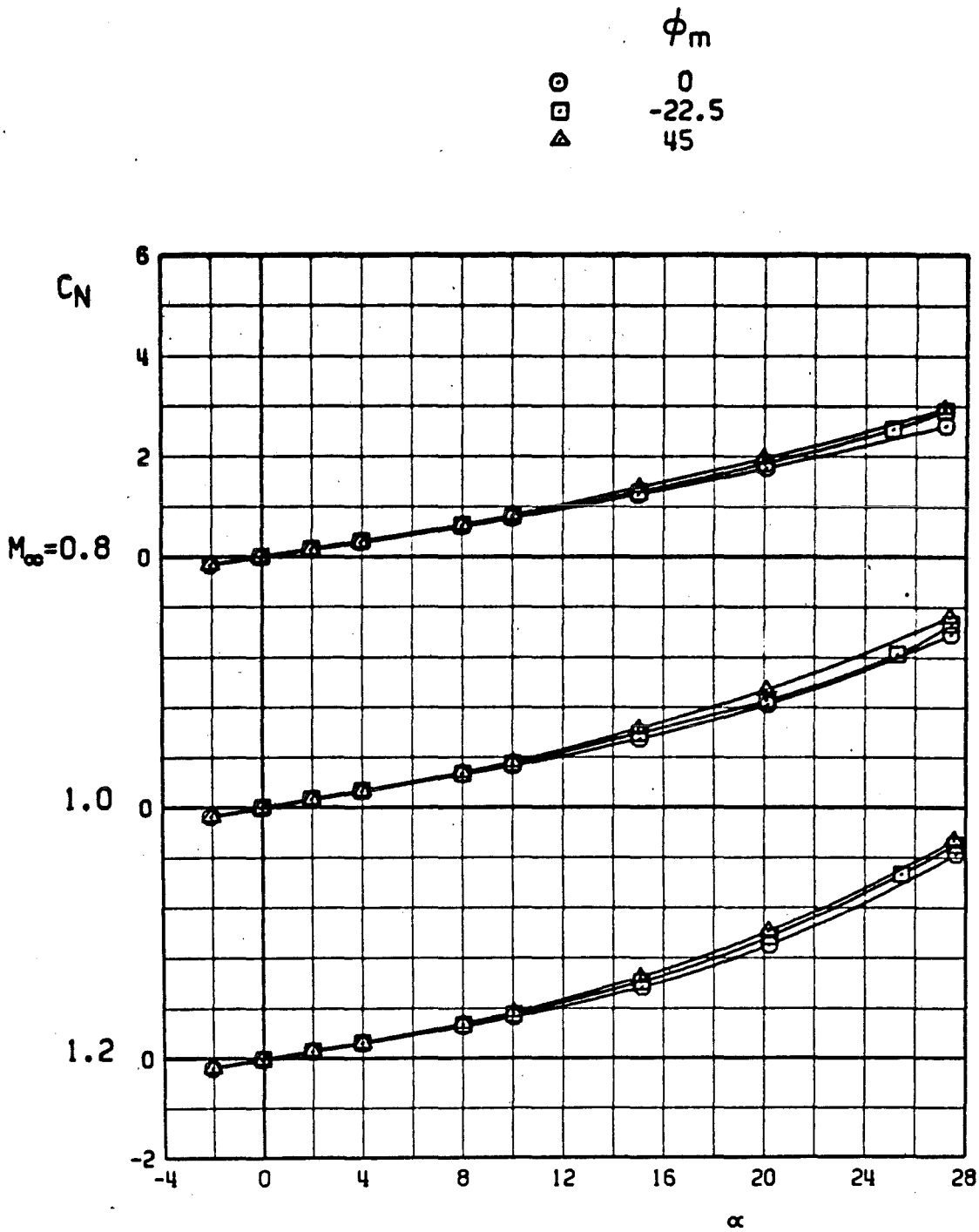
e. Rolling-moment coefficients  
 Figure 11. Continued.



f. Yawing-moment coefficients  
Figure 11. Continued.



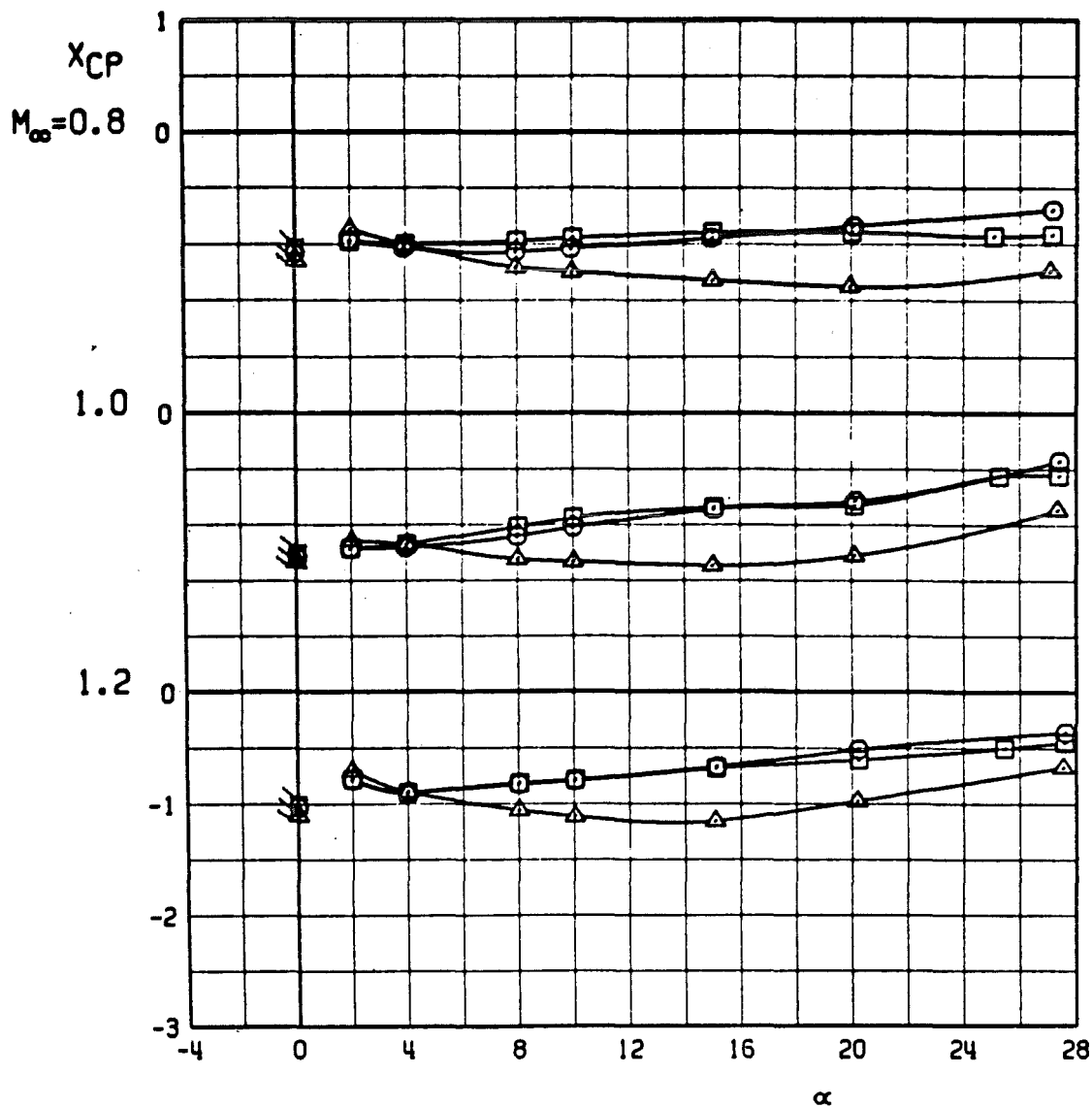
g. Side-force coefficients  
 Figure 11. Concluded.



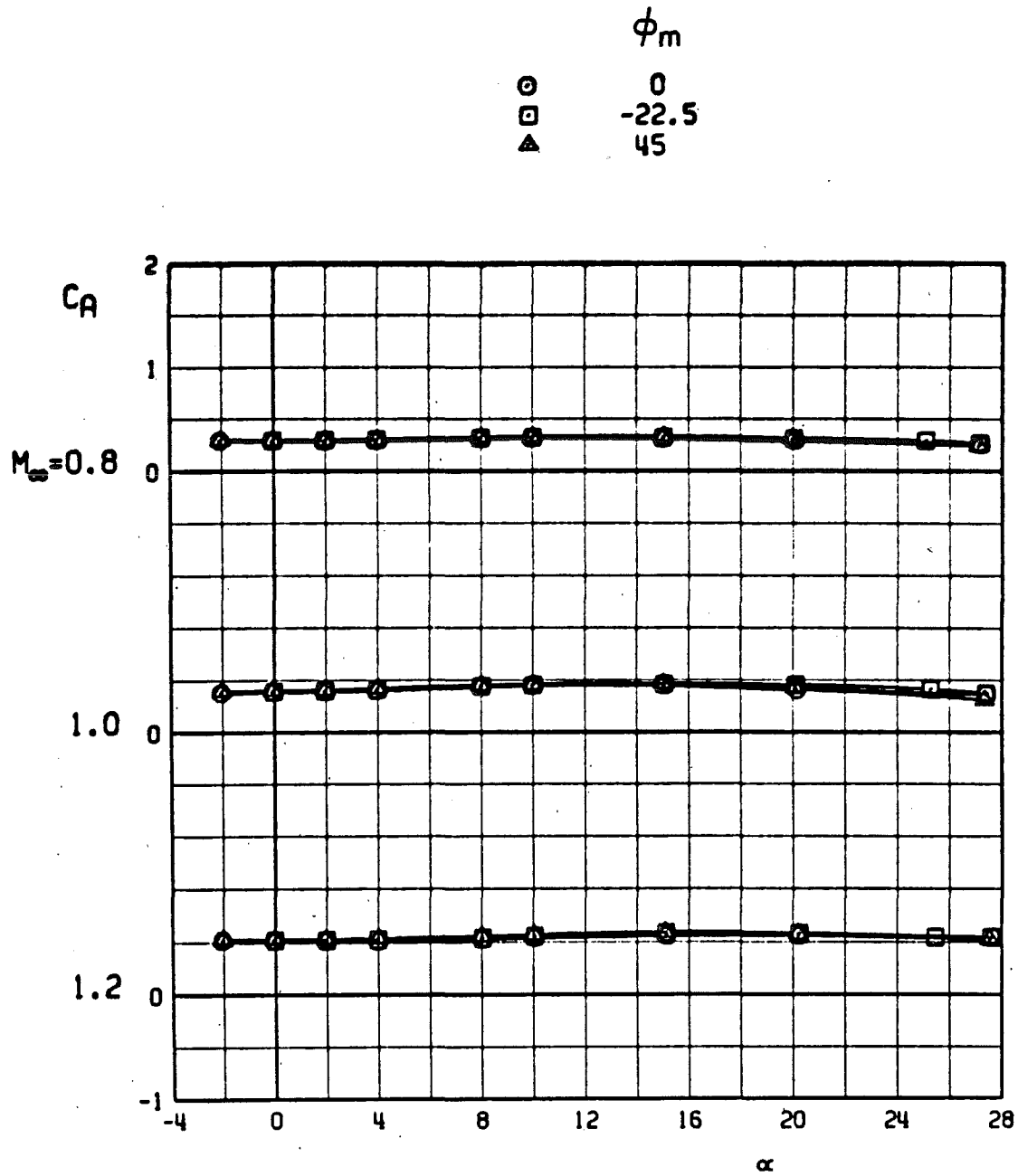
a. Normal-force coefficients  
 Figure 12. Effects of roll angle on the static stability characteristics of configuration FFSW1.

	$\phi_m$
○	0
□	-22.5
△	45

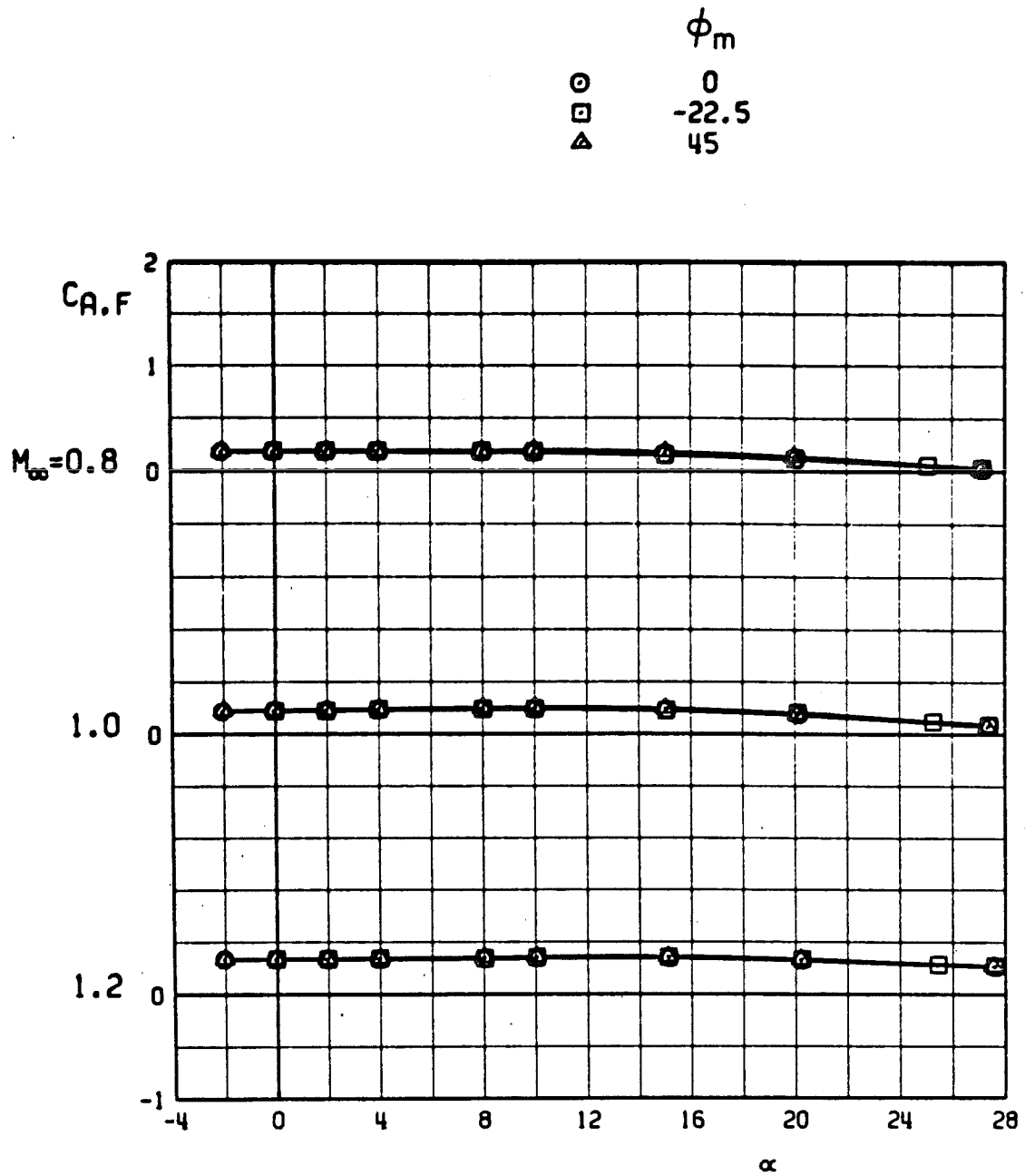
FLAGGED SYMBOLS INDICATE NEUTRAL-POINT LOCATION



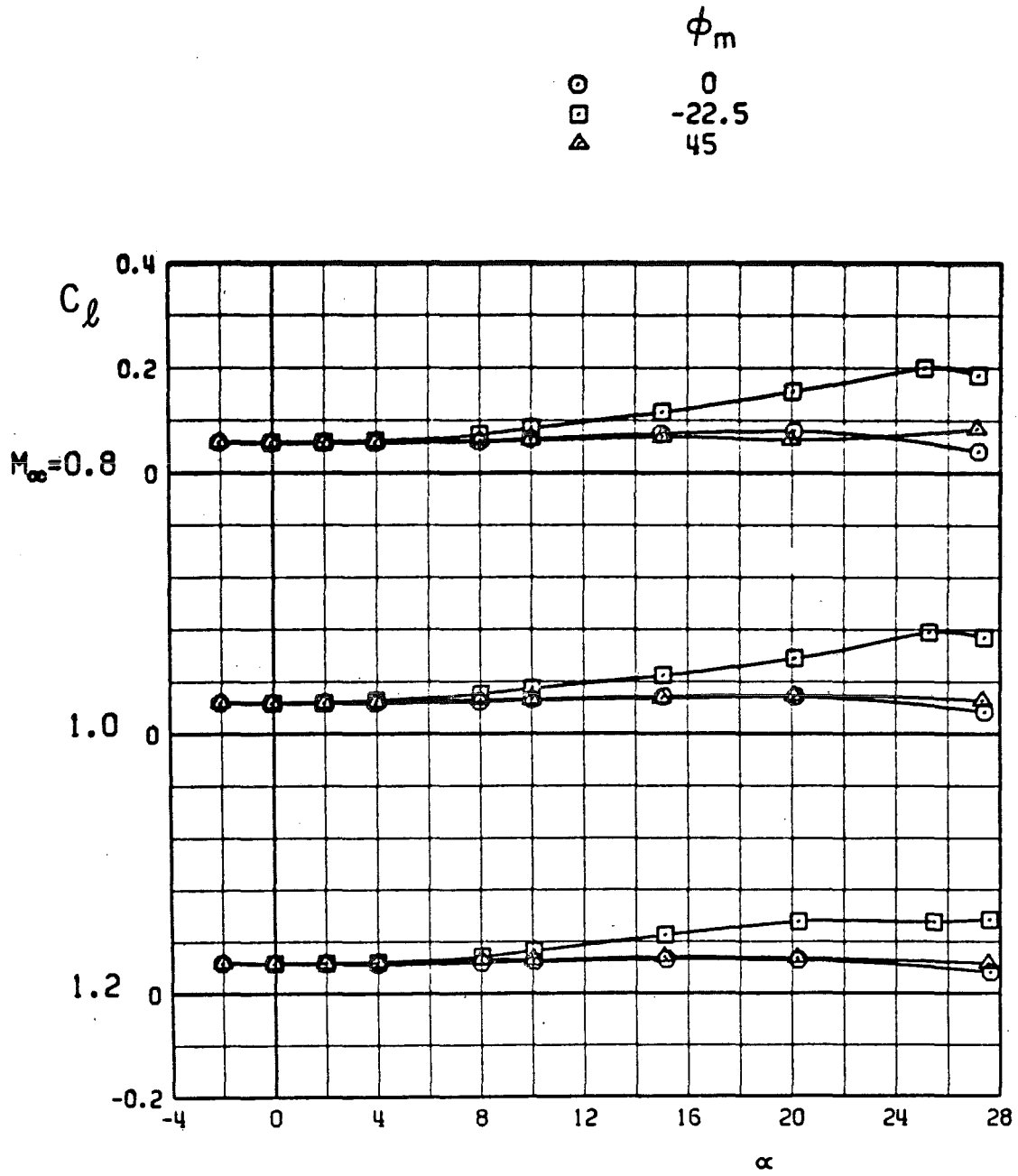
b. Center-of-pressure locations  
Figure 12. Continued.



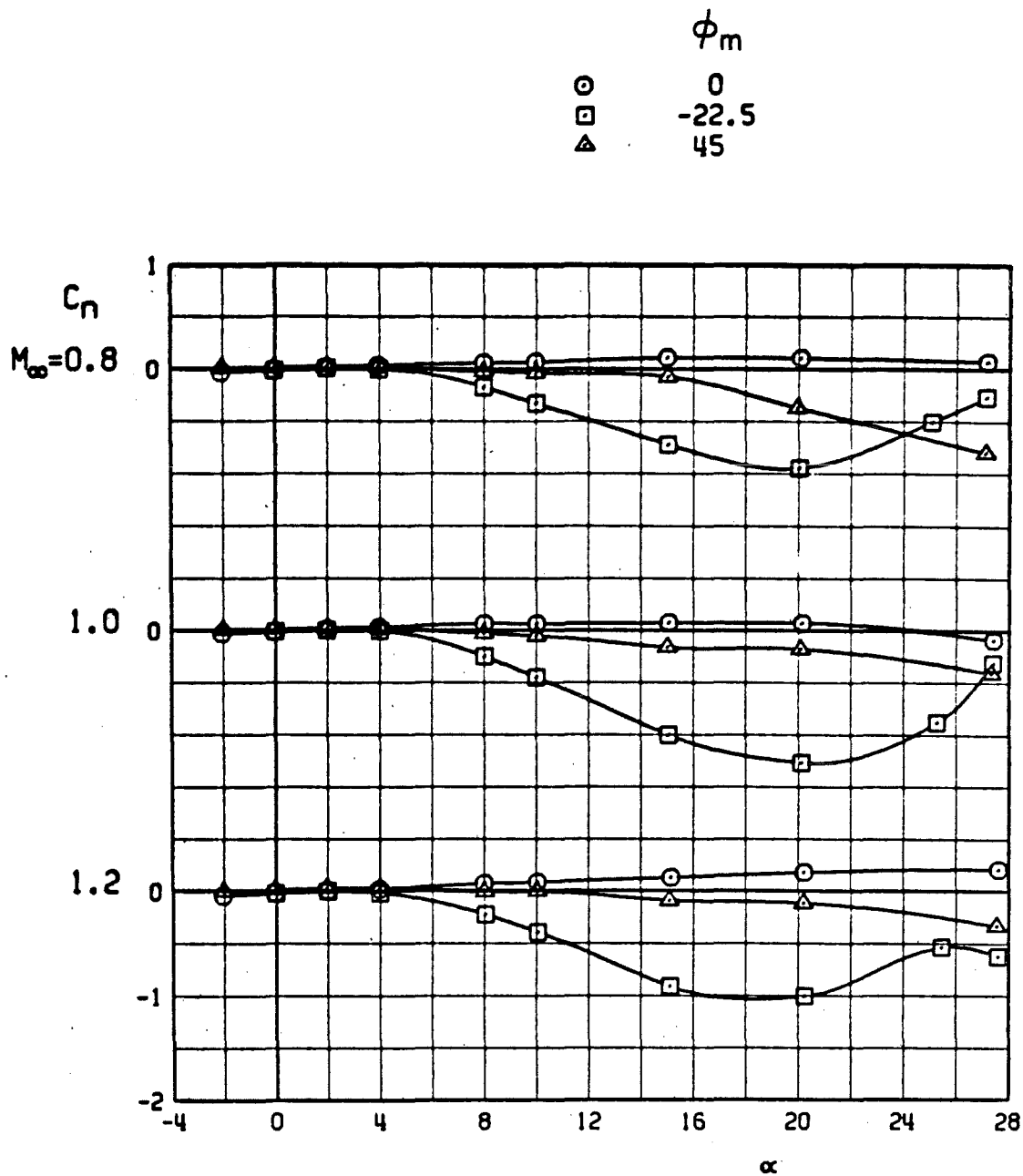
c. Axial-force coefficients  
Figure 12. Continued.



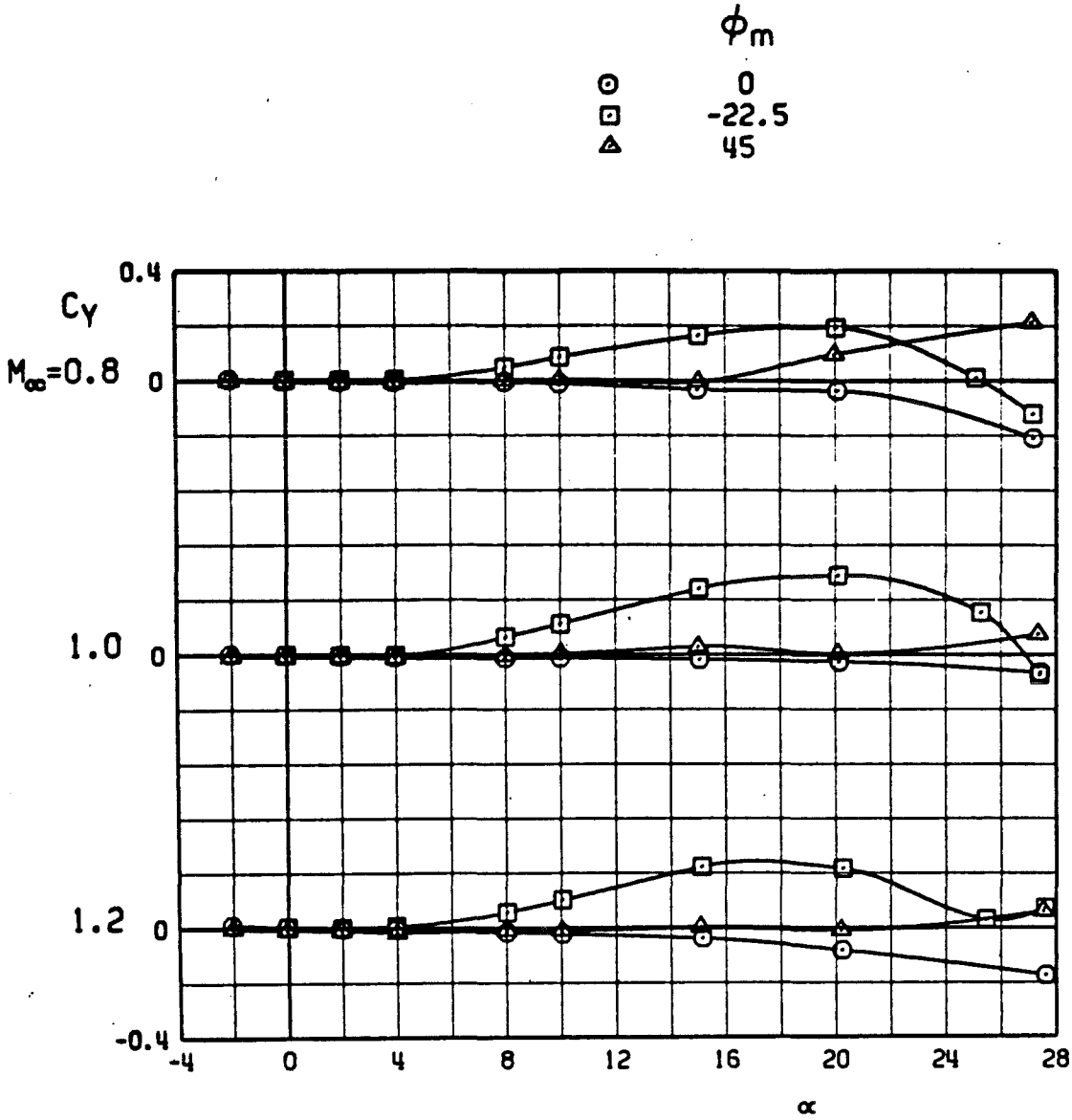
d. Forebody axial-force coefficients  
Figure 12. Continued.



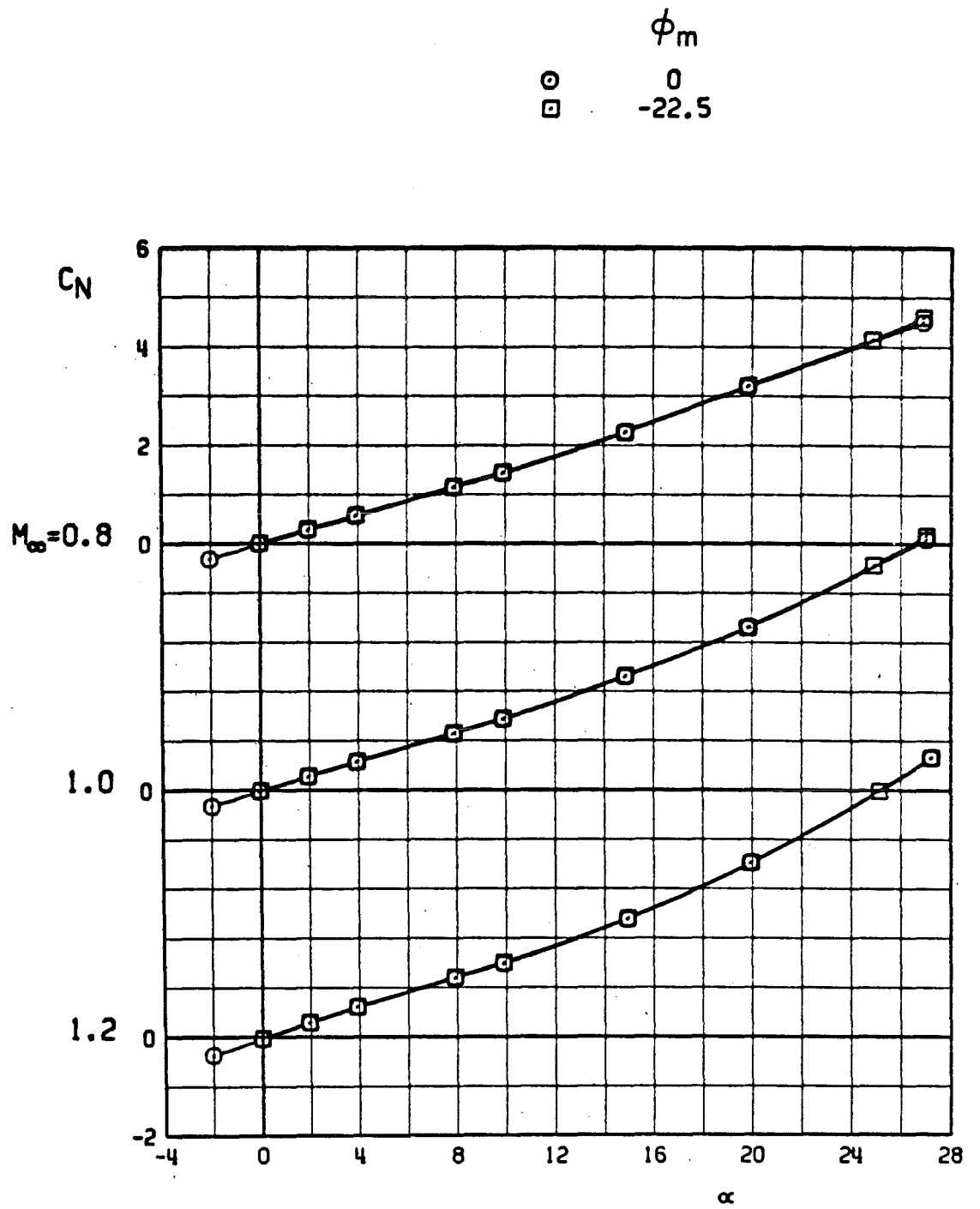
e. Rolling-moment coefficients  
Figure 12. Continued.



f. Yawing-moment coefficients  
Figure 12. Continued.



g. Side-force coefficients  
Figure 12. Concluded.

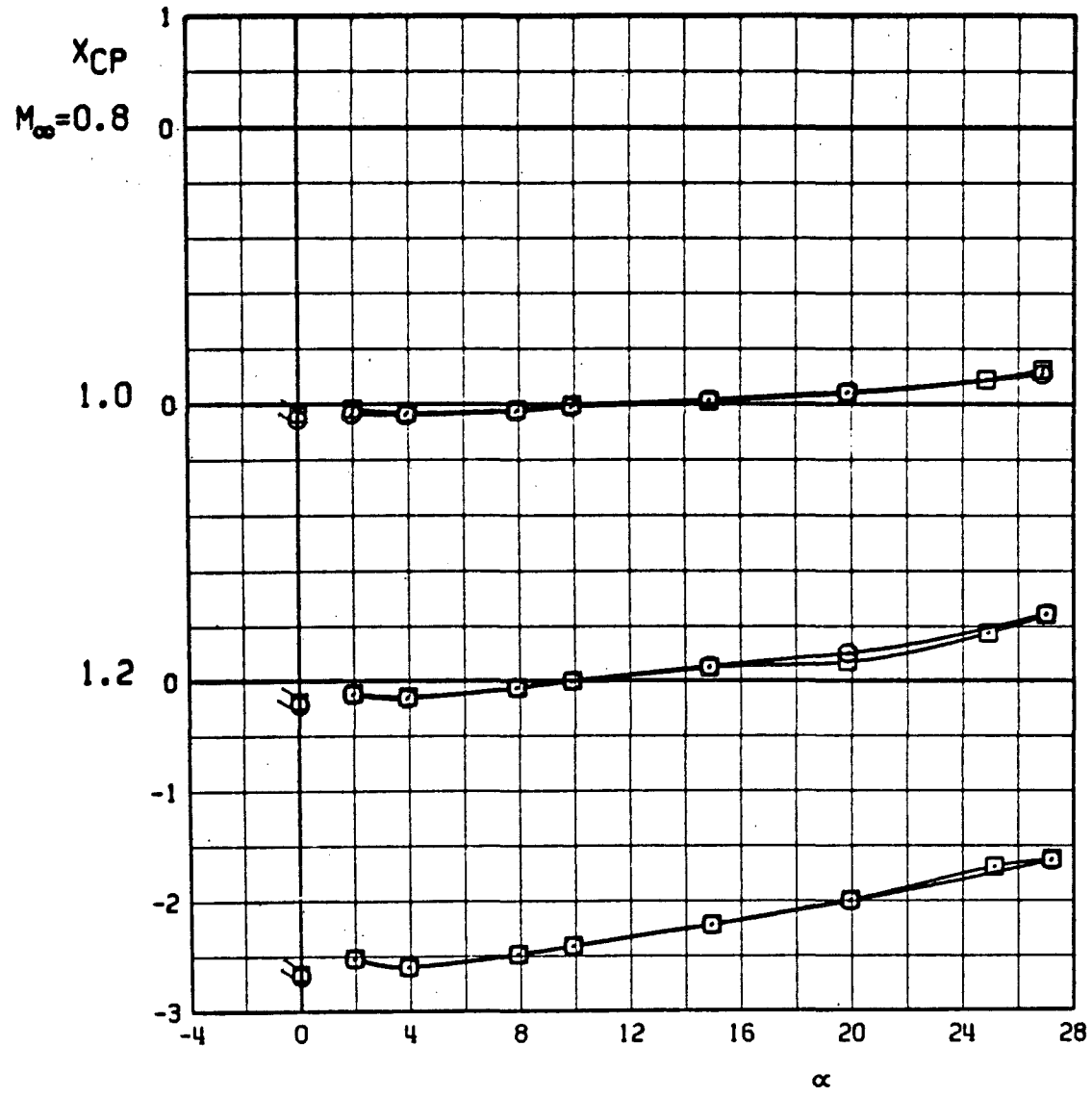


a. Normal-force coefficients  
 Figure 13. Effects of roll angle on the static stability characteristics of configuration ISReW1.

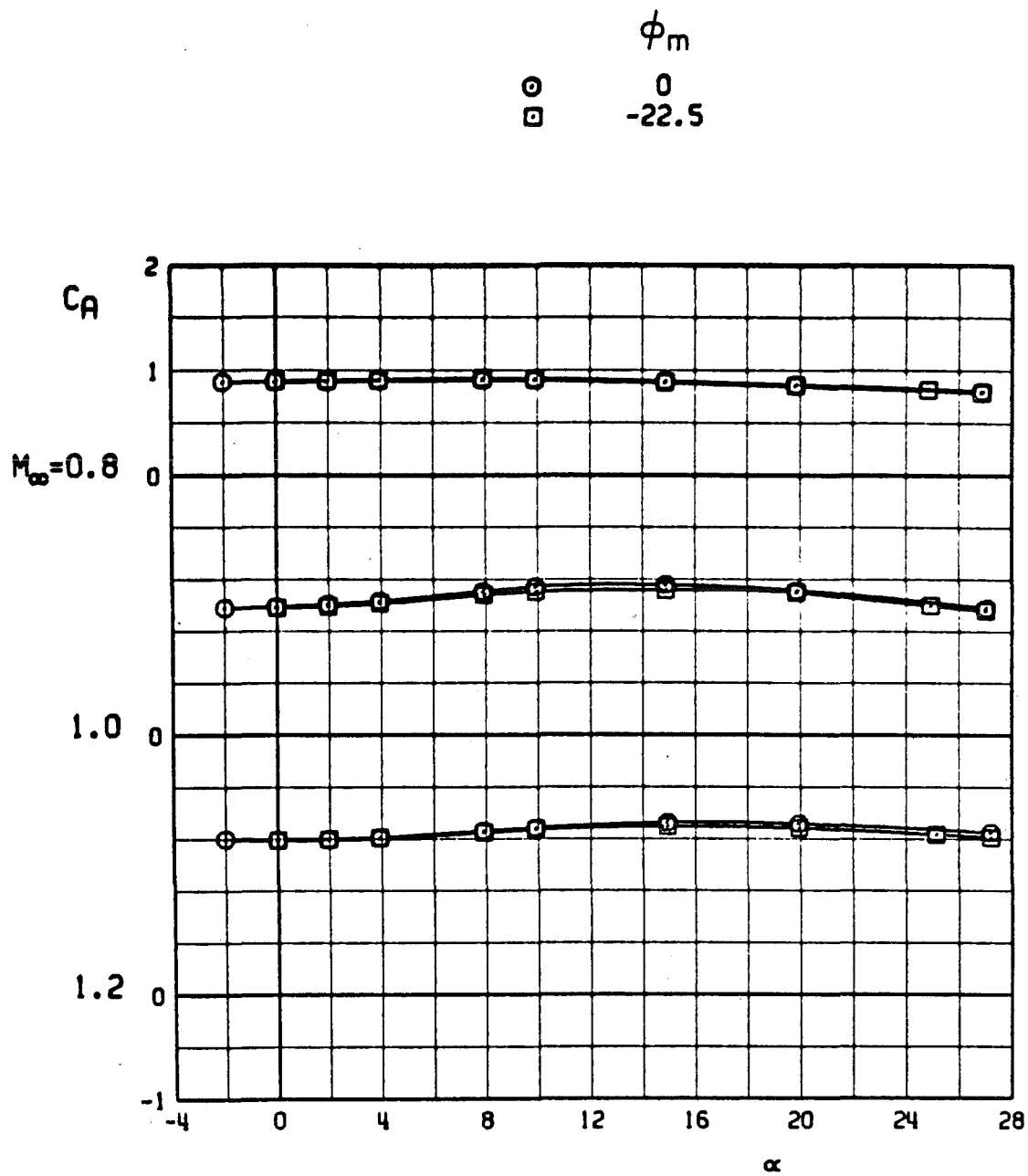
$\phi_m$

○ 0  
 □ -22.5

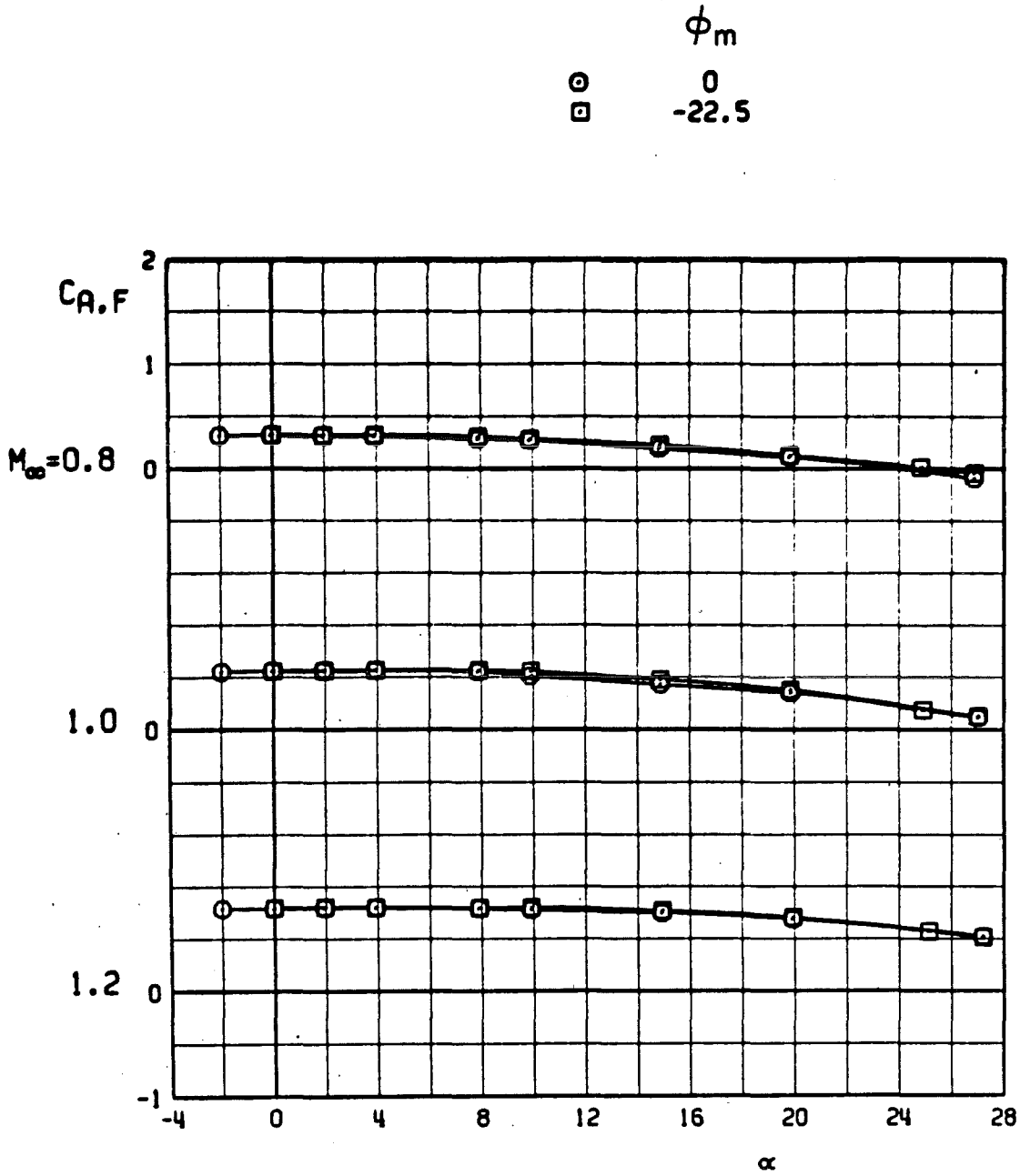
FLAGGED SYMBOLS INDICATE NEUTRAL-POINT LOCATION



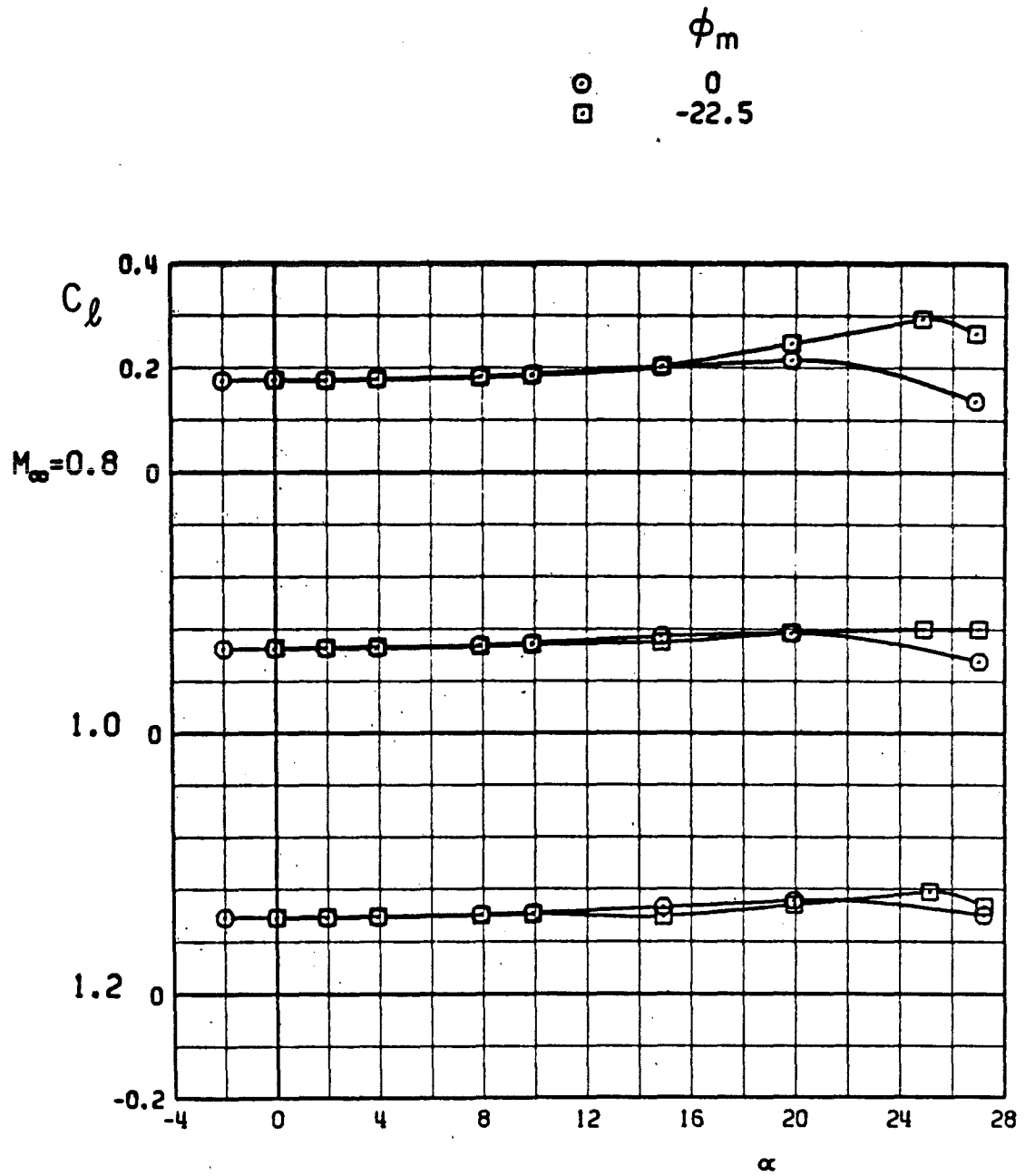
b. Center-of-pressure locations  
 Figure 13. Continued.



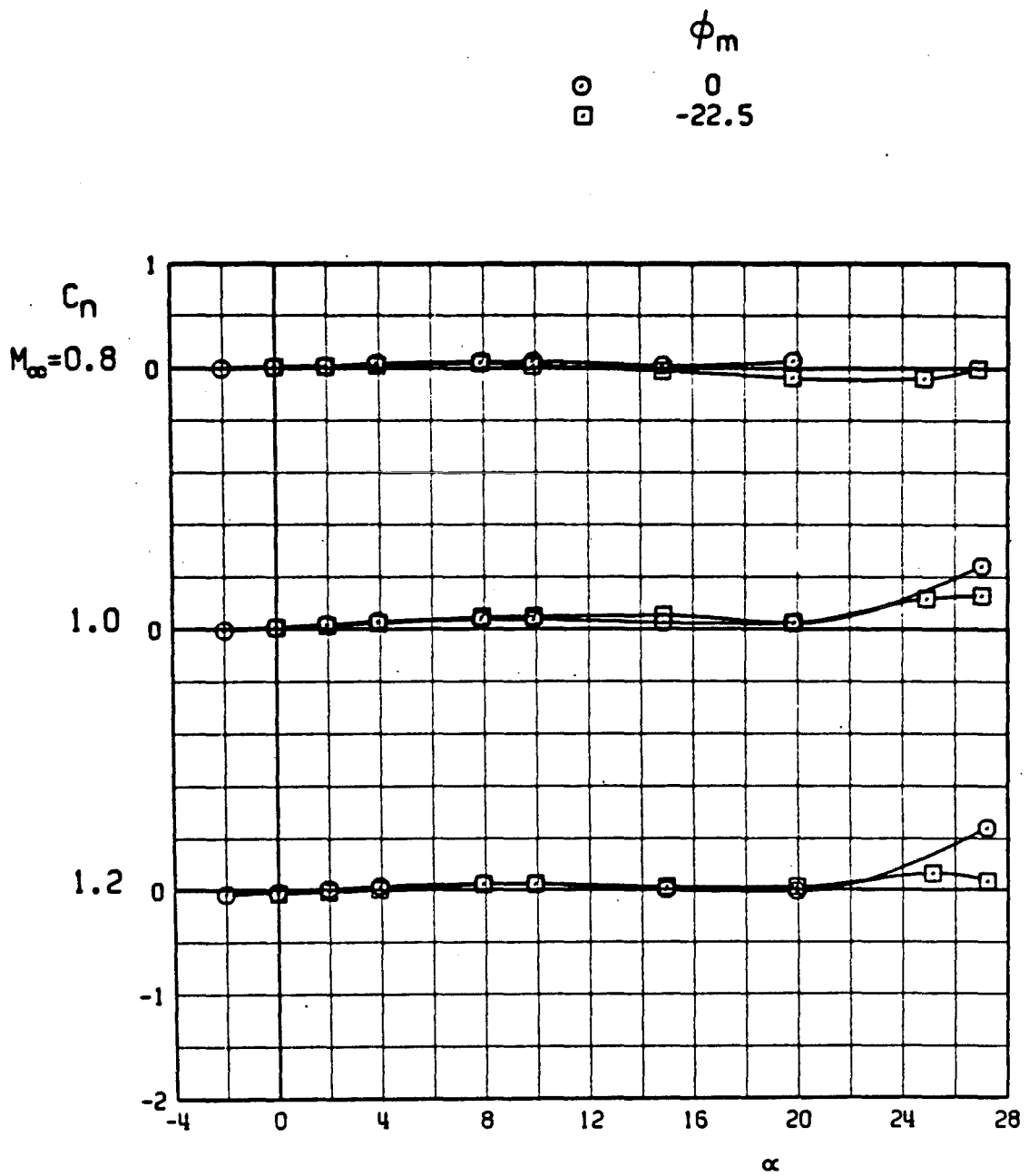
c. Axial-force coefficients  
Figure 13. Continued.



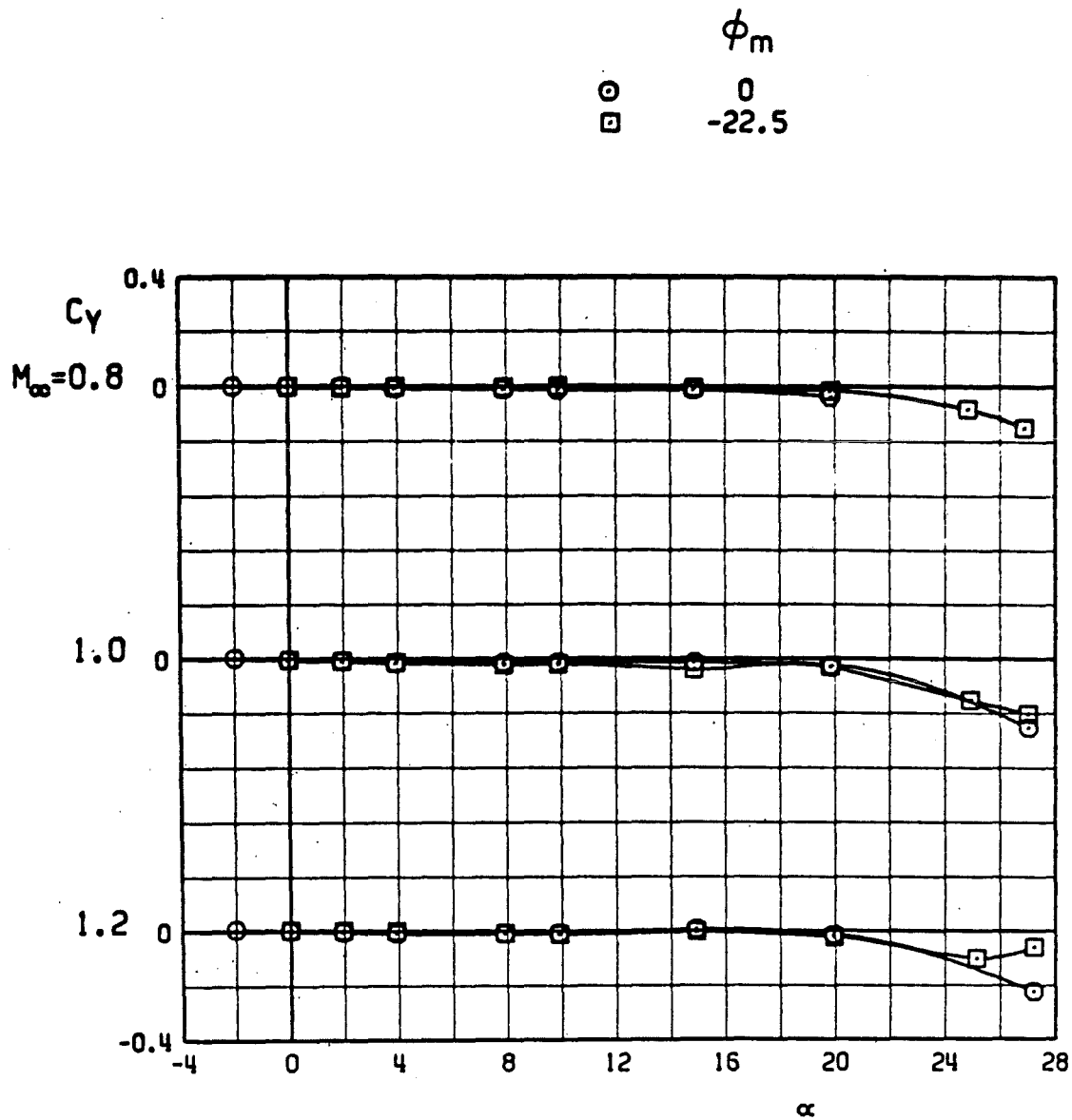
d. Forebody axial-force coefficients  
 Figure 13. Continued.



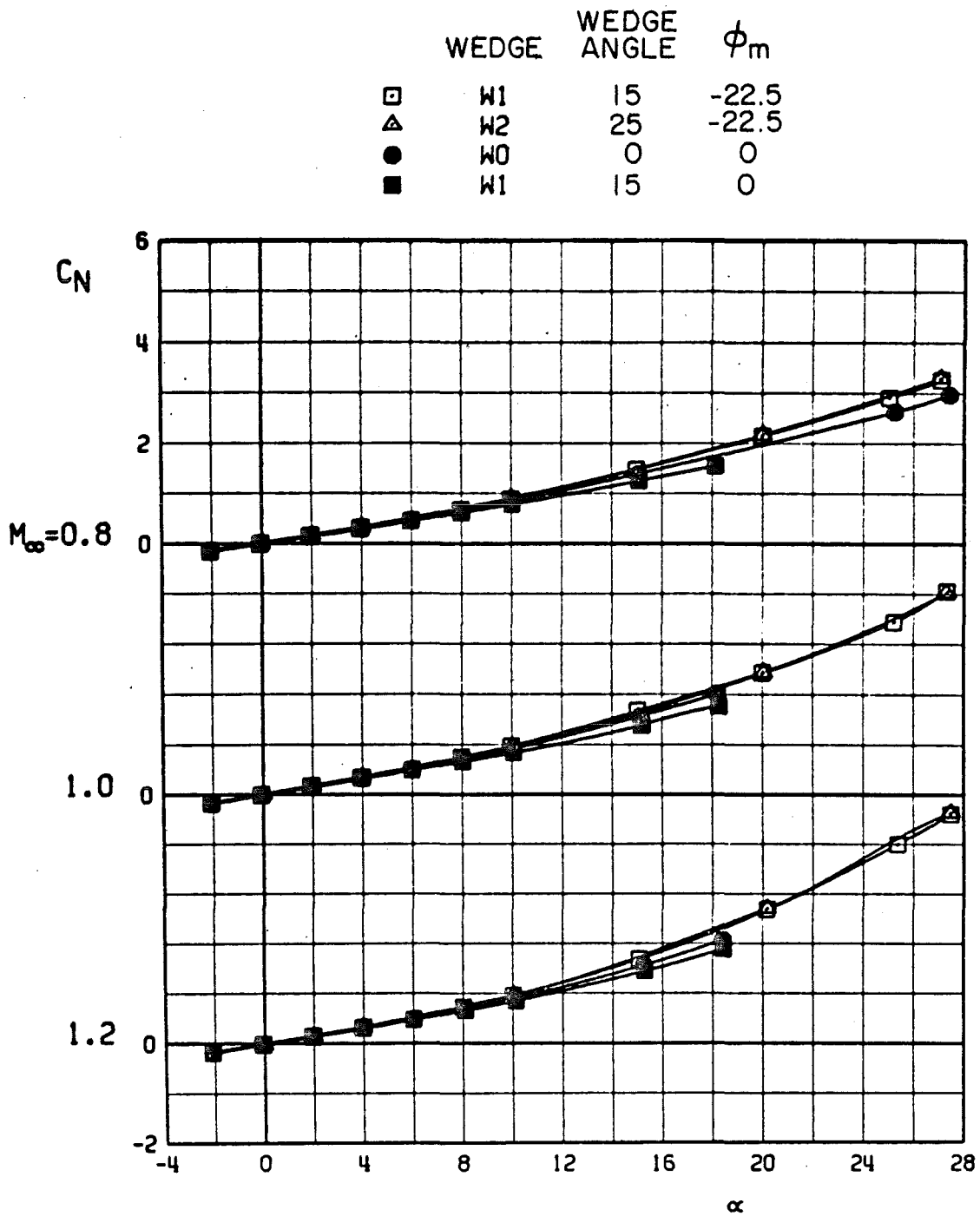
e. Rolling-moment coefficients  
Figure 13. Continued.



f. Yawing-moment coefficients  
Figure 13. Continued.



g. Side-force coefficients  
Figure 13. Concluded.

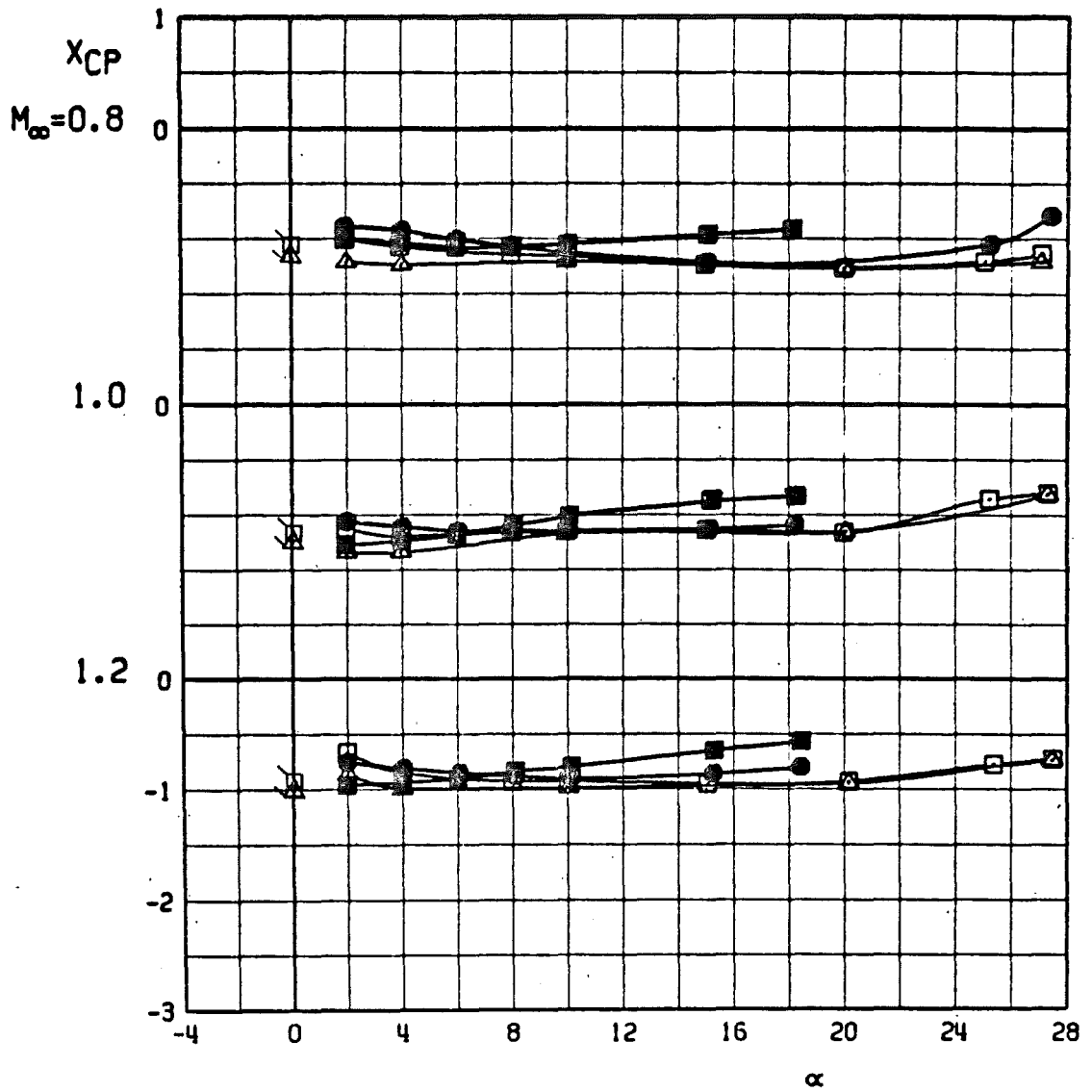


a. Normal-force coefficients

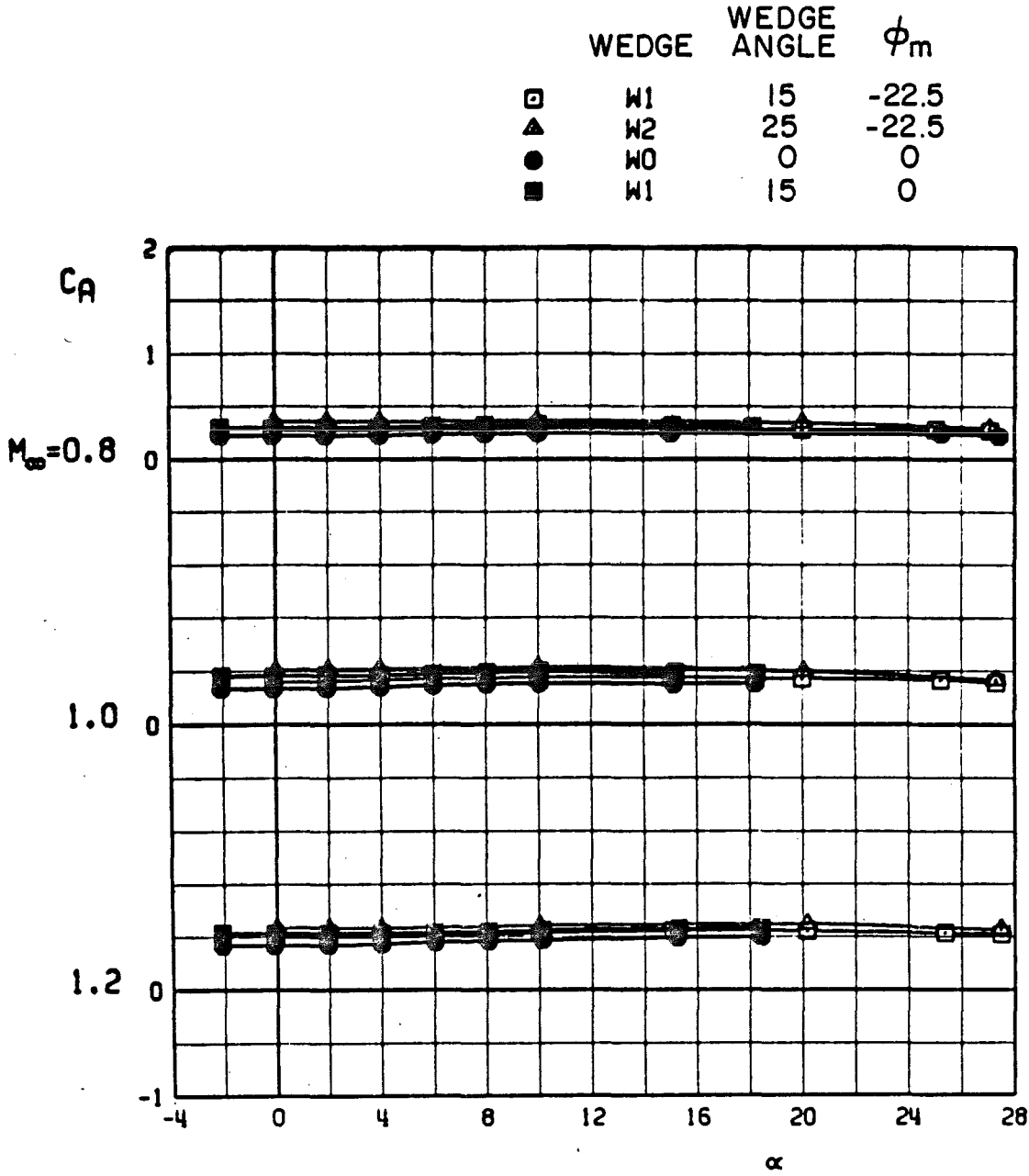
Figure 14. Effects of fin spin wedge angle on the static stability characteristics of the FF configuration.

	WEDGE	WEDGE ANGLE	$\phi_m$
□	W1	15	-22.5
△	W2	25	-22.5
●	W0	0	0
■	W1	15	0

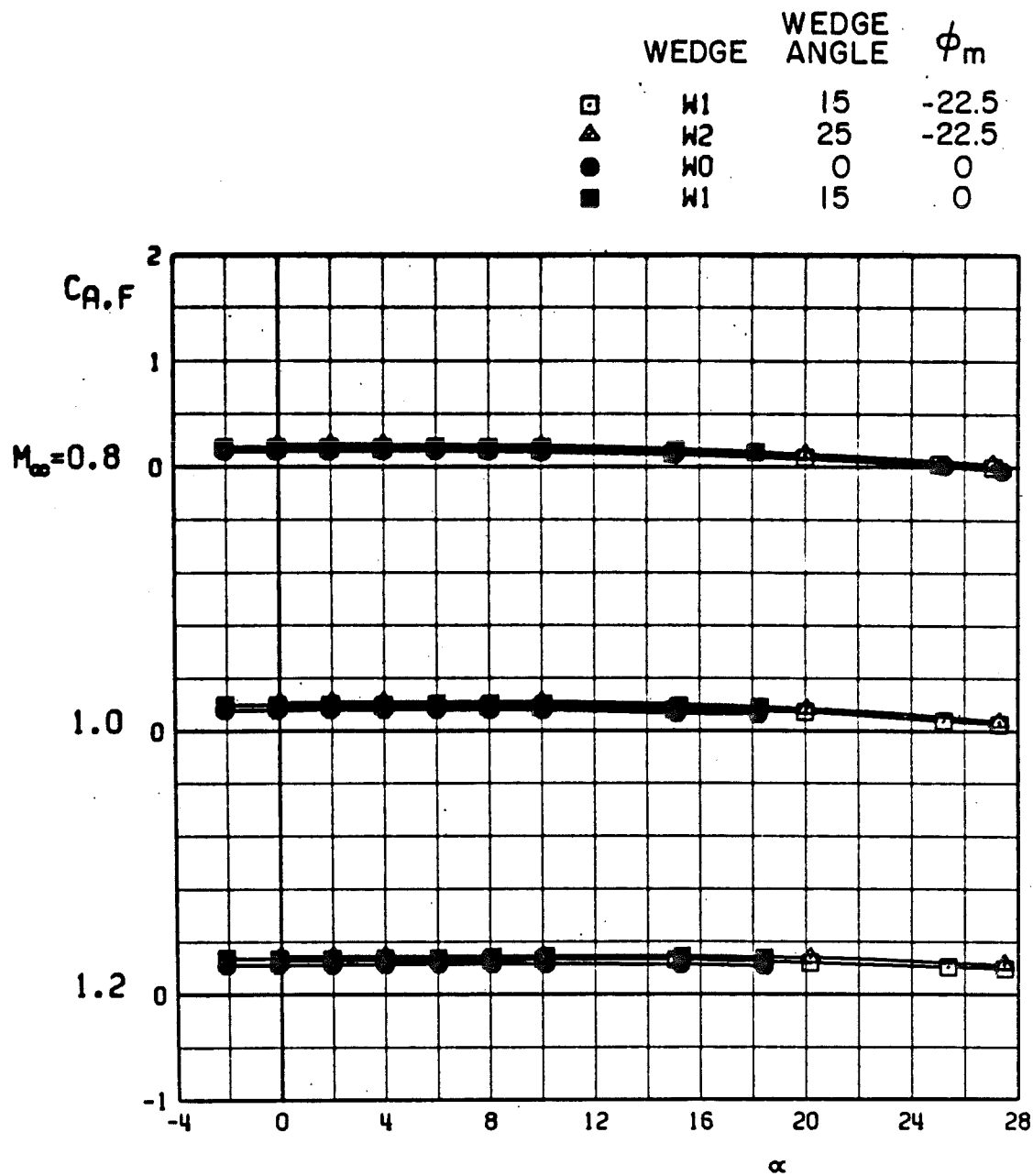
FLAGGED SYMBOLS INDICATE NEUTRAL-POINT LOCATION



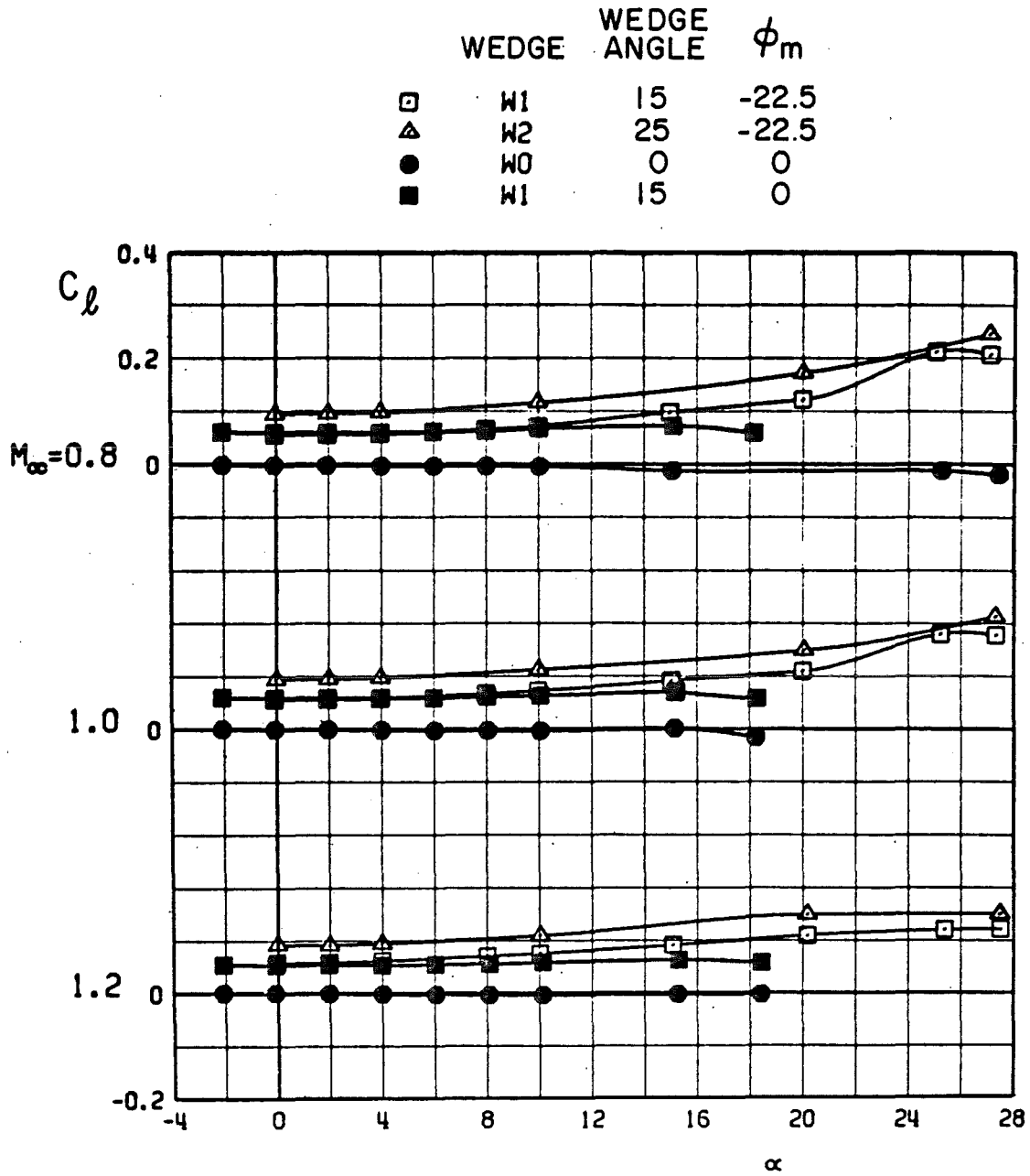
b. Center-of-pressure locations  
Figure 14. Continued.



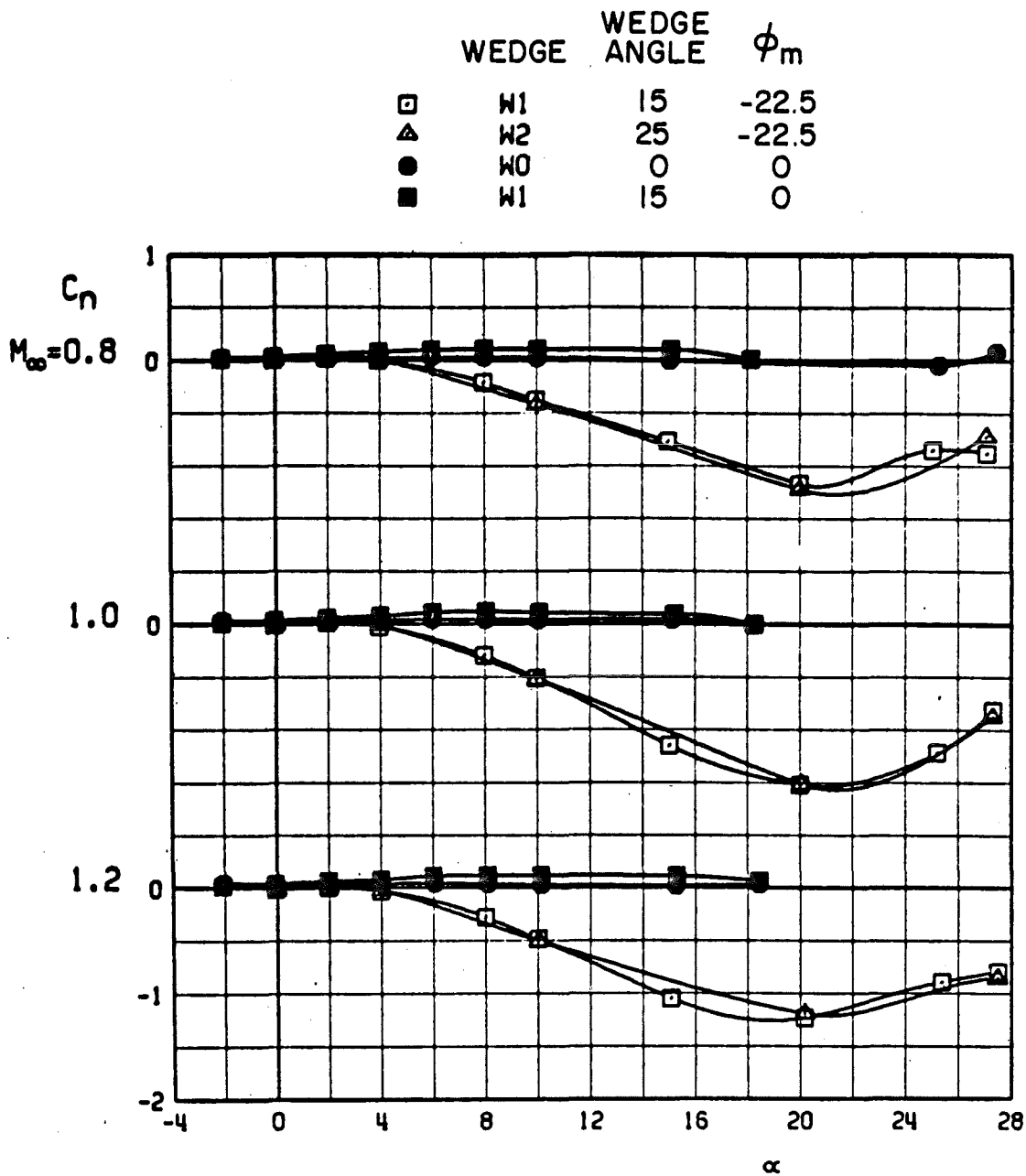
c. Axial-force coefficients  
 Figure 14. Continued.



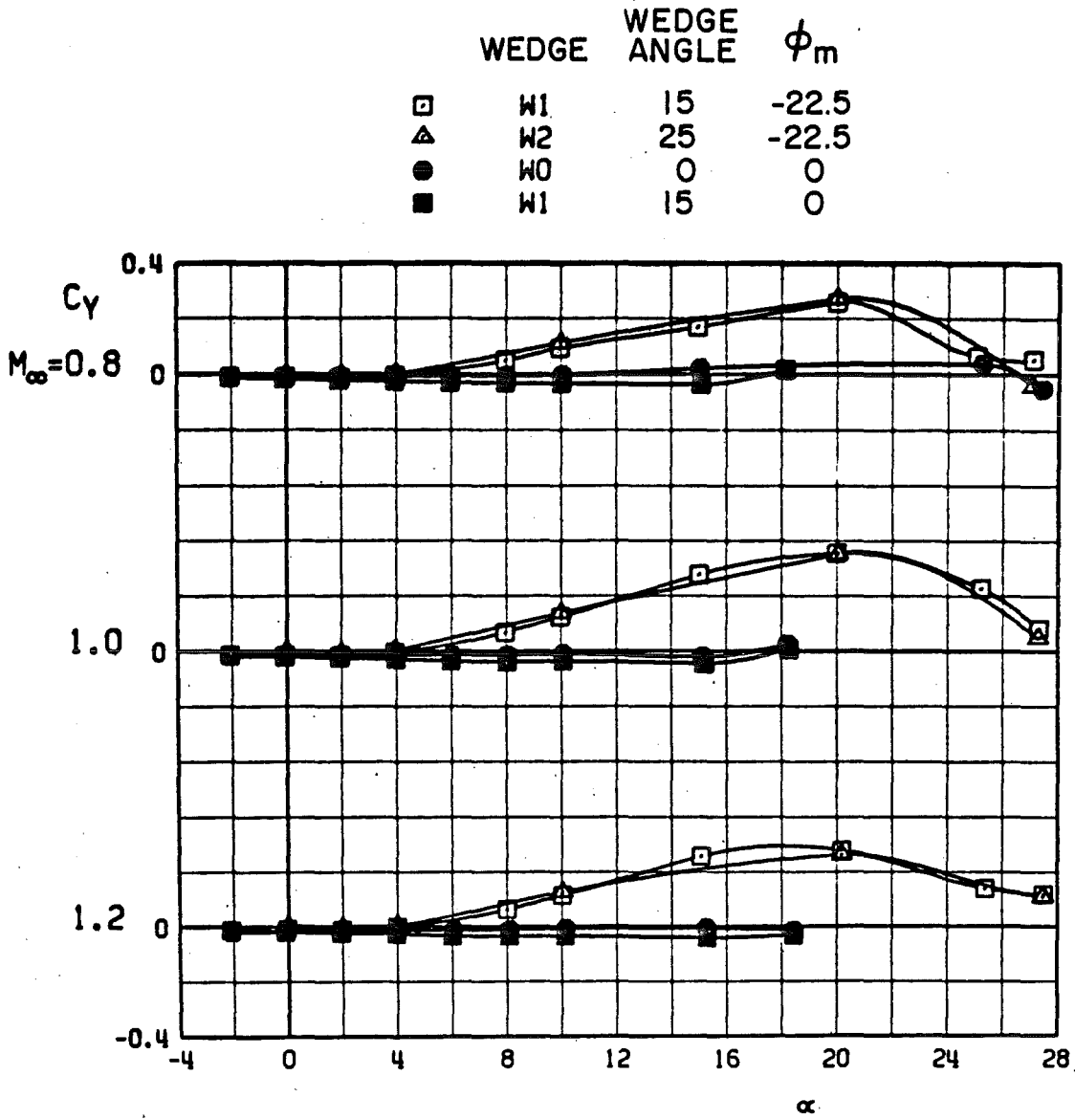
d. Forebody axial-force coefficients  
Figure 14. Continued.



e. Rolling-moment coefficients  
Figure 14. Continued.

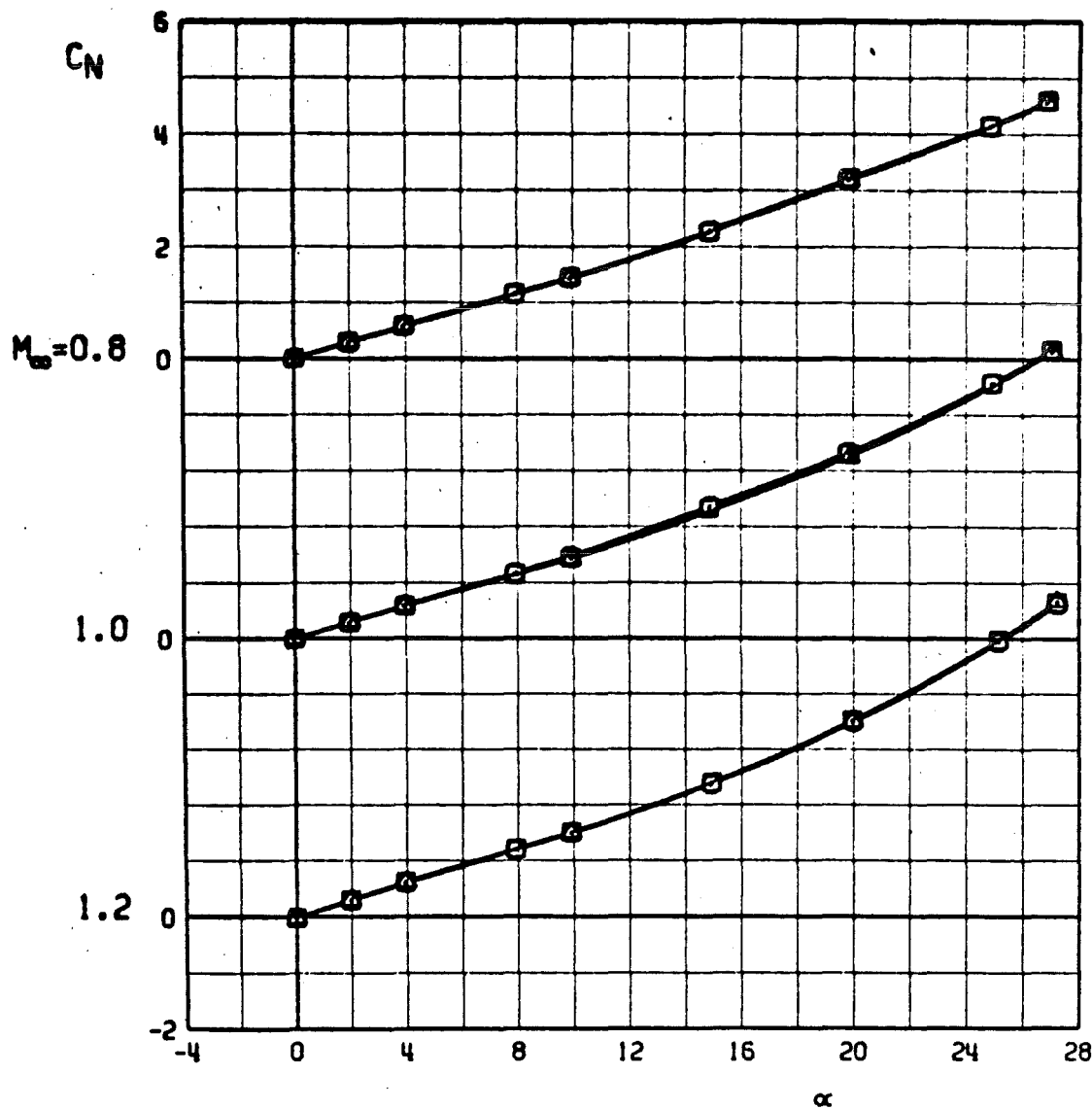


f. Yawing-moment coefficients  
Figure 14. Continued.



g. Side-force coefficients  
Figure 14. Concluded.

	WEDGE	WEDGE ANGLE
⊙	W0	0
□	W1	15
△	W2	20

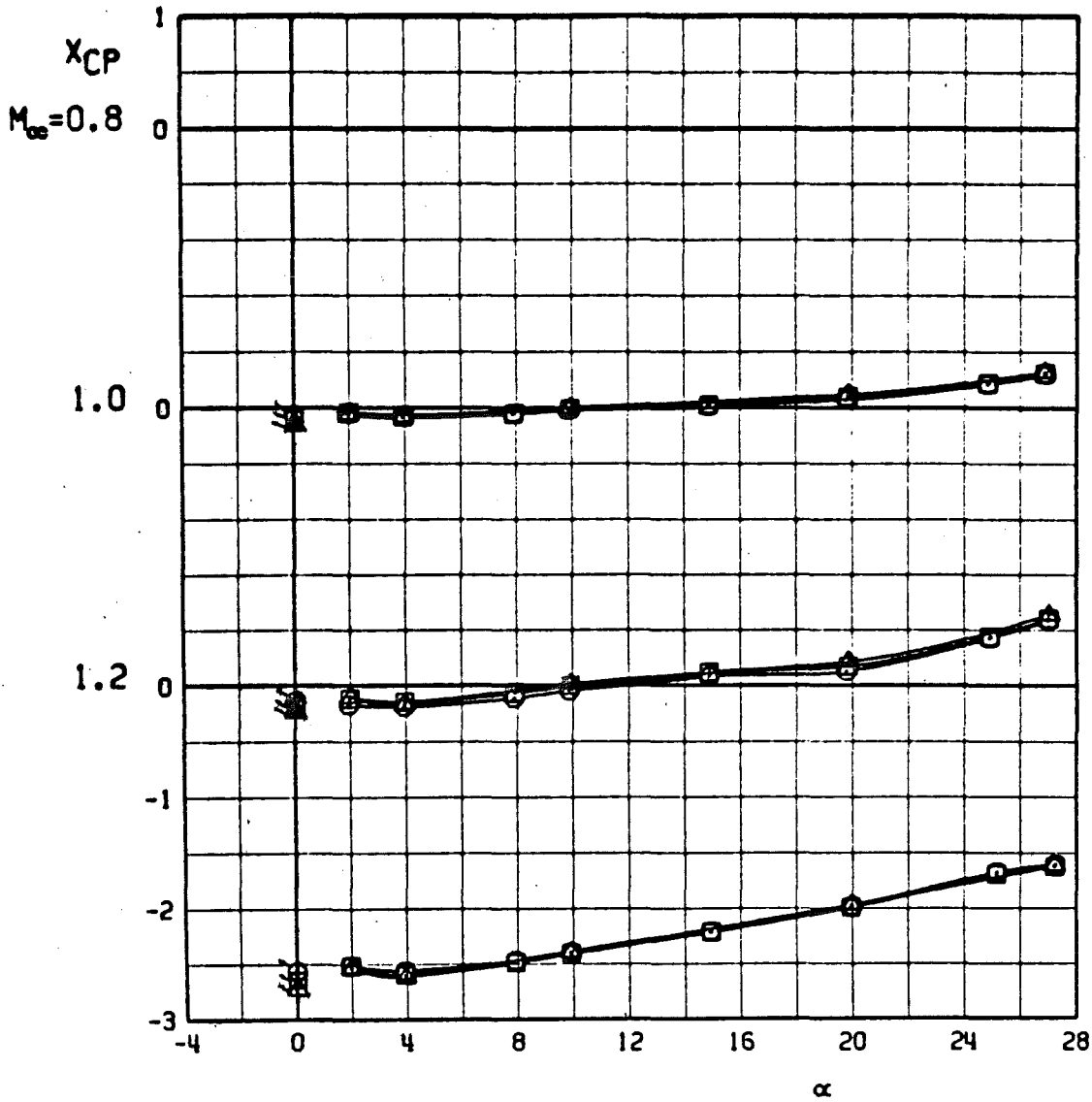


a. Normal-force coefficients

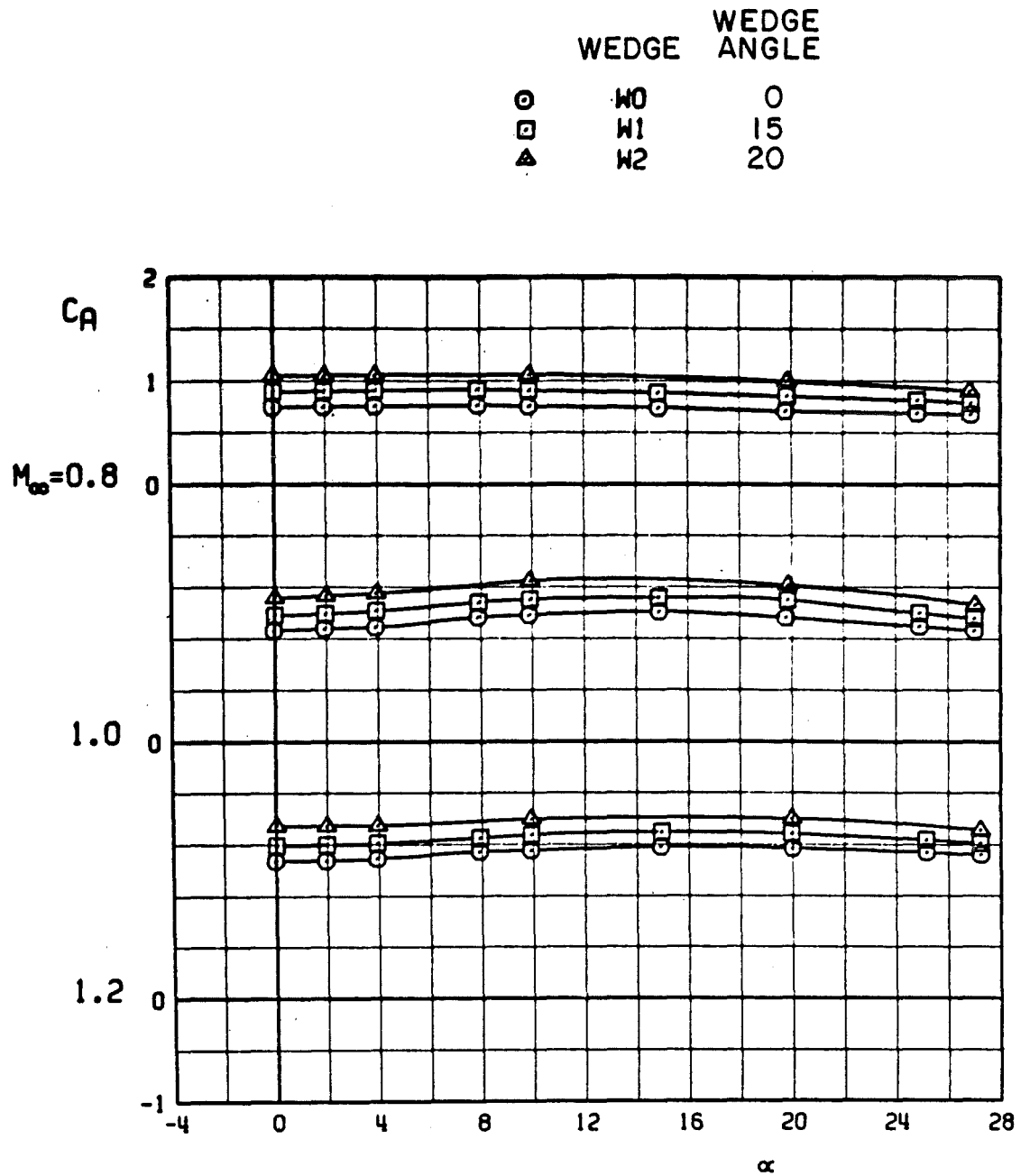
Figure 15. Effects of fin spin wedge angle on the static stability characteristics of the ISRe configuration,  $\phi_m = -22.5$ .

	WEDGE	WEDGE ANGLE
○	W0	0
□	W1	15
△	W2	20

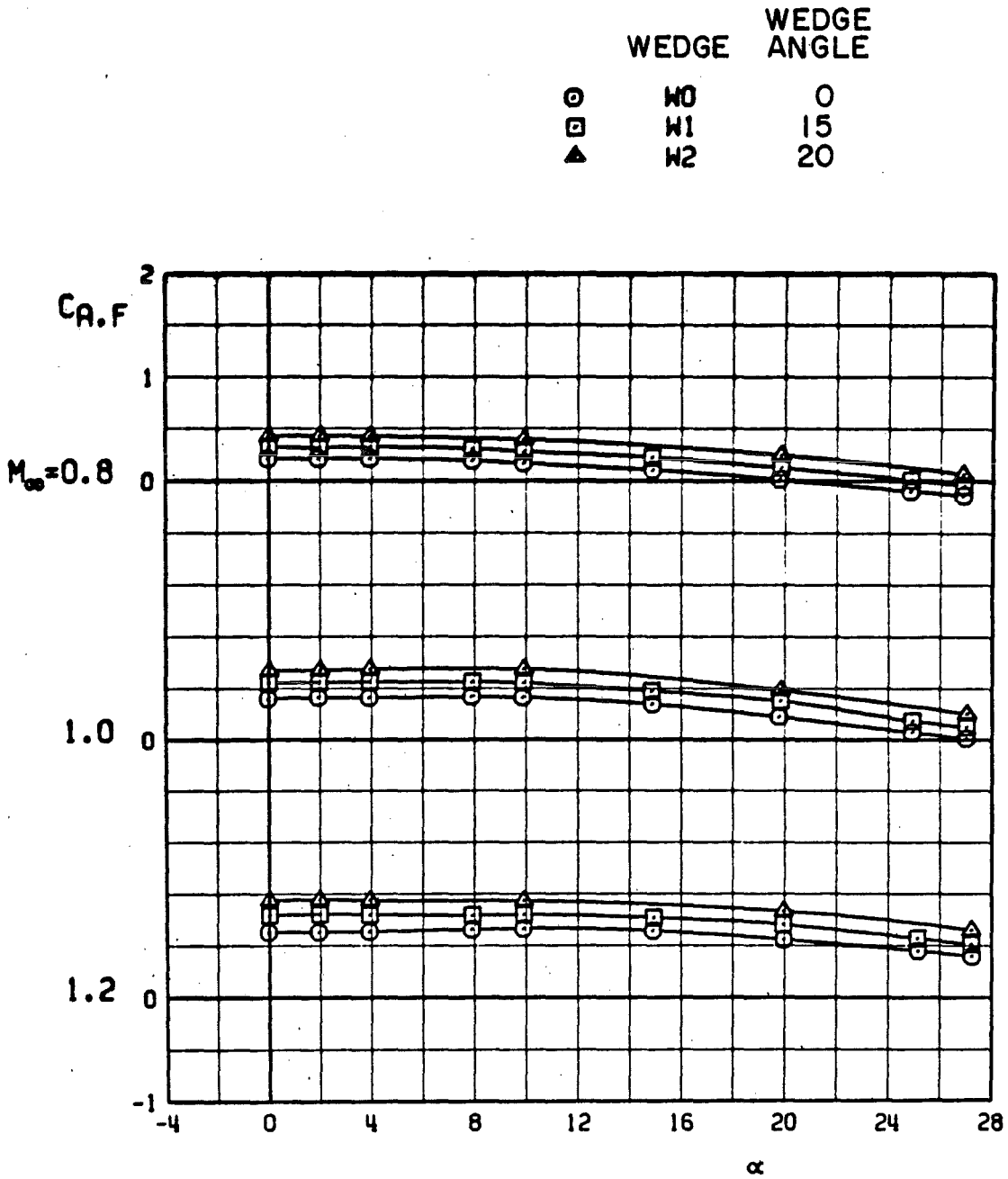
FLAGGED SYMBOLS INDICATE NEUTRAL-POINT LOCATION



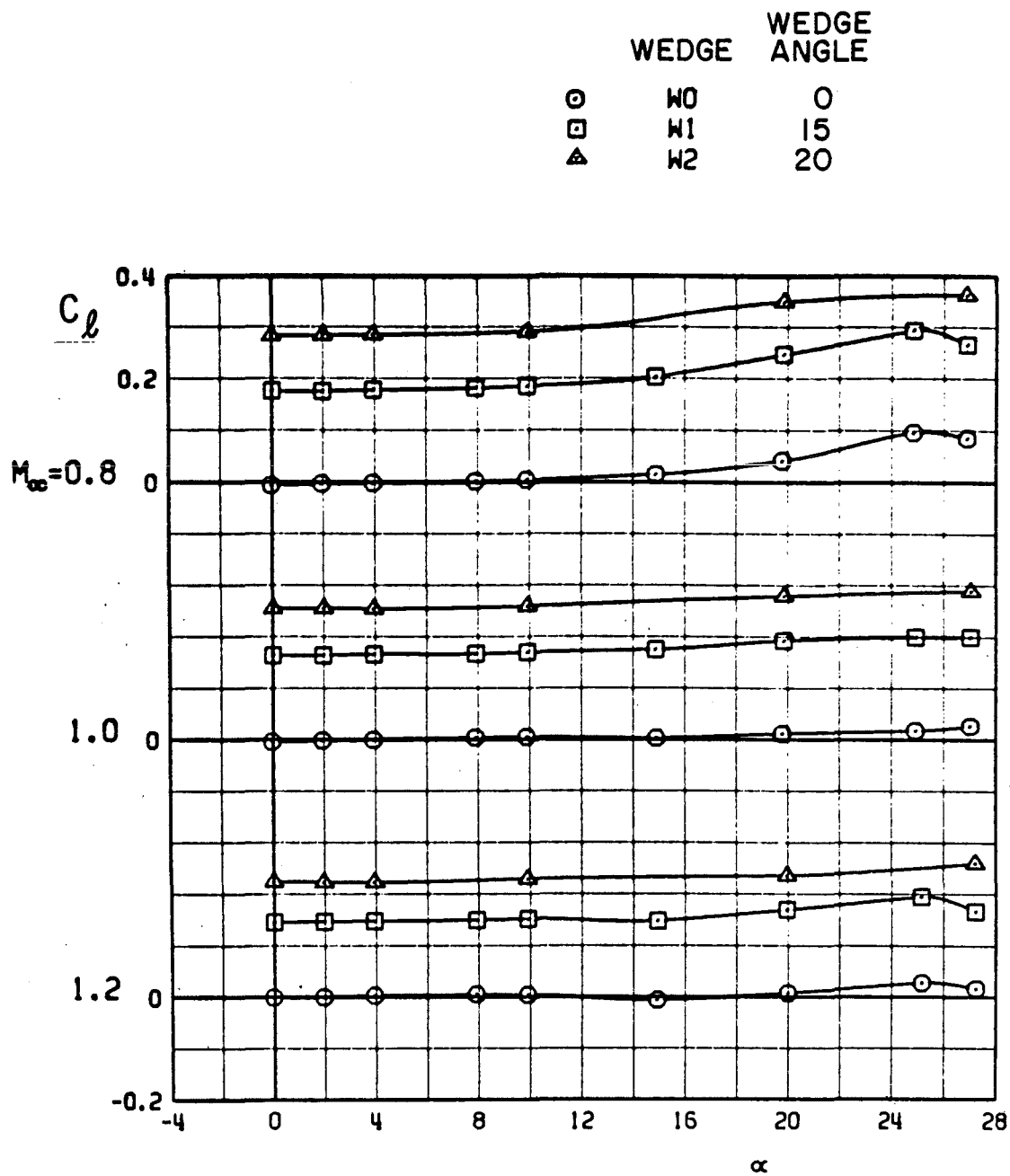
b. Center-of-pressure locations  
Figure 15. Continued.



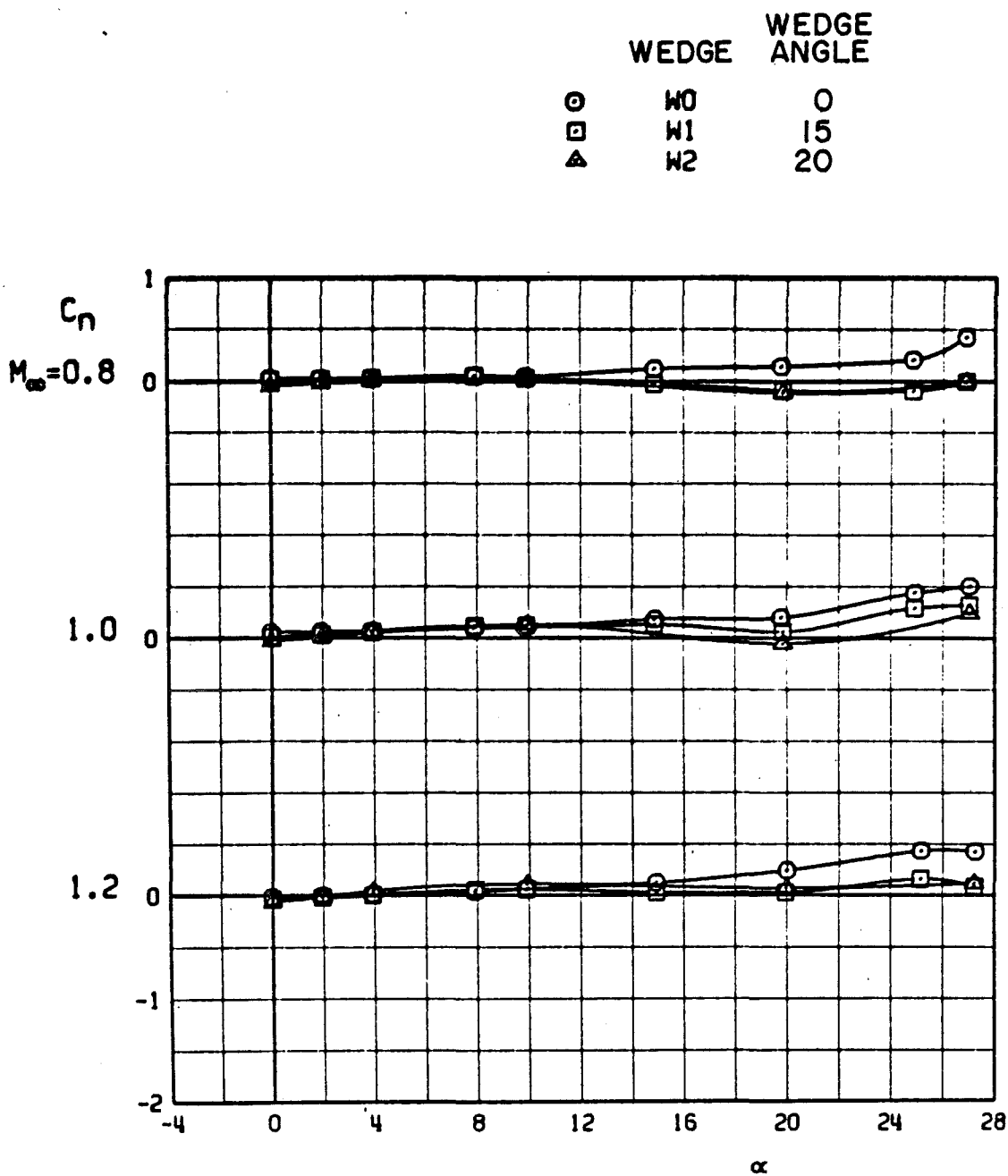
c. Axial-force coefficients  
Figure 15. Continued.



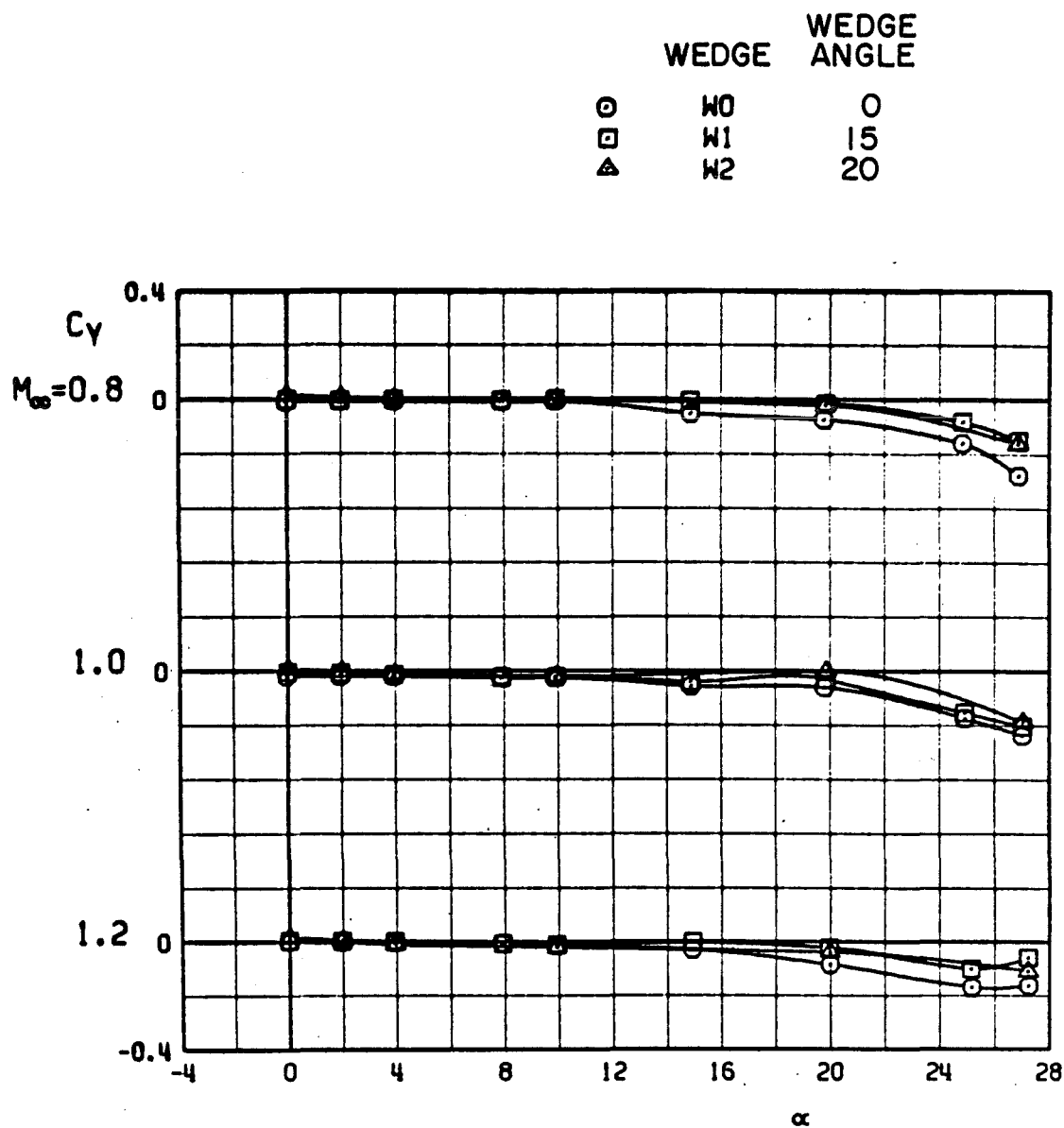
d. Forebody axial-force coefficients  
Figure 15. Continued.



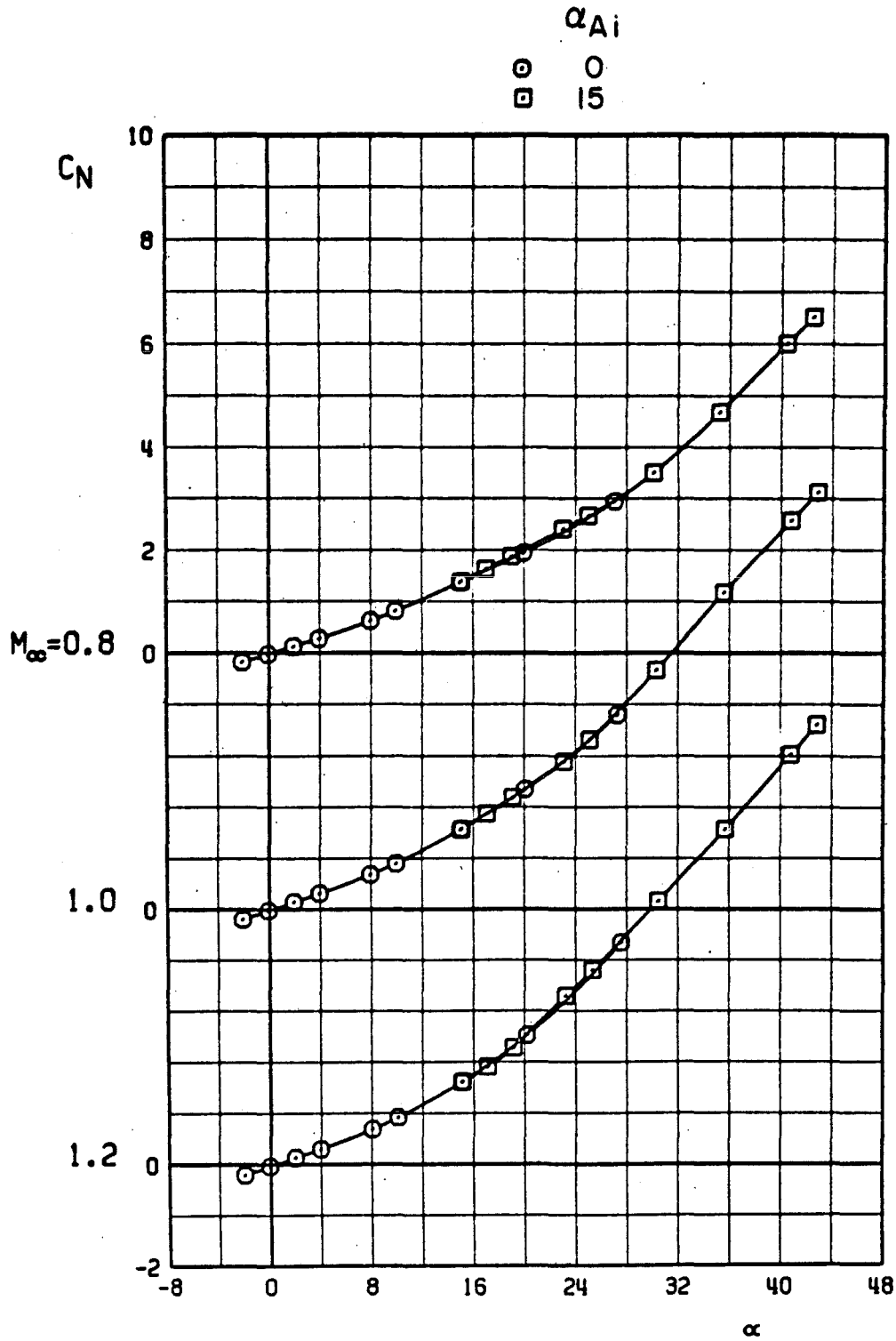
e. Rolling-moment coefficients  
 Figure 15. Continued.



f. Yawing-moment coefficients  
Figure 15. Continued.



g. Side-force coefficients  
Figure 15. Concluded.

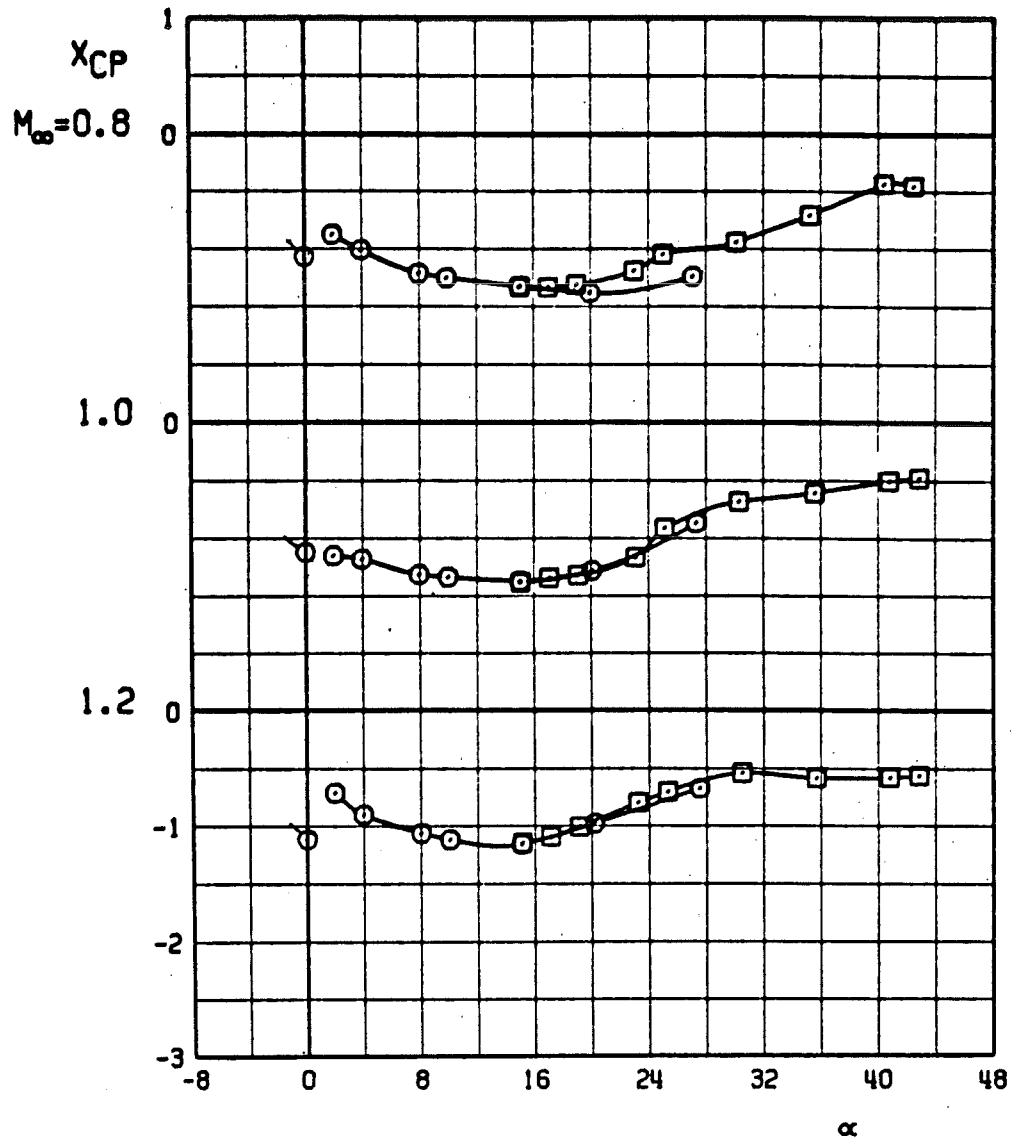


a. Normal-force coefficients

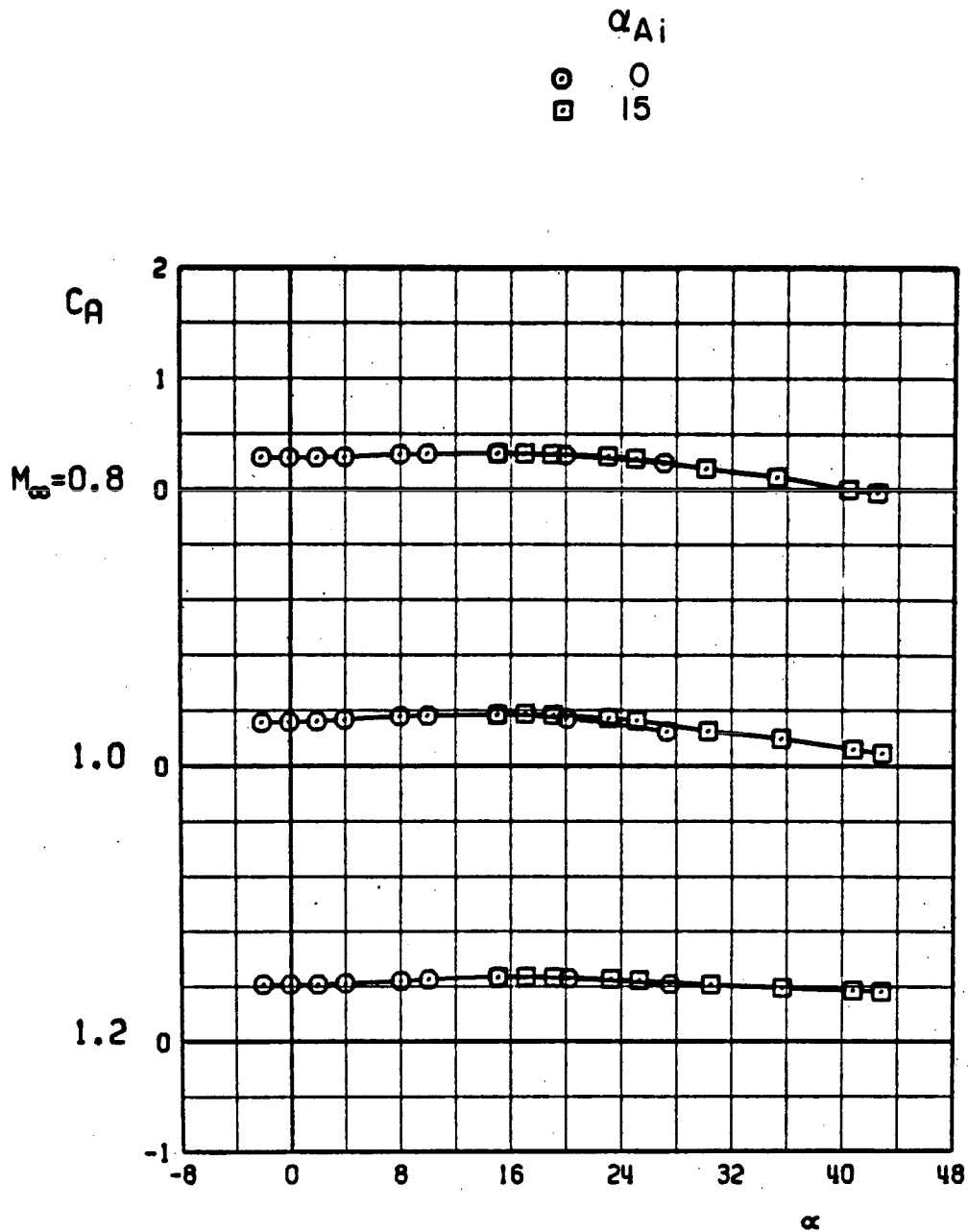
Figure 16. Effects of high angles of attack on the static stability characteristics of configuration FFSW1 with  $\phi_m = 45$ .

$\alpha_{Ai}$   
 ○ 0  
 □ 15

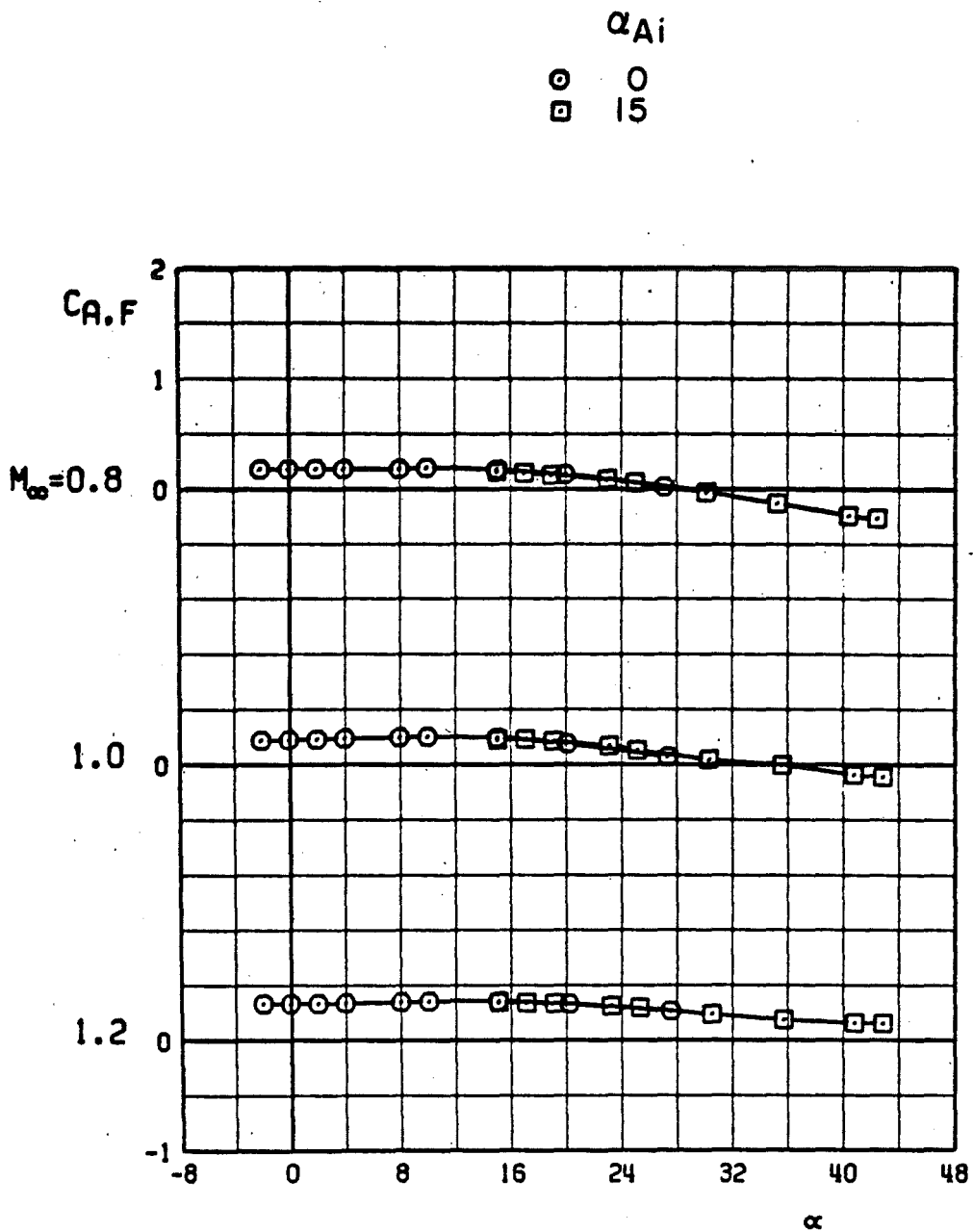
FLAGGED SYMBOLS INDICATE NEUTRAL-POINT LOCATION



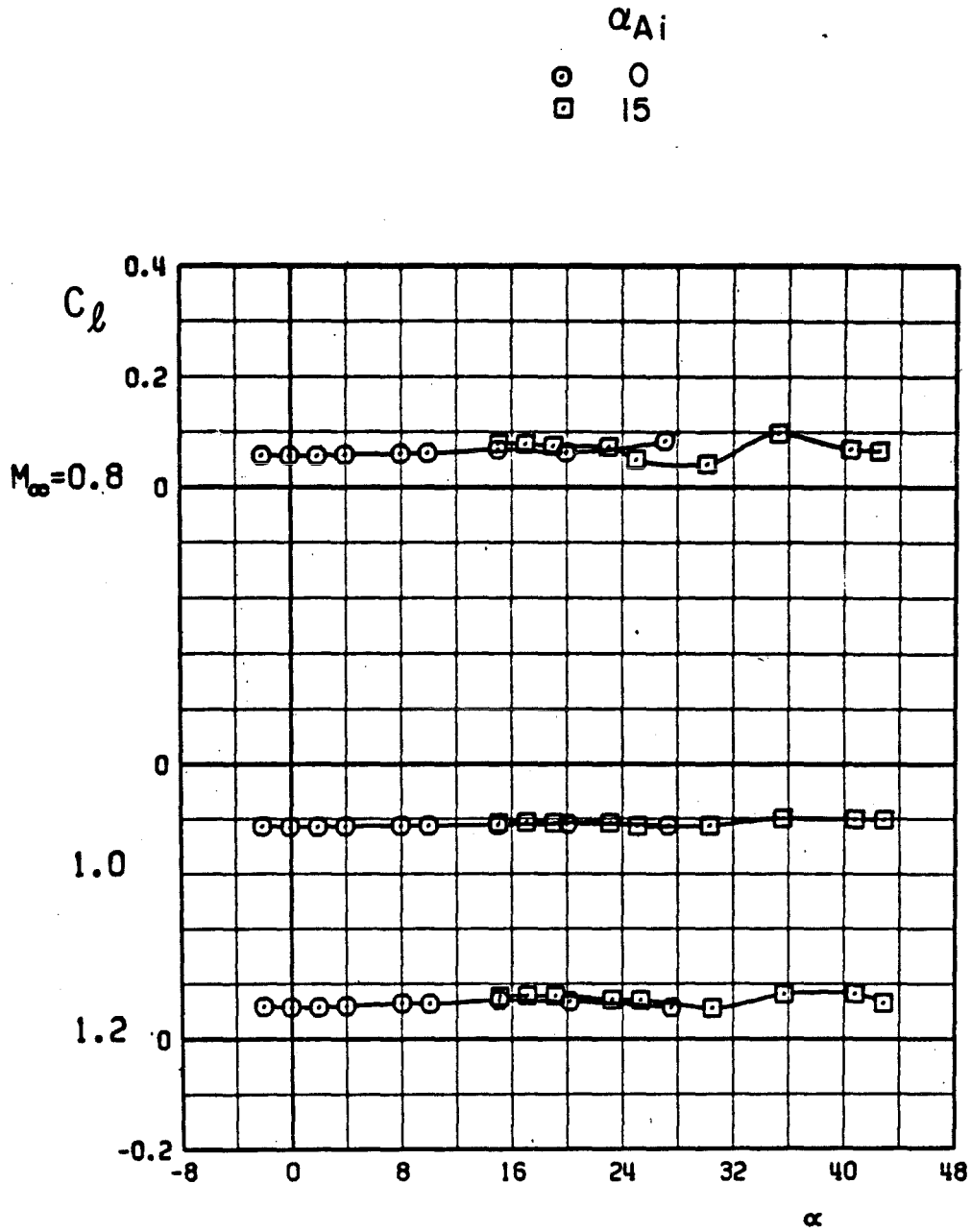
b. Center-of-pressure locations  
 Figure 16. Continued.



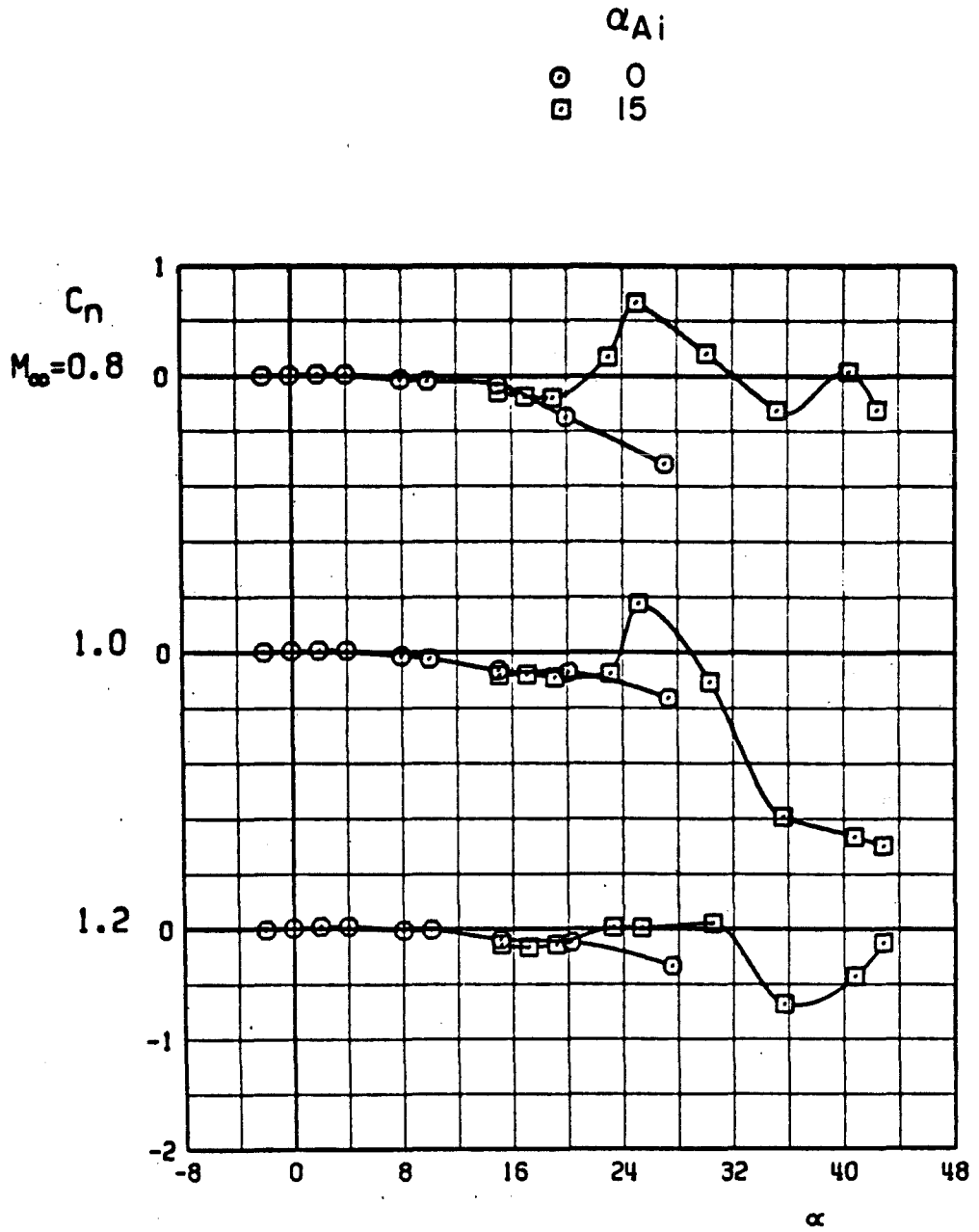
c. Axial-force coefficients  
Figure 16. Continued.



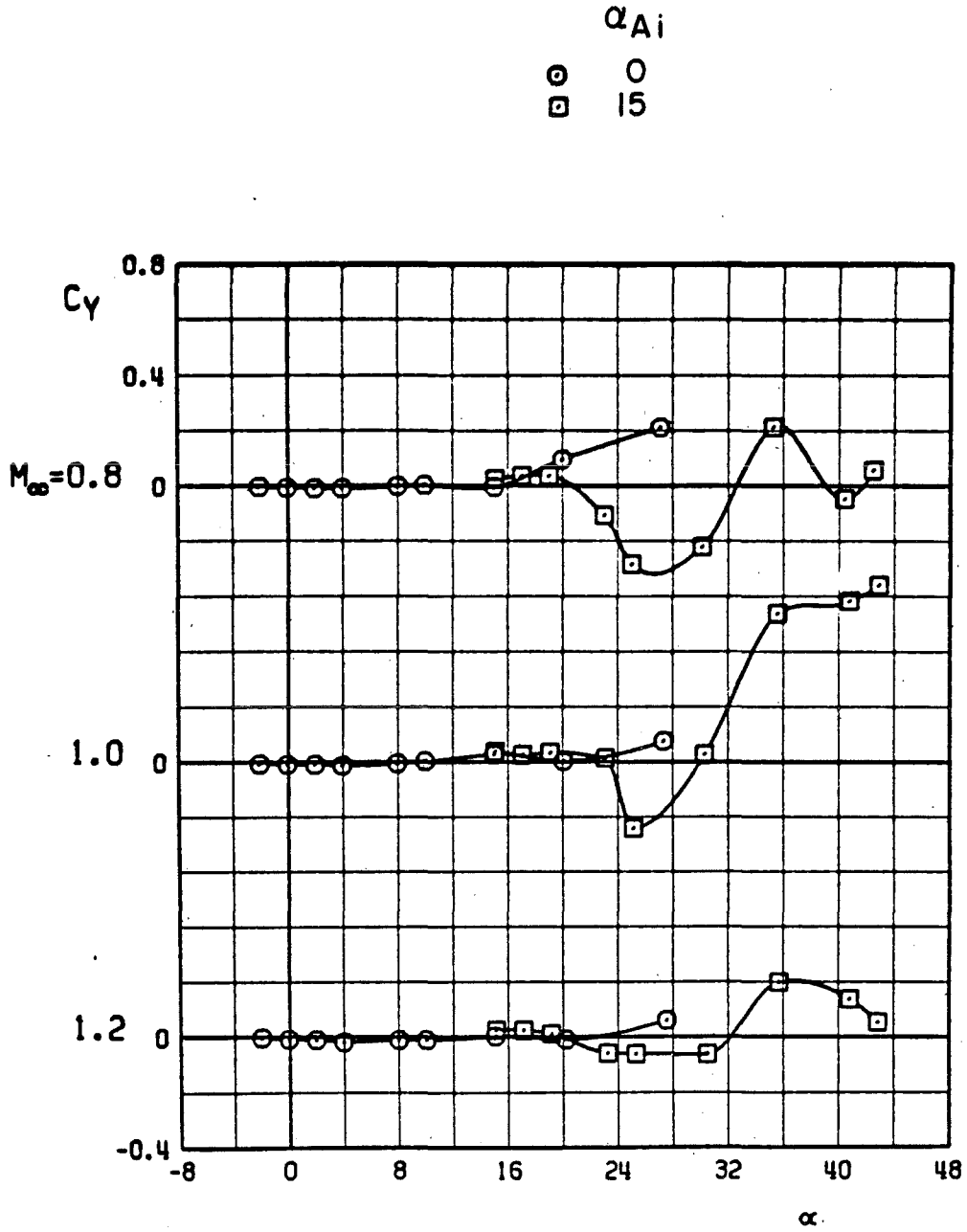
d. Forebody axial-force coefficients  
Figure 16. Continued.



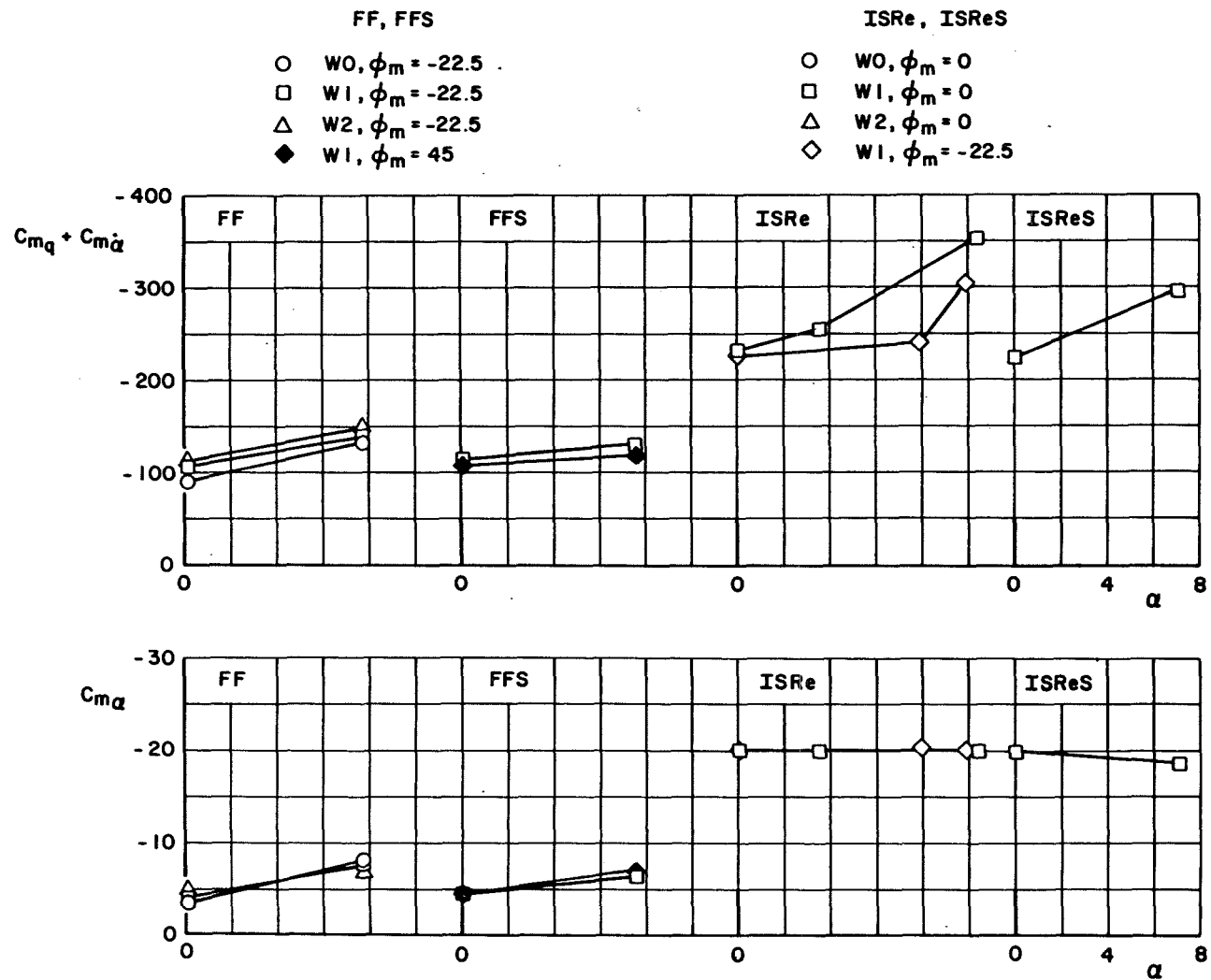
e. Rolling-moment coefficients  
Figure 16. Continued.



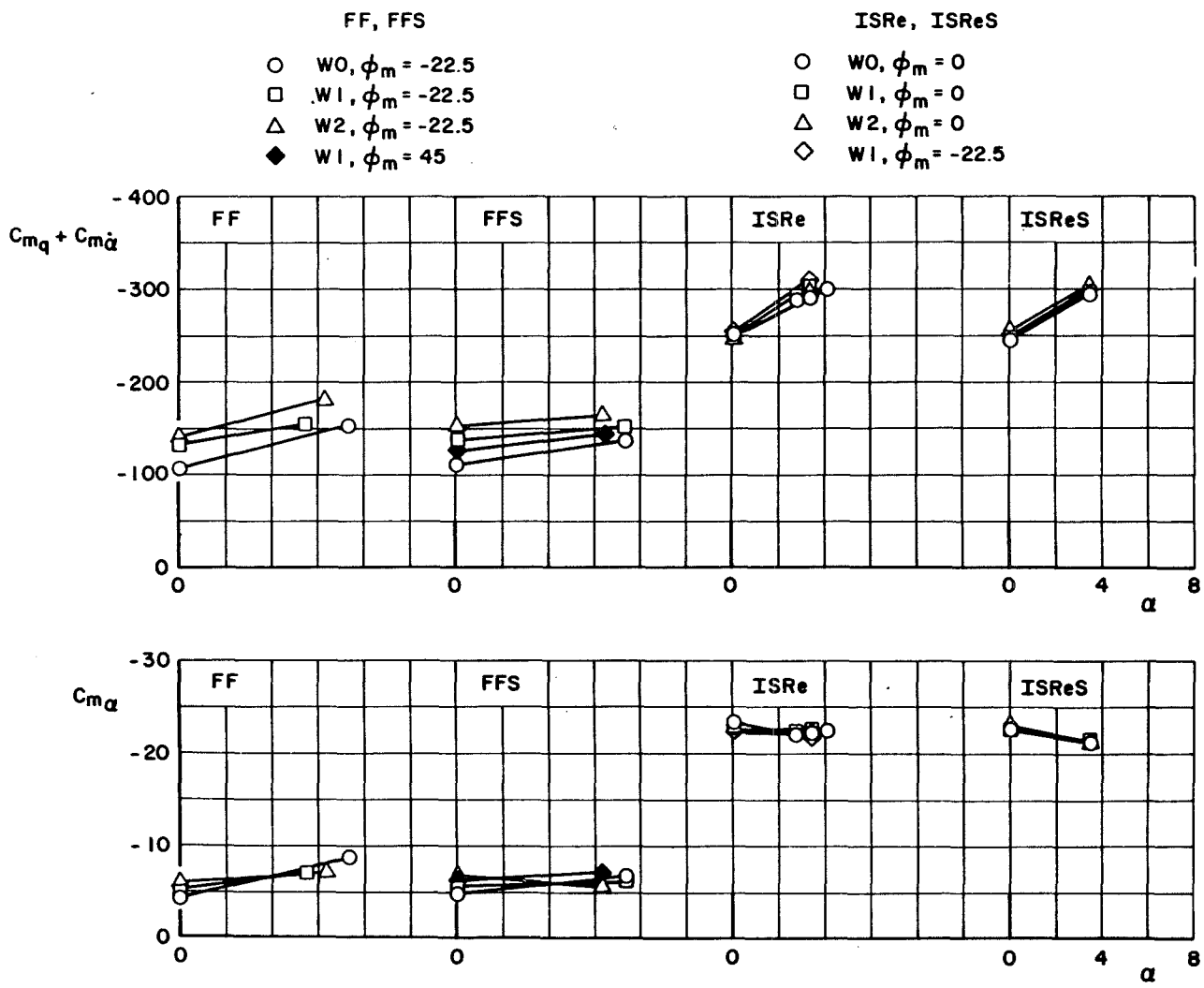
f. Yawing-moment coefficients  
Figure 16. Continued.



g. Side-force coefficients  
Figure 16. Concluded.

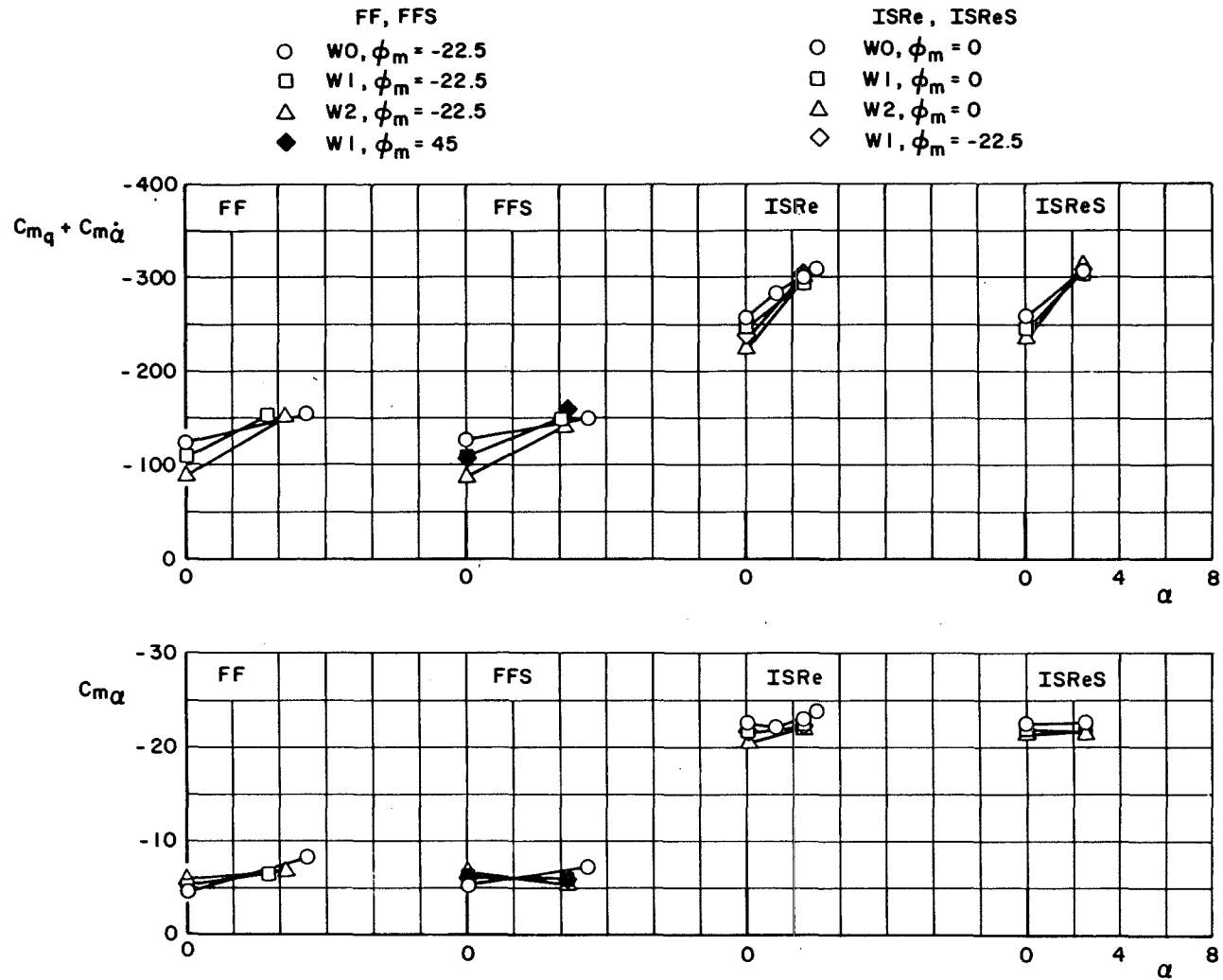


a. Mach number 0.40  
 Figure 17. Variation of  $C_{m_q} + C_{m_{\dot{\alpha}}}$  and  $C_{m_{\alpha}}$  with angle of attack.

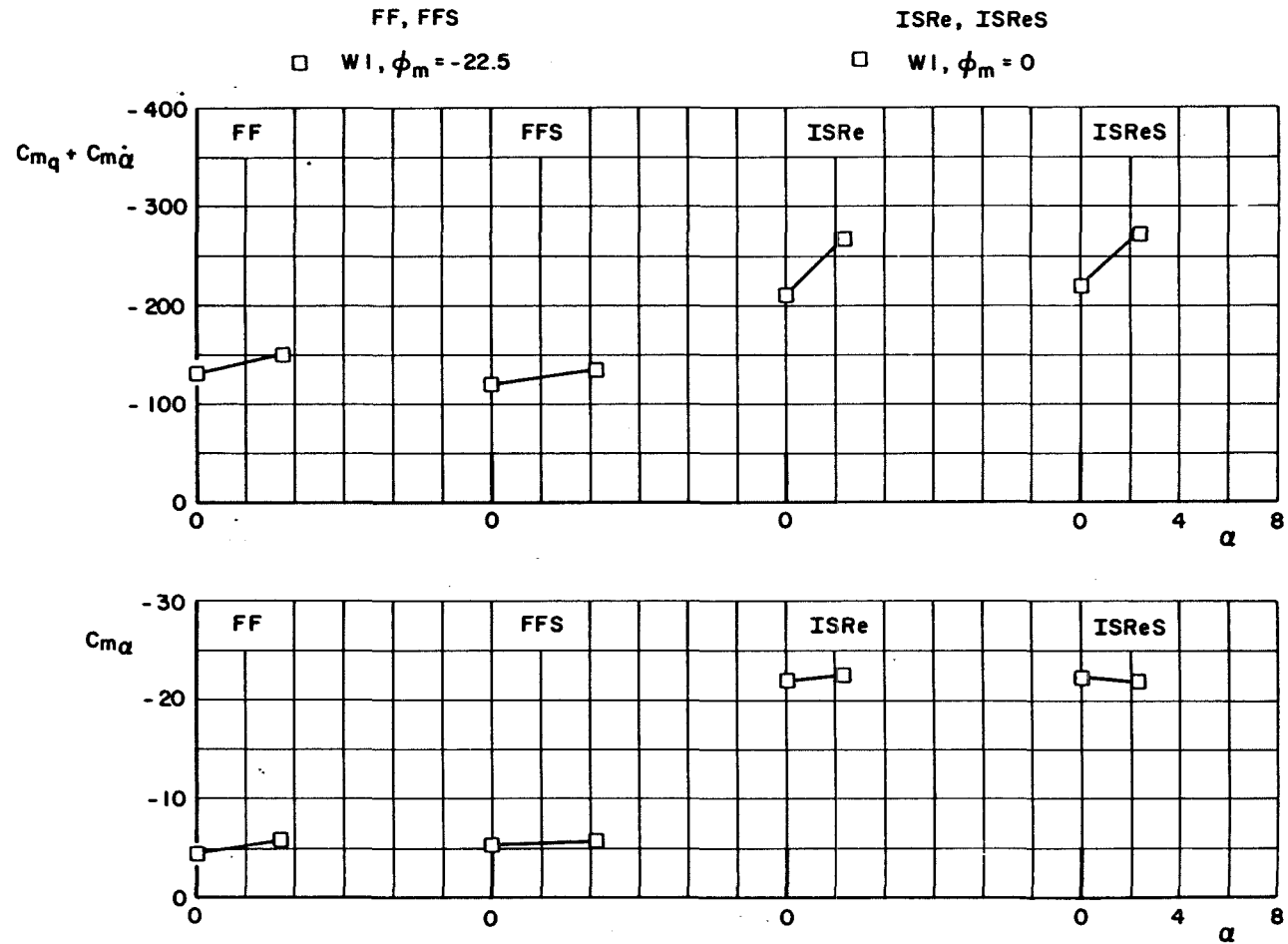


b. Mach number 0.80  
Figure 17. Continued.

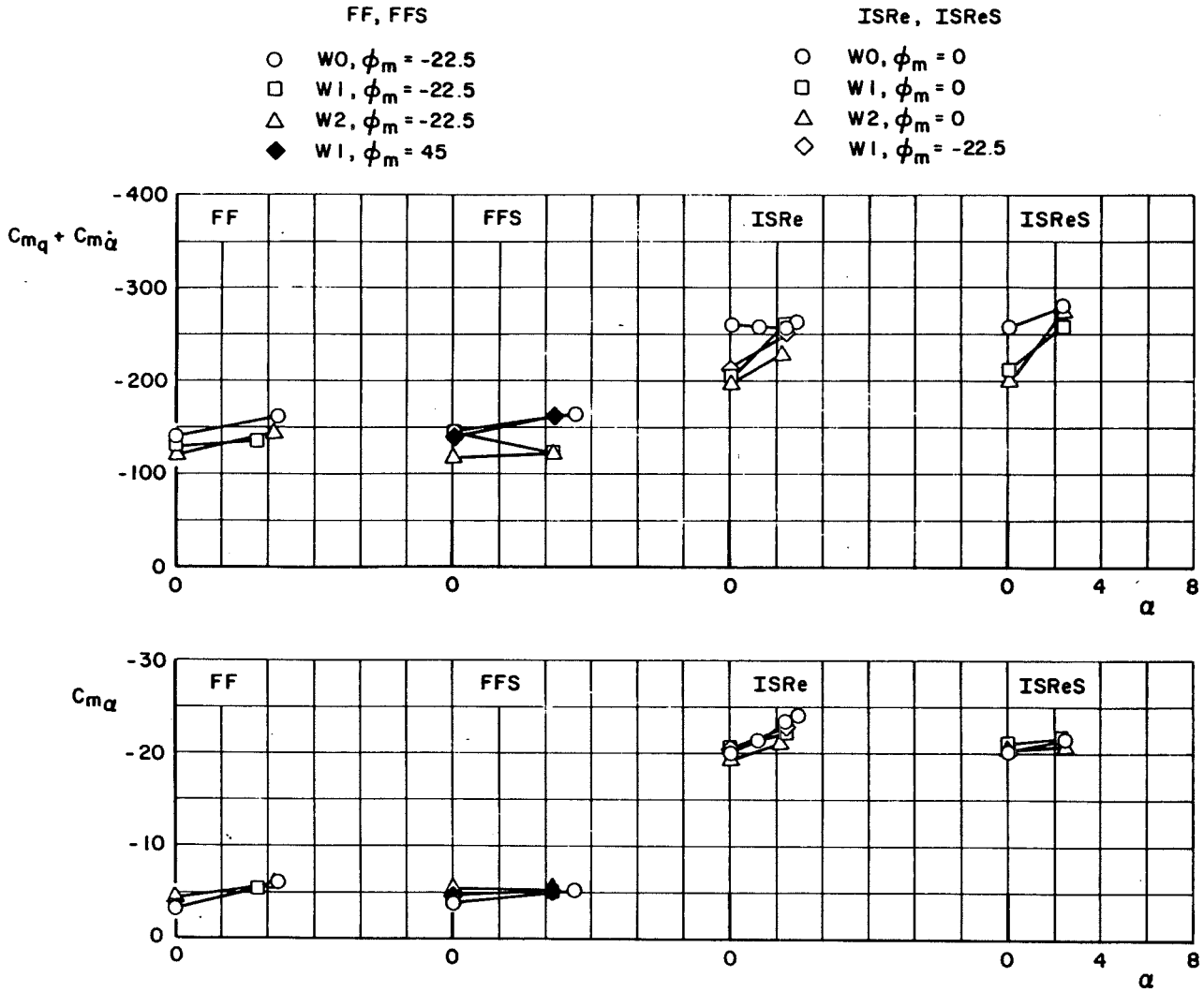




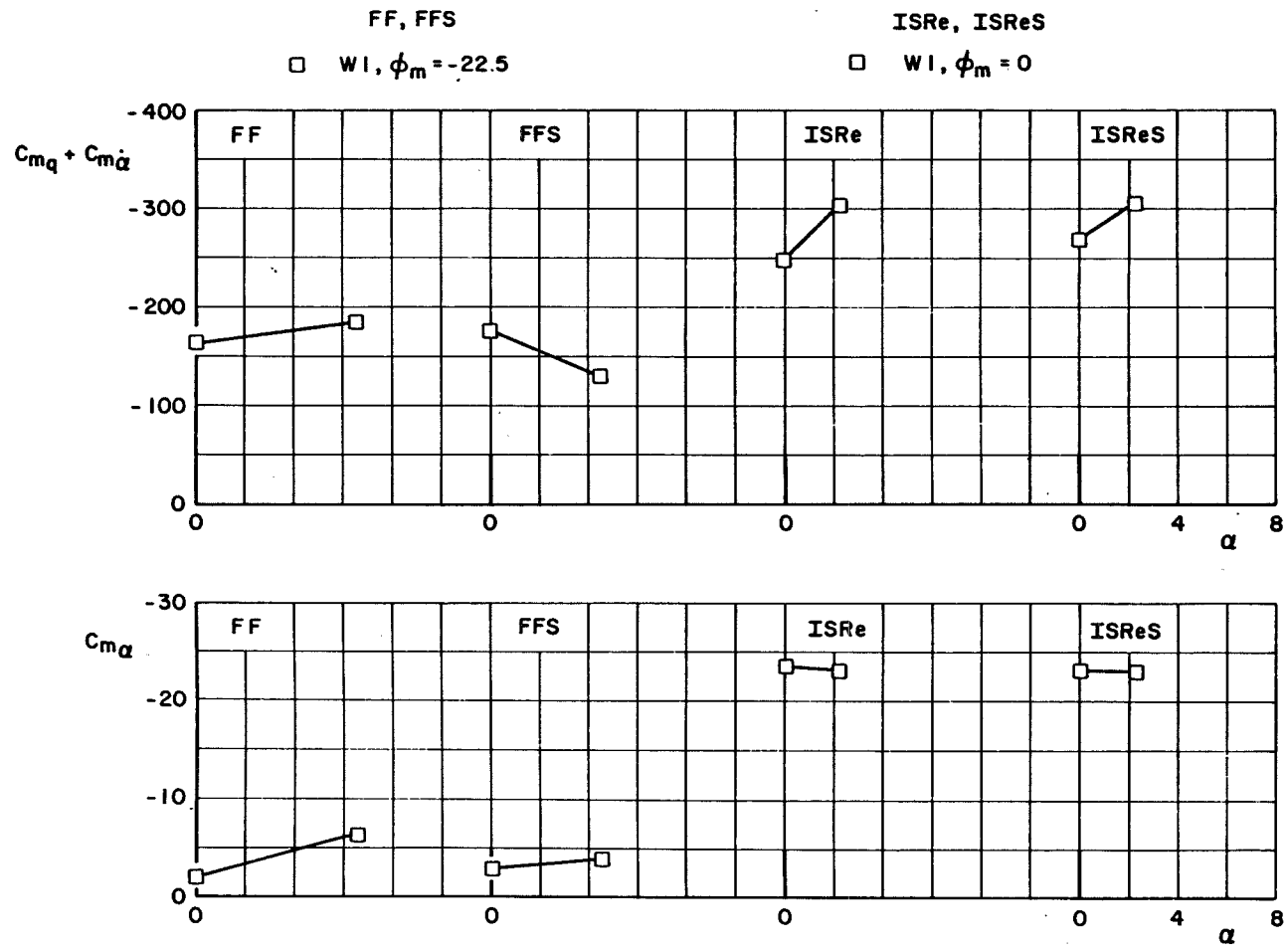
d. Mach number 1.00  
Figure 17. Continued.



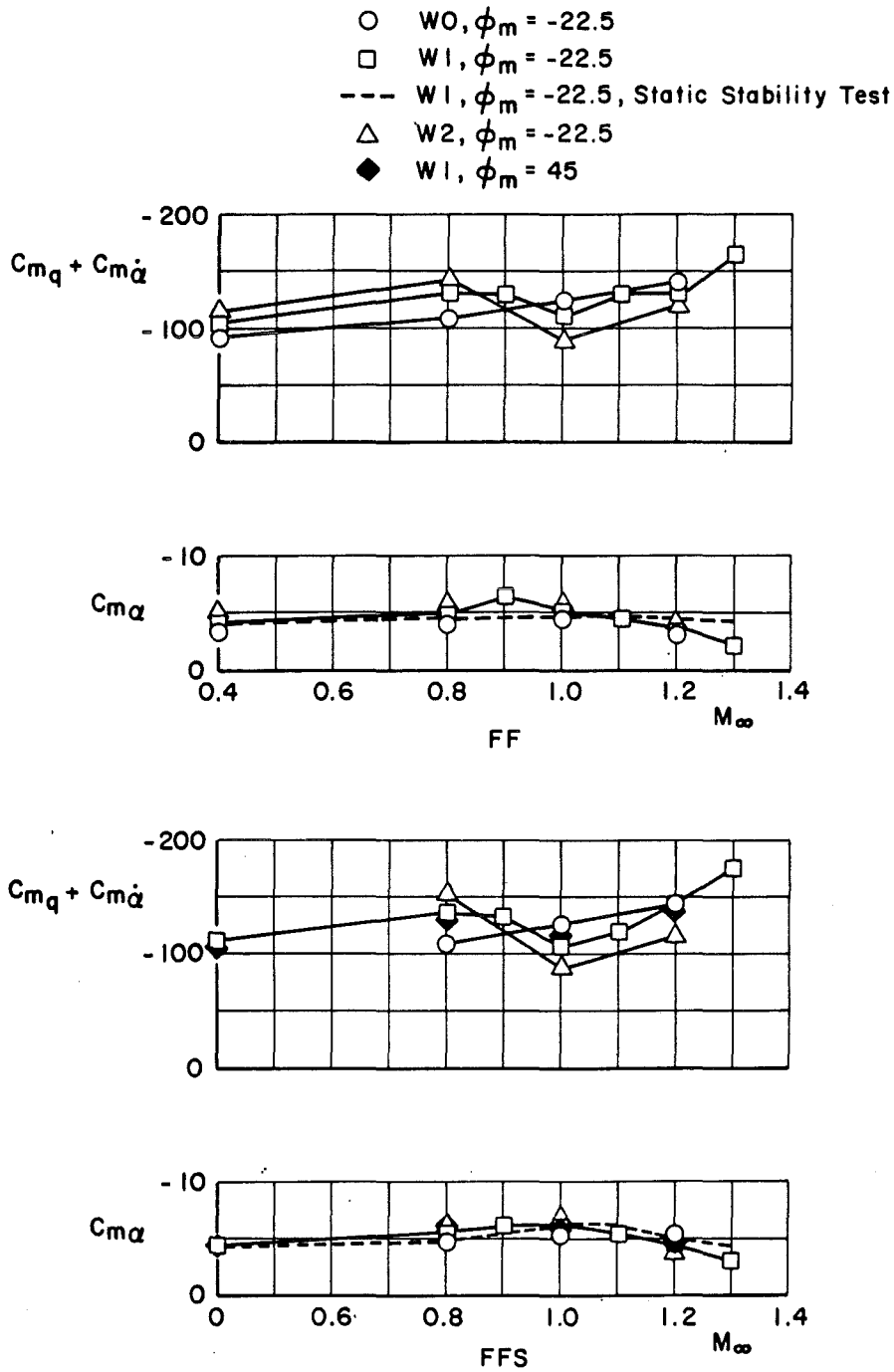
e. Mach number 1.10  
Figure 17. Continued.



f. Mach number 1.20  
Figure 17. Continued.

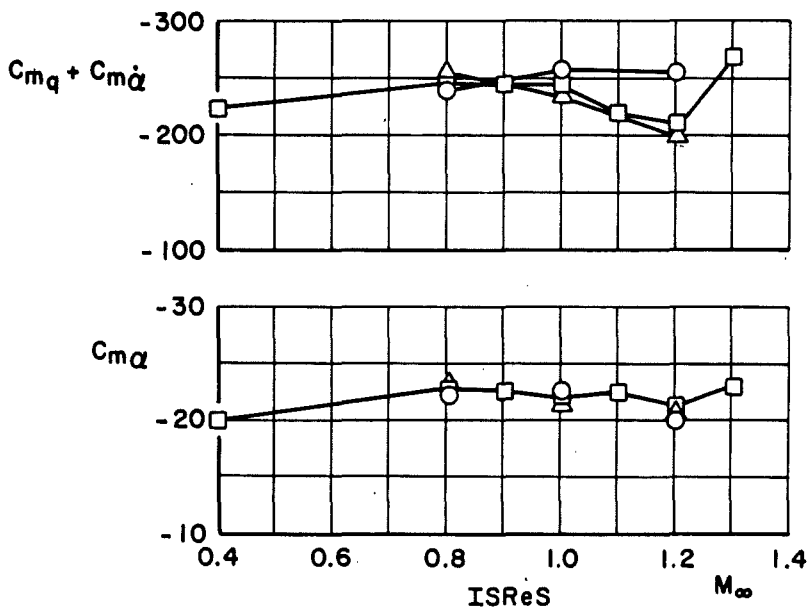
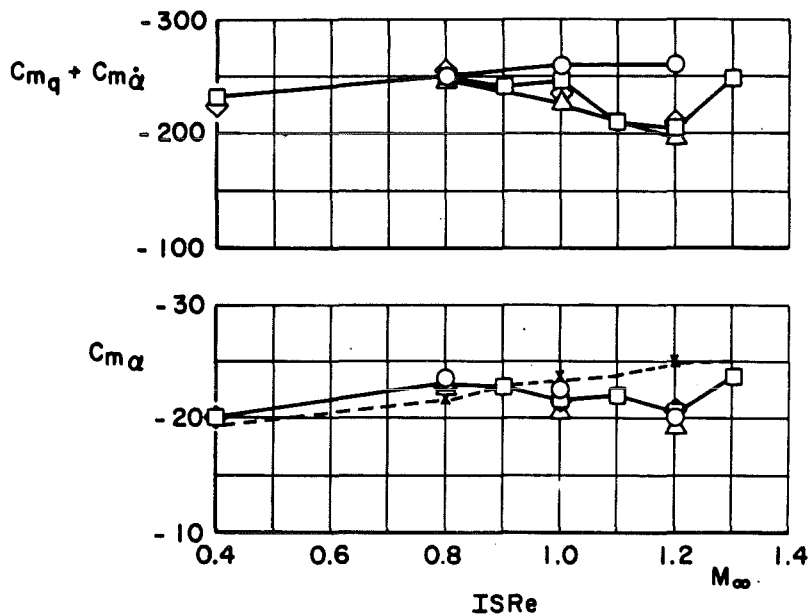


g. Mach number 1.30  
Figure 17. Concluded.



a. Configurations FF and FFS  
 Figure 18. Variation of  $C_{m_q} + C_{m_{\dot{\alpha}}}$  and  $C_{m_{\alpha}}$  with Mach number at zero angle of attack.

- W0,  $\phi_m = 0$
- W1,  $\phi_m = 0$
- x- W1,  $\phi_m = 0$ , Static Stability Test
- △ W2,  $\phi_m = 0$
- ◇ W1,  $\phi_m = -22.5$
- W1,  $\phi_m = -22.5$ , Static Stability Test



b. Configuration ISRe and IRSeS  
Figure 18. Concluded.

## NOMENCLATURE

$A_b$	Model base area, ft <sup>2</sup>
$C_A$	Axial-force coefficient, $F_A/q_\infty S$
$C_{A,b}$	Base axial force, $(p_\infty - p_b)A_b/q_\infty S$
$C_{A,F}$	Forebody axial force, $C_A - C_{A,b}$
$C_\ell$	Rolling-moment coefficient, $M_\ell/q_\infty Sd$
$C_m$	Pitching-moment coefficient, $M_m/q_\infty Sd$ (see Figs. 3 and 4) for moment reference locations
$C_{m_q}$	Pitching-moment coefficient due to pitching velocity, $\partial C_m/\partial(qd/2V_\infty)$ , rad <sup>-1</sup>
$C_{m_\alpha}$	Pitching-moment coefficient due to angle of attack, $\partial C_m/\partial\alpha$ , rad <sup>-1</sup>
$C_{m_{\dot{\alpha}}}$	Pitching-moment coefficient due to rate of change of angle of attack, $\partial C_m/\partial(\dot{\alpha}d/2V_\infty)$ , rad <sup>-1</sup>
$C_N$	Normal-force coefficient, $F_N/q_\infty S$
$C_n$	Yawing-moment coefficient, $M_n/q_\infty Sd$
$C_Y$	Side-force coefficient, $F_Y/q_\infty S$
$d$	Reference length, maximum diameter of the model centerbody, static model 0.1792 ft, pitch-damping model, 0.3958 ft
$F_A$	Measured axial force, lb
$F_N$	Measured normal force, lb
$F_Y$	Measured side force, lb
$I$	Mass moment of inertia, slug-ft <sup>2</sup>
$M_\ell$	Measured rolling moment, ft-lb
$M_m$	Measured pitching moment, ft-lb
$M_n$	Measured yawing moment, ft-lb

$M_\infty$	Free-stream Mach number
$p_b$	Average model base static pressure, psfa
$p_\infty$	Free-stream static pressure, psfa
$q$	Pitching velocity, rad/sec
$q_\infty$	Free-stream dynamic pressure, psf
$Re$	Reynolds number based on $d$
$S$	Reference area (static model $0.0252 \text{ ft}^2$ ) (pitch-damping model, $0.1231 \text{ ft}^2$ )
$V_\infty$	Free-stream velocity, ft/sec
$X_{cp}$	Center of pressure, $C_m/C_N$ (body diameters from moment reference point, positive when forward of moment reference)
$X_{np}$	Neutral-point location, $(dC_m/dC_N)_{\alpha=0}$ (body diameters from moment reference point, positive when forward of moment reference)
$\alpha$	Model angle of attack, deg
$\alpha_{Ai}$	Sting offset angle, deg
$\bar{\theta}$	Model oscillation amplitude, deg
$\omega_m$	Model angular oscillation frequency, rad/sec
$\omega_s$	Support sting angular oscillation frequency, rad/sec
$\phi_m$	Model roll angle, deg

#### TAIL CONFIGURATION CODE

FF	Fixed fins
FFS	Fixed slotted fins
ISRe	Inflatable stabilizer retarder with extender and solid fins
ISReS	Inflatable stabilizer retarder with extender and slotted fins
W0	No fin spin wedges

W1            15-deg fin spin wedges

W2            25-deg fin spin wedges